UCLA
UCLA Electronic Theses and Dissertations

Title

The Microbiome: Micro and Macro Community Dynamics in the Human Oral Cavity and in Space

Permalink

https://escholarship.org/uc/item/87s2c271

Author

Bedree, Joseph

Publication Date

2020

Supplemental Material

https://escholarship.org/uc/item/87s2c271#supplemental

Peer reviewed|Thesis/dissertation

UNIVERSITY OF CALIFORNIA

Los Angeles

The Microbiome: Micro and Macro Community Dynamics in the Human Oral Cavity and in

Space

A dissertation partially satisfying the requirements for the degree

Doctor of Philosophy

in Oral Biology

by

Joseph Kernan Bedree

2020

ABSTRACT OF THE DISSERTATION

The Microbiome: Micro and Macro Community Dynamics in the Human Oral Cavity and in

Space

by

Joseph Kernan Bedree

Doctor of Philosophy in Oral Biology

University of California, Los Angeles 2020

Professor Renate Lux, Co-Chair

Professor Wenyuan Shi, Co-Chair

The 'Great Plate Anomaly' described by Staley and Konopka has presented two significant

obstacles in the field of microbiology, (1) to cultivate as well as characterize all of the microbial

diversity within the natural environment as individual species, the uncultivated organisms being

'microbial dark matter', and (2) as a community, such as the microbiome. Importantly, the

characterization of bacterial organisms involved in human health and disease is of particular

importance. To further illuminate these implicated 'microbial dark matter', a *Schaalia*

odontolytica (formerly *Actinomyces odontolyticus subsp. actinosynbacter*) strain, XH001, the

bacterial basibiont, was recently co-cultivated from the human oral cavity along with its epibiont, a *Nanosynbacter lyticus* type strain TM7x (HMT_952), which thrives on surface of XH001, for characterization. Surprisingly, TM7x, is a member of the Saccharibacteria phylum (formerly TM7 phylum) that is part of a new bacterial lineage denoted as the Candidate Phyla Radiation (CPR), which may comprise of more than 25 percent of all bacterial diversity.

To determine genetic mediators in their relationship, RNA-seq was performed and found the highest upregulated gene in TM7x-asssociated XH001 versus XH001 to be *lsrB*, the receptor for the Auto-Inducer-2 molecule. We confirmed the *lsrB* upregulation via quantitative real time PCR from the transcriptomic analysis and developed a genetic modification system to create deletion mutants to elucidate the genetic determinants involved in the establishment of XH001 and the association with its parasitic epibiont, TM7x. We targeted the *lsrB* and *luxS* (encodes AI-2 synthase) homologues in XH001 and successfully generated an XH001ΔlsrB and XH001ΔluxS single deletion mutants. Phenotypic analyses provided data suggesting that the association with TM7x enhances wildtype XH001's biofilm formation capability in a *lsrB* and *luxS* dependent manner. Herein we also present an established genetic system, including a high-throughput mutagenesis platform (Tn-seq), that enabled a full conditionally essential gene study of XH001 and evaluation of the genetic mediators during the TM7x-associated parasitic event with XH001 in real time. This essential gene study revealed 10.5% of genome to be necessary for growth and elucidated several genes in XH001 directly involved in the epibiotic-parasitic relationship between TM7x and XH001.

Bridging the second knowledge-gap of microbial community dynamics stated above, the oral and gut microbiome of BALB/c mice as part of NASA's Rodent Research 5 mission were assessed for longitudinal changes upon returning to earth for the first time in US/NASA history

as well as the effects of long duration microgravity exposure. Intriguingly, overall microbial diversity was shown to be increased in microgravity conditions, as corroborated by recent human astronaut studies, and found to reduce to pre-flight levels, albeit permanently shifted away from baseline upon returning to earth as show in this study. Furthermore, *Lactobacillus murinus* and *Dorea spp.* were enriched, along with functionally assigned metabolic pathways involved with short-chain fatty acid production, in microgravity compared to terrestrial ground controls revealing a potential mechanism for mediating bone homeostasis.

The dissertation of Joseph Kernan Bedree is approved

Anahid Jewett

Robert Gunsalus

Xuesong He

Renate Lux, Committee Co-Chair

Wenyuan Shi, Committee Co-Chair

University of California, Los Angeles

2020

In loving memory of my grandparents Jerome, Elizabeth, and Virginia

I also dedicate this work to my parents, Melvin and Kathleen, as well as my siblings, Samuel

and Helen

TABLE OF CONTENTS

LIST OF FIGURES

LIST OF TABLES

CHAPTER 4

ACKNOWLEDMENTS

The completion of my PhD has been a wonderful accomplishment and an excellent opportunity to grow as a human being and as a scientist. I have immense gratitude for this endeavor that spans not only experiences and accomplishments, but most importantly the lifelong connections with people I have made along the way. Since science is not a solitary experience and growth is inexorably connected to those who teach you, I must now graciously thank the many people who helped me along the way: I first want to thank my thesis advisor, Dr. Wenyuan Shi, for his mentorship and support to enhance my training and growth as a scientist. I also would like to thank my committee members Drs. Xuesong He, Renate Lux, Anahid Jewett, and Rob Gunsalus for their excellent scientific insight and assistance with completing my thesis project.

One of my most important influences in graduate school was Dr. Aida Kaplan, who I am proud to call a close friend. I also must thank Dr. Bruno Lima, who is also a great friend and colleague that exposed me to complex bacterial genetics early on in graduate school seeding my future interests in synthetic biology and educating me on techniques that made a seminal publication possible. Drs. Daniel Ferrer, Melissa Agnello, and Jonathan Baker thank you for being such an excellent friends and lab partners. Thank you all so much for your sage wisdom, support, and technical expertise throughout my PhD.

The intellectual growth that led to this opportunity to study at a such world class institution has been a life-long pursuit that will finally culminate with the completion of this Doctor of Philosophy in Oral Biology degree. I cannot express in words the appreciation I have for all the love and support my family has provided over the years. Mom, Dad, Helen, and Sam, thank you for everything you have done and helping me develop into the person that I have become today.

VITA

2013	B.Sc. in Biology (Minor: Organizational Leadership) Purdue University
2016	Awarded UCLA MBI Whitcome Training Grant University of California, Los Angeles
2017	Awarded Ruth L. Kirschstein Predoctoral Individual National Research Service Award (NIH-NIDCR NRSA Award Number F31DE026057) University of California, Los Angeles
2018	Awarded The Richard and Mary Finkelstein Student Travel Award American Society of Microbiology (2018 ASM Microbe Meeting)
2018	Best Student Poster Lake Arrowhead Microbial Genomics Conference

PUBLICATIONS AND PRESENTATIONS

Bor, B., Collins, A.J., Murugkar, P.P., Balasubramanian, S., To, T.T., Hendrickson, E.L., **Bedree, J.K**., Bidlack, F.B., Johnston, C.D., Shi, W. and McLean, J.S., (2020). Insights obtained by culturing Saccharibacteria with their bacterial hosts. Journal of Dental Research, 99(6), 685-694.

Bor, B., **Bedree, J.K.,** Shi, W., McLean, J.S., He, X. Saccharibacteria (TM7) in The Human Oral Microbiome. (2019). *Journal of Dental Research*. *98*(5), 500-509.

Bedree JK, Bor B, Cen L, Edlund A, Lux R, McLean JS, Shi W and He X (2018). Quorum Sensing Modulates the Epibiotic-Parasitic Relationship Between *Actinomyces odontolyticus* and Its Saccharibacteria epibiont, a *Nanosynbacter lyticus* Strain, TM7x. *Front. Microbiol.* 9:2049. doi: 10.3389/fmicb.2018.02049

McLean, J. S., Liu, Q., Bor, B., **Bedree, J. K.**, Cen, L., Watling, M., ... & Shi, W. (2016). Draft genome sequence of Actinomyces odontolyticus subsp. actinosynbacter strain XH001, the basibiont of an oral TM7 epibiont. *Genome announcements*, *4*(1), e01685-15.

Bor, B., Poweleit, N., Bois, J. S., Cen, L., **Bedree, J. K**., Zhou, Z. H., ... & Shi, W. (2015). Phenotypic and physiological characterization of the epibiotic interaction between TM7x and its basibiont Actinomyces. *Microbial ecology*, *71*(1), 243-255.

Bedree, J., Huang, Y., Shi J., Ha, P., Pan, H.C., Stodieck, L., Kim, J.K., Wu, B., He, X., Kwak, J.H., Ting, K., Soo, C., Shi, W. Microgravity Modulates Bacterial Diversity and Abundance in the

Rodent Gut Microbiome. *Section: Microbes-3*. The American Society for Gravitational and Space Research Conference 2018, Bethesda, MD. **Invited Oral Presentation.**

Bedree, J., Bor, B., Cien, L, McLean, J., Edlund, A, He, X., Shi, W. Shedding light on Oral Microbial Dark Matter Shedding light on Oral Microbial Dark Matter: Quorum-Sensing Modulates the Epibiotic-Parasitic Relationship between *Actinomyces Odontolyticus* Subspecies *Actinosynbacter* Strain (XH001) and its Epibiont, A TM7 Phylotype (TM7x). IADR/PER 96th General Session & Exhibition of the IADR PAN European Regional Congress 2018, London, England. **Invited Oral Presentation.**

Bedree, J., Bor, B., Cien, L, McLean, J., Edlund, A, He, X., Shi, W. Shedding light on Oral Microbial Dark Matter Shedding light on Oral Microbial Dark Matter: Quorum-Sensing Modulates the Epibiotic-Parasitic Relationship between *Actinomyces Odontolyticus* Subspecies *Actinosynbacter* Strain (XH001) and its Epibiont, A TM7 Phylotype (TM7x). *Gordon Research Seminar-Microbial Toxins and Pathogenicity-Bacterial Pathogenesis: Exploring Molecular Conflicts Between Host and Pathogen.* GRS-Microbial Toxins and Pathogenicity 2018, Waterville, NH. **Invited Oral Presentation.**

Bedree, J., Bor, B., Cien, L, McLean, J., Edlund, A, He, X., Shi, W. Shedding light on Oral Microbial Dark Matter: Quorum Sensing Modulates the Epibiotic-Parasitic Relationship Between XH001 and TM7x *American Society of Microbiology-Richard and Mary Finkelstein Student Travel Award Ceremony.* ASM Microbe 2018, Atlanta, Georgia. **Invited Oral Presentation.**

Bedree, J., Bor, B., McLean, J., He, X., Shi, W. Quorum sensing modulates the epiparasitic relationship between XH001 and TM7x. *J Dent Res Vol 95*(A): 0081(Oral Section-Microbiology/Immunology-Biofilms I), 2016. AADR/CADR 45th Annual Meeting and Exhibition, Los Angeles, California. **Invited Oral Presentation.**

Forsyth Institute Symposium 2018: The Uncultivatable Bacteria (October 11-12th, Cambridge, MA). Poster Title: **Bedree J.K.**, Bor B, Cen L, Edlund A, Lux R, McLean JS, Shi W and He X. Quorum Sensing Modulates the Epibiotic-Parasitic Relationship Between *Actinomyces odontolyticus* and Its Saccharibacteria epibiont, a *Nanosynbacter lyticus* Strain, TM7x. **Poster Presentation.**

Lake Arrowhead Microbial Genomics Conference 2018 (LAMG September 16-20th Lake Arrowhead, CA). Poster Title: **Bedree J.K.**, Bor B, Cen L, Edlund A, Lux R, McLean JS, Shi W and He X. Quorum Sensing Modulates the Epibiotic-Parasitic Relationship Between *Actinomyces odontolyticus* and Its Saccharibacteria epibiont, a *Nanosynbacter lyticus* Strain, TM7x. **Poster Presentation.**

Gordon Research Conference-Microbial Toxins and Pathogenicity-Bacterial Pathogenesis: From Pathogen Physiology to Interactions with the Host Microbiota and Immune System (GRC 2018-July 8-13th Waterville, NH) Poster Title: **Bedree, J.**, Bor, B., Cien, L, McLean, J., Edlund, A, He, X., Shi, W. Shedding light on Oral Microbial Dark Matter: Shedding Light on Oral Microbial Dark Matter: Quorum-Sensing Modulates the Epibiotic-Parasitic Relationship between *Actinomyces Odontolyticus* Subspecies *Actinosynbacter* Strain (XH001) and its Epibiont, A TM7 Phylotype (TM7x). **Poster Presentation.**

FOREWORD

Recent metagenomic analyses revealed a whole class of bacteria, denoted Candidate Phyla Radiation (CPR), including over 35 phyla, comprising of >25% of the bacterial domain (Brown et al. 2015, Hug et al. 2016). This CPR class is detected in a vast range of natural habitats, as well as the human body. CPR organisms also encompass unique characteristics such as small cell sizes and reduced genomes, lacking a variety of essential genes required to exist as an independent, free-living cell, suggestive of obligate-symbiotic relationships with other organisms. However, illuminating direct evidence supporting this notion, as well as detailed knowledge regarding their interaction with their hosts, is an obstacle due to recalcitrance of CPR to in vitro cultivation (McLean et al. 2020). As the first cultivated representative of the CPR group, Nanosynbacter lyticus type strain, TM7x (HMT_952), of the Saccharibacteria phylum (formerly TM7 phylum) was recently co-cultivated with its bacterial basibiont host, *Schaalia odontolytica*, formerly *Actinomyces odontolyticus subsp. actinosynbacter* (Nouioui et al. 2018), strain, XH001 (He et al. 2015). Initial studies indicated that TM7x is obligate, epibiotic-parasite living on the surface of XH001, and was also shown to induce morphological changes when associating with XH001 (Bor et al. 2016). However, there have since been other Saccharibacteria members with established hosts, but these relationships and TM7x alike are specific in nature and evolutionarily related (Bor et al. 2018, Bor et al. 2020, Utter et al. 2020). To indirectly determine the underlying genetic mechanisms of TM7x in the epibiotic-parasitic relationship, metatranscriptomic analysis (RNA-seq) was performed and revealed a set of differentially regulated genes within XH001 when associated with TM7x as compared to parasite-free XH001. The most highly upregulated gene, a *lsrB* ortholog, encodes a periplasmic binding protein for the auto inducer (AI) 2 signaling molecule (He et al. 2015). The focus of this initial work was to elucidate the role of AI-2 quorum sensing affecting the epibiotic-parasitic relationship between XH001 and TM7x as well as create an initial genetic system for XH001 since TM7x is recalcitrant to standard mutant selection methodology (Bedree et al. 2018). To elucidate the remaining genetic factors mediating the relationship

2

between XH001 and TM7x, a combination of additional approaches would be required and warranted further enhancement of the first described genetic system (Bedree et al. 2018), thus to this end, a high-throughput mutagenesis tool (Tn-seq) was implemented to perform a crucial conditionally essential gene study and selection screen to elucidate the genetic constituents involved in the TM7x and XH001 relationship.

The first chapter of the dissertation consists of a complete copy of a published review in the *Journal of Dental Research* (https://doi.org/10.1177/0022034519831671), of which I am co-author (Bor et al. 2019). This introduction details a comprehensive history of Saccharibacteria/TM7 consisting of a general introduction to the phylum, its biodiversity and biogeography, and the first cultivable representative of Saccharibacteria, *Nanosynbacter lyticus* type strain TM7x (HMT_952), with its host bacterium, *Schaalia odontolytica*, XH001 (He et al. 2015, McLean et al. 2016). As stated by the *Journal of Dental Research* "Author re-use policy", the citations listed above are the only requirements for re-use for academic and non-profit purposes. Author contributions for chapter one of the thesis: B. Bor, contributed to design, data interpretation, drafted and critically revised the manuscript; J. K. Bedree, W. Shi contributed data interpretation and critically revise the manuscript; J. McLean, X. He, contributed to conception, design, and data interpretation, drafted, and critically revised the manuscript. All authors give final approval and agree to be accountable for all aspects of the work.

The second chapter describes how quorum sensing modulates the epibiotic-parasitic relationship between a *Schaalia odontolytica* (formerly *Actinomyces odontolyticus subsp. actinosynbacter*) strain*,* XH001, and its Saccharibacteria epibiont, a *Nanosynbacter lyticus* strain, TM7x (Bedree et al. 2018). This chapter is a complete copy of the manuscript published in *Frontiers in Microbiology* (https://doi.org/10.3389/FMICB.2018.02049). *Frontiers in Microbiology* is an open-

access journal under the CC-BY Creative Commons attribution license (the current version is CC-BY, version 4.0 http://creativecommons.org/licenses/by/4.0/). Author contributions for chapter two: JB, BB, AE, RL, JM, WS, and XH designed the research. JB, BB, LC, AE, JM, and XH performed the research. JB, BB, LC, AE, RL, JM, WS, and XH analyzed the data. JB, BB, AE, RL, JM, WS, and XH wrote the manuscript.

The third chapter comprises of two major components for advanced genetic tool development of *Schaalia odontolytica* strain, XH001, which includes construction of a high throughput mutagenesis platform (Tn-seq) and fluorescent protein expression constructs. These two genetic tools accomplished the three aims of this chapter, which were to elucidate the conditionally essential genes in XH001, the host of TM7x, Tn-seq selection screening with TM7x against XH001::Tn5 to determine genetic mediators involved in the epibiotic parasitic relationship, and real time monitoring of XH001 and TM7x parasitism using fluorescence. The author contributions for chapter three: Joseph K. Bedree, Jake Bourgeois, Pooja Balani, Andrew Camilli, Xuesong He, and Wenyuan Shi designed the research. Joseph K. Bedree, Jake Bourgeois, Pooja Balani, Andrew Camilli, Xuesong He, and Wenyuan Shi performed the research. Joseph K. Bedree, Jake Bourgeois, Pooja Balani, Andrew Camilli, Xuesong He, and Wenyuan Shi analyzed the data. Joseph K. Bedree, Jake Bourgeois, Pooja Balani, Andrew Camilli, Xuesong He, and Wenyuan Shi wrote the manuscript.

The fourth and final chapter of this dissertation describes a broad view of bacterial-bacterial interactions within the oral and gut microbiome context and is tangentially related to the first three chapters in this respect, however, the context for understanding the microbiome is quite different. This work uniquely describes how microgravity modulates bacterial diversity in the rodent oral and gut microbiome as part of NASA's Rodent Research 5 mission. This chapter is a

manuscript in preparation for submission to the journal *Nature*. As such, the chapter content is formatted for submission aside from compliance with UCLA thesis submission guidelines. Author contributions for chapter four: Joseph K. Bedree, Kristopher Kerns, Tsute Chen, Bruno P. Lima, Samuel S. Minot, Erik L. Hendricksen, Ella Lamont, Guo Liu, Pin Ha, Jiayu Shi, Jong Kil Kim, Hsin Chuan Pan, Luan Tran, Alexis Kokaras, Louis Stodieck, Yasaman Shirazi, Benjamin Wu, Jin Hee Kwak, Kang Ting, Chia Soo, Jeffrey S. McLean, Xuesong He, Wenyuan Shi designed the research. Joseph K. Bedree, Kristopher Kerns, Tsute Chen, Bruno P. Lima, Samuel S. Minot, Erik L. Hendricksen, Ella Lamont, Guo Liu, Pin Ha, Jiayu Shi, Jong Kil Kim, Hsin Chuan Pan, Luan Tran, Alexis Kokaras, Louis Stodieck, Yasaman Shirazi, Benjamin Wu, Jin Hee Kwak, Kang Ting, Chia Soo, Jeffrey S. McLean, Xuesong He, Wenyuan Shi performed the research. Joseph K. Bedree, Kristopher Kerns, Tsute Chen, Bruno P. Lima, Samuel S. Minot, Erik L. Hendricksen, Ella Lamont, Guo Liu, Pin Ha, Jiayu Shi, Jong Kil Kim, Hsin Chuan Pan, Luan Tran, Alexis Kokaras, Louis Stodieck, Yasaman Shirazi, Benjamin Wu, Jin Hee Kwak, Kang Ting, Chia Soo, Jeffrey S. McLean, Xuesong He, Wenyuan Shi wrote the manuscript.

Chapter 1: Saccharibacteria (TM7) in the Human Oral Microbiome

Abstract

Bacteria from the Saccharibacteria phylum (formerly known as TM7) are ubiquitous members of the human oral microbiome. Recent studies revealed remarkable 16S rRNA diversity in the environmental and mammalian host-associated members across this phylum and their association with oral mucosal infectious diseases has been observed. However, due to their recalcitrance to conventional cultivation, their physiology, lifestyle, and role in health and diseases remain elusive. The recent cultivation of *Nanosynbacter lyticus* type strain TM7x (HMT_952), the first Saccharibacteria strain co-isolated as an ultra-small obligate parasite with its bacterial host from human oral cavity, provides a rare glimpse into the novel symbiotic lifestyle of these enigmatic, human-associated bacteria. Here, we review the current knowledge on the diversity and unique biology of TM7. Furthermore, insight into the potential impact of TM7 on modulating the human oral microbial ecology is highlighted. However, to understand their relationship, a genetic toolset was developed in the bacterial host of TM7x, *Actinomyces odontolyticus* subspecies *actinosynbacter*, XH001. This toolset consisted of methodologies for chromosomal deletions and a high-throughput genetic screening tool known as Tn-seq. As such, an XH001 Tn-seq library was constructed and enabled elucidation of the conditionally essential genes required for *in vitro* growth.

Introduction

A monumental milestone in human microbiology within the past few decades was uncovering the vast microbial abundance and diversity associated with the human body (Peterson et al. 2009, Chen et al. 2010, Dewhirst et al. 2010). These microbial communities co-evolve with their host and significantly influence health and disease in humans (Nishihara et al. 2004, Ley et al. 2006). Due to its easy access and clinical relevance, human oral cavity has become a model for advanced microbiome analysis seeking to gain an understanding of microbial ecology and functionality (Chen et al. 2010, Edlund et al. 2013, Edlund et al. 2015, Baker et al. 2017, Nowicki et al. 2018). However, a significant portion (≈30%) of oral microbial species remains uncultivable (http://www.homd.org), thus, their metabolic potential, physiological properties, ecological function, and influence in human health are unknown. A primary example is the bacterial phylum Saccharibacteria (also formerly known as phylum TM7 and will be referred to as such in this review for brevity). Members of the TM7 phylum are ubiquitous in the human oral microbiome and accumulating evidence links their association with periodontal disease. However, due to the lack of cultivated representatives, knowledge of TM7 was scarce until the recent cultivation of the first oral strain, which provided the first view on its unique cell size, lifestyle and the means to study these bacteria (He et al. 2015). In this review, we provide an update on the current knowledge of this enigmatic bacterial phylum.

8

I. TM7: Ubiquitous yet "Enigmatic" Bacterial Phylum Associated with the Human Oral Cavity

General introduction to TM7

TM7 rRNA gene sequences were first detected from a peat bog sample (TM stands for "Torf, mittlere. Schicht," German for a middle layer of peat) in northern Germany in the mid-1990s by using a culture-independent molecular approach (Rheims et al. 1996, Rheims et al. 1996), along with highly divergent sequences from a number of additional candidate bacteria such as TM6 (McLean et al. 2013). TM7 was later proposed as a distinct bacterial phylum based on partial 16S rDNA sequences (Hugenholtz et al. 1998, Hugenholtz et al. 2001) and designated "Candidate Division TM7". Subsequently, its presence has been detected in extremely diverse natural habitats, including soil, seawater, underground water, rhizospheres, deep-sea sediments, wastewater treatment plant, hot springs, termite guts, and mammals (Hugenholtz et al. 2001, Brinig et al. 2003, Kumar et al. 2003, Nakajima et al. 2005, Dewhirst et al. 2012, Kindaichi et al. 2016, Dudek et al. 2017, Zhang et al. 2017, Starr et al. 2018), using 16S rRNA-based molecular approaches. As of 2011, a total of 255 TM7 phylotypes have been indicated by 16S rRNA gene sequencing with 160 listed as environmental, 42 as animal associated, and 53 as human-associated (Dinis et al. 2011). This list continues to expand as studies unveil new phylotypes (distinct sequences with no cultured representatives) from increasingly diverse environmental niches (Liu et al. 2012, Lowe et al. 2012, Segata et al. 2012, Winsley et al. 2014, Dudek et al. 2017, Zhang et al. 2017, Starr et al. 2018). Single cell sequencing approaches then provided the first fragmented partial genomes of the oral TM7a (Marcy et al. 2007) and the soil harboring TM7 bacterium, GTL1 (Podar et al. 2007). While valuable, these incomplete genomes provided limited power to predict the functional capacities present in this diverse phylum (Dinis et al. 2011). In 2013, four complete TM7 genomes were assembled through differential coverage binning sampled from an activated sludge bioreactor (Albertsen et al. 2013). '*Candidatus*

Saccharibacteria' was proposed as the new phylum name for TM7 based on the genomic analysis, which suggested these bacteria, with reduced genomes, consume primarily sugar compounds.

While TM7 bacteria can be found in a wide distribution of habitats, their physiology, lifestyle, and ecological role or pathogenic nature (for host-associated phylotypes) remained elusive due to their apparent recalcitrance to conventional cultivation methods. Attempts were made to isolate TM7 bacteria but failed to achieve sustainable growth. A soil-slurry membrane system, which combined a polycarbonate membrane as growth support and the soil extract acting as growth substrate, was implemented to cultivate the environmental TM7 phylotypes as tiny microcolonies (Ferrari et al. 2005, Abrams et al. 2012), albeit with no success in further enrichment. Intriguingly, these microcolonies were composed of a mixture of different bacterial species suggesting TM7 may require co-cultivation in order to propagate (Abrams et al. 2012). These results were consistent with previous studies evaluating uncultivable microorganisms from the environment, which revealed that many recalcitrant bacteria rely on metabolic cooperation with other species for the provision of nutrients (Zengler et al. 2002, Vartoukian et al. 2010, Pham et al. 2012). Furthermore, using a cultivation-independent metagenomic approach, Banfield and colleagues recovered the complete genome of a TM7 representative (RAAC3) from an acetate-stimulated aquifer sediment (Kantor et al. 2013). Genomic analysis revealed that RAAC3 is missing pathways for biosynthesis of nucleotides, lipids and amino acids, and suggested that TM7 could be auxotrophic and metabolically dependent on other organisms (Kantor et al. 2013).

Human oral TM7

TM7 bacteria are commonly found constituents of the human microbiome and are detected in various human body sites, including the gastrointestinal tract, skin, and the female genital tract

(Brinig et al. 2003, Eckburg et al. 2005, Fredricks et al. 2005, Gao et al. 2007). Additionally, 16S rRNA gene sequencing indicates that TM7 has been continuously prevalent in the human oral microbiome from Neanderthals (Weyrich et al. 2017) to modern-day Homo sapiens (Brinig et al. 2003). The association of TM7 with inflammatory mucosal diseases, such as vaginosis and inflammatory bowel disease has been suggested from studies that found TM7 sequences differentially abundant in the disease state (Brinig et al. 2003, Fredricks et al. 2005, Kuehbacher et al. 2008). Typically found at low abundance, approximately 1% of the whole oral microbial population based on culture independent molecular analyses (Brinig et al. 2003, Podar et al. 2007), an increase in the abundance (as high as 21% of the whole oral bacterial population in some cases) of TM7 members was detected in patients with mucosal infections (Rylev et al. 2011). Even greater abundances of TM7 were associated with gingivitis severity and periodontal disease (Paster et al. 2002, Brinig et al. 2003, Rylev et al. 2011, Liu et al. 2012, Kistler et al. 2013, Camelo-Castillo et al. 2015, Sousa et al. 2017, Nowicki et al. 2018). Certain oral TM7 phylotypes, such as TM7 clones, AF125206 (HMT_356, 99.7% identity) and AY134895 (HMT_952, Strain: TM7x , 98.9% identity), can even be detected on or within the host crevicular epithelial cells (Paster et al. 2002). Moreover, the reduction in the abundance of TM7 can be consistently observed in plaque-induced gingivitis after treatment intervention (Huang et al. 2016). This clinical evidence suggests the correlation of TM7 with gingivitis and periodontitis, and therefore justifies that several TM7 taxa have been included in the core microbiome associated with periodontitis (Abusleme et al. 2013). Despite these associations, no causative relationship between TM7 and periodontal diseases has been established, which warrants further study.

Oral TM7: biodiversity and biogeography

As high through-put DNA sequencing studies accumulated, many inadvertently grouped these candidate phylum sequences into bins designated as "other" or "unclassified", primarily as a result

of lacking close representative sequences in databases. In addition, although some related sequences were deposited in databases, many were not classified as phylogenetically related to TM7, which we now hypothesize to be driven by sequence divergence across the phylum. Thorough 16S rRNA gene sequence analyses from publicly available databases have subsequently revealed the diversity of TM7 across many environments. Development of the Human Oral Microbiome Database (Chen et al. 2010), which contains deposited, full length 16S rRNA gene sequences with group level designations, allows evaluation of the distribution of these TM7 sequences in datasets that originally did not report group resolved TM7 hits. One study performed this type of contemporary 're-analysis', using recently developed oligotyping techniques (250 bp sequences grouped at 99% sequence identity) that were applied across the oral samples within the Human Microbiome Project high throughput 16S rRNA marker gene dataset (Eren et al. 2014). The distribution of the oligotypes reported indicated a best 'hit' match with TM7 groups, G1, G3, and G5, which were found across nine oral sites in healthy humans with no oral disease (Eren et al. 2014). Consequently, recent studies using available 16S rRNA gene phylogeny revealed six major TM7 phylum groups (G1- G6), which are detected in the oral cavity alone (Camanocha et al. 2014). Collectively, the groups vary in prevalence across subjects within the oral cavity and the enrichment of some groups within specific anatomical sites is evident (Figure 1). Over two decades past the first reported 16S rRNA sequence in 1996 (Rheims et al. 1996), only genomes from the G1 group have been uncovered from single cells or metagenomic binning approaches. Very recent studies however have uncovered additional genomes from the other diverse groups within the phylum from humans and mammals (McLean et al. 2018), including the dolphin oral cavity (Dudek et al. 2017).

II. TM7x: The First Cultivated TM7 Strain

TM7x—an obligate parasite that infects oral bacteria

Utilizing a newly developed culturing medium that was able to support the growth of multiple TM7 phylotypes within an *in vitro* multispecies oral microbial community (Tian et al. 2010, Edlund et al. 2013), and combined with targeted antibiotic enrichment, He *et al.* were able to achieve the successful co-isolation of the first cultivable representative of TM7, *Nanosynbacter lyticus* type strain TM7x (HMT_952), with its host bacterium, *Actinomyces odontolyticus actinosynbacter* strain, XH001 (He et al. 2015, McLean et al. 2016).

Initial observations showed for the first time that TM7x has an ultra-small cell size (200–300 nm) and was attached to a bacterial host. The TM7x genome is also reduced (about 700 genes) and lacks the ability to produce membrane lipids or nucleotides. Additionally, genes required for *de novo* biosynthesis of essential amino acids, nucleotides and cofactors are lacking (He et al. 2015), which could explain the previous failed attempts in isolating TM7 species as a pure monoculture. TM7x has a high coding density genome and ranks among the smallest bacteria found in the human body in both genome size and gene count to date. TM7x falls within the G1 Phylum group, which also has several environmental G1 relatives; this group contains members from mixed sources from mammals to deep groundwater(McLean et al. 2018). In comparison to the environmental genomes available, the oral TM7x genome is smaller and therefore likely has become reduced within mammalian hosts over time (He et al. 2015). The gene loss, however, is clustered mostly within a single genomic region. The rest of the genome is highly syntenic compared with the metagenomically derived and closed environmental genomes isolated from an aquifer (RAAC3) as well as a sludge bioreactor ("*Ca. Sachharibacteria. Aalborgensis*") (He et al. 2015). The genome of TM7x bears some similarities to known bacterial symbionts in insects (McCutcheon et al. 2011), specifically the highly reduced gene content with diminished functional

capacity and auxotrophy for various vitamins as well as minerals. Unlike TM7x, insect symbionts are in general reliant on a eukaryotic host instead of a free-living bacterium.

Further studies demonstrated a highly dynamic interaction between TM7x and its bacterial host, in response to physical association and environmental conditions such as oxygen level and nutritional availability. This is reflected by their reciprocal morphological and physiological changes during episymbiotic growth (Bor et al. 2016). Specifically, XH001 cells grow as short rods when alone, but exhibit elongated cell morphology when physically associated with TM7x under nutrient-replete conditions. In contrast, upon starvation, TM7x-associated host cells manifest a variety of cell morphologies, including swollen cell body, clubbed-ends, and even cell lysis. In addition, a large portion of the TM7x cells transform from ultra-small cocci into more elongated cells under starvation condition (Bor et al. 2016). Transcriptomic gene profiling of the roughly 2000 genes in XH001 revealed roughly 340 differentially regulated genes. A total of 70 genes were up-regulated (greater than threefold) when XH001 was physically associated with TM7x. Most interestingly, of the 35 most up-regulated genes, eight (23%) encoded functions related to the stress response and eight more (23%) were involved in carbohydrate metabolism (He et al. 2015). The gene expression data aligned with the physical observation that the association of TM7x resulted in a slightly reduced growth in XH001, a characteristic feature of a parasitic relationship (Bor et al. 2016). Overall, the combined physiological, genomic and transcriptional characteristics led to the classification of TM7x as an obligate epibiont that is parasitic (an epiparasite) (He et al. 2015).

Although epiparasitism is widespread between microorganisms and domain Eukarya (Bidartondo et al. 2002), TM7x represents the first epiparasite discovered within the domain Bacteria that requires other bacteria as a host (Bor et al. 2016). Interestingly, similar symbiotic relationships have been reported in domain Archaea. The first evidence was reported in 2002, when a

nanosized hyperthermophilic archaeon, *Nanoarchaeum equantum*, was found to proliferate while attached to a specific archaeal host, a member of the genus, Ignicoccus (Huber et al. 2002). Like TM7x, *N. equitans* is an obligate parasite with reduced genome capacity that cannot sustain host-free, independent cellular growth. In high cell density, *N. equitans* is inhibitory and prevents *Ignicoccus* host growth (Jahn et al. 2008). Further studies indicated that these ultra-small archaeal "parasites" can be found in various environmental settings, particularly in extreme environments, including deep sea hydrothermal vents (Huber et al. 2002), acid mine drainage (Baker et al. 2006), and hot springs (Wurch et al. 2016). These nanoarchaeum species are the member of a larger lineage termed DPANN archaea, which are inferred to be mostly symbionts based on the genomic information similar to CPR, and it is even shown that they share similar metabolic traits (Castelle et al. 2018).

One of the key features of parasites is their metabolic dependency on their hosts, which is evident from the minimal metabolic pathways predicted in TM7x, as shown in Figure 2. These annotated genes in pathways are derived from our collaboration with BioCyc (Pathway/Genome Database Collection) and displayed with Pathway Tools (Caspi et al. 2016, Karp et al. 2016). XH001 genome is teeming with a multitude of pathways that can satisfy the cellular requirements of TM7x. Genome scale, flux balance model (Orth et al. 2010) predicting the metabolic interactions of TM7x and XH001 in minimal media, indicates that lactate is likely the main carbohydrate source for TM7x derived from XH001 (Figure 2). This was generated using the Seed Models (Henry et al. 2010) and combined with a community metabolic model (Henry et al. 2016), and subsequently visualized in Kbase (Arkin et al. 2018). Additionally, there is a predicted flux of L-arginine as well as other amino acids, peptides (Gly-glu-L, Gly-Phe), and fatty acid metabolites. Validation of these predictions and the mechanisms by which TM7x transports these components can now be investigated with the strains available in stable co-culture (He et al. 2015, Bor et al. 2018).

TM7x – a bacterial parasite that enjoys long-term stable relationship with its host

Once the epiparasitic relationship between TM7x and its bacterial host XH001 is established, it remains stable and easily maintained under nutrient replete, *in vitro,* laboratory conditions (He et al. 2015, Bor et al. 2016). This long-term, stable relationship is possible because the TM7x/XH001 coculture appears to maintain a subpopulation of uninfected XH001 bacterial cells, which accounts for ~28-52% of the population on average (Bor et al. 2018). While the TM7x-infected host cell population in the coculture display reduced growth and severely inhibited cell division, the uninfected XH001 population exhibits normal cell division and could serve as a reservoir to facilitate another infection cycle by TM7x via horizontal transmission (Bor et al. 2018).

Further knowledge was gained by infecting naïve hosts, an independent *Actinomyces odontolyticus* isolate from human oral cavity that has not been exposed to TM7x in the laboratory (designated as XH001n), using isolated TM7x. Bor *et al.* observed that XH001n suffered a dramatic cell death, which was a result of an overwhelmingly high number (on average >50 cells) of TM7x infecting individual host cells (Bor et al. 2018). This virulent killing is transient however, where the XH001n cells can quickly evolve a reduced-susceptibility to TM7x infection and enter a stable long-term epiparasitic relationship akin to XH001. This reduced susceptibility is hypothesized to be driven by rapid host evolution via genetic adaptation, where genome sequencing revealed these stable host cells gained multiple mutations in the transporter and regulatory genes potentially allowing partial protection from infection (Bor et al. 2018).

The rapidly developed, long-term association between TM7x with XH001n was also observed through infection of a number of closely related *Actinomyces* species with TM7x (Bor et al. 2018). The ability of TM7x to quickly adapt to multiple hosts post infection and the subsequent establishment of the stable epiparasitic relationship could potentially allow TM7 species to associate with many bacterial lineages and persist within the oral cavity or other natural

environmental niches. This is an intriguing evolutionary question that warrants further investigation.

TM7x—a parasite with benefits

As an obligate epiparasite, TM7x represents a burden to its host bacteria, and exerts various negative impacts, including increased stress responses (Bor et al. 2016), reduced cellular growth rate and cell division (Bor et al. 2016), and even cell lysis under nutrient starvation conditions in batch culture (He et al. 2015). However, recent studies also indicated that the association with TM7x could potentially be beneficial to the host bacteria, for example via promoting biofilm formation (Bedree et al. 2018).

In most ecological habitats, including the human oral cavity, microbes form complex and highly structured, multi-species communities known as biofilms. This structure is facilitated through an intricate extracellular matrix consisting of polysaccharides, proteins, DNA, and lipids, and it is an essential part of the many microbial lifecycle in the oral cavity (Bowen et al. 2018). It protects oral bacteria from saliva flow, daily oral hygiene interventions, and clearance by the human immune system, thereby allowing persistence within the oral cavity (Sanz et al. 2017). Bedree *et al.* recently demonstrated that the association of TM7x with XH001 promotes biofilm formation partially via auto inducer (AI)-2 quorum sensing (QS) (Bedree et al. 2018). This was validated by chromosomal deletions of key AI-2 QS genes, *luxS* and *lsrB*, encoding the AI-2 QS molecule synthase and binding receptor, respectively, in XH001, which resulted in biofilm formation deficiencies of TM7x-associated XH001 (Bedree et al. 2018). In addition to TM7x and its host withstanding physical disturbances within oral cavity, a plausible advantage could be evading the immune system *in vivo* by directly reducing inflammation via biofilm formation. While this recent study did not directly evaluate this possibilities in the oral cavity, existing literature reports that

biofilm inducing bacteria impede activation of the immune system (Donlan et al. 2002, Domenech et al. 2013) and diminish the pro-inflammatory response by reducing TNF-α production (Thurlow et al. 2011). This is consistent with the observation that TM7x association repressed XH001-induced TNF-α expression in macrophages, which suggests that TM7x may prevent detection of XH001 by macrophages or possibly directly suppress TNF-α expression in macrophages (He et al. 2015). Altogether, these data are suggestive of ultra-small bacteria potentially having the capacity to modulate the normal host immune response (He et al. 2015). The full molecular mechanism behind this QS-regulated, enhanced biofilm formation phenotype in TM7x-associated XH001 remains to be elucidated. Furthermore, determining if biofilm formation could provide evolutionary fitness in the survival of TM7x's bacterial hosts merits further investigation.

Conventionally, a parasitic relationship is commonly defined as one partner gains benefit at the expense of its counterpart. While recent evaluation of the epiparasitic relationship between TM7x and XH001 corroborates the increasing lines of evidence showing that while parasites negatively impact the growth of their hosts, they also could offer evolutionary advantages by enabling the persistence of their host species (Dunn et al. 2008). Thus, when assessing the benefits and disadvantages of parasitism, the outcome of the relationship should not solely be studied in isolation, but rather in a natural context.

III. Beyond TM7x: Into the Ultra-Small World

TM7 and Candidate Phyla Radiation (CPR)

The Candidate Phyla Radiation (CPR) is a newly described bacterial major lineage (superphylum) containing over 70 phyla, potentially accounting for more than 25% of bacterial diversity, and until recently, no cultured representative had been reported (Brown et al. 2015, Hug et al. 2016, Castelle et al. 2018). This discovery has greatly expanded the view of microbial diversity, but simultaneously engendered fundamental questions that remain unanswered regarding their biology and their potential influence on microbial ecology. TM7, in addition to the SR1 and GN02 phyla, are among the only CPR that are detected within the human microbiome, specifically enriched in the oral cavity (Camanocha et al. 2014). Other members of the TM7 and CPR share similar characteristics with TM7x including highly reduced genomes, restricted metabolic capacities and an inferred ultra-small cell size (Kantor et al. 2013, Brown et al. 2015, Luef et al. 2015, McLean et al. 2018). Strikingly, since most of the available genomes reveal numerous absent biosynthetic pathways across the CPR lineage, they are predicated to have a symbiotic lifestyle similar to TM7x (Kantor et al. 2013, McLean et al. 2013, Brown et al. 2015, Castelle et al. 2018). TM7x represents the first cultivated member of CPR and has thus far enabled detailed studies of these ultrasmall epiparasites, such as the dynamic interaction with their hosts, host preference and range, biofilm formation and their pathogenic potential (Figure 3). As the impetus for studying the CPR increases (Brown et al. 2015, Attar 2016, Burstein et al. 2016, Castelle et al. 2017, Danczak et al. 2017, Castelle et al. 2018), TM7x/XH001 may continue to provide fundamental knowledge on the underlying mechanisms governing the lifestyle of bacteria with reduced genomes, such as those belonging to the CPR group.

Novel approach for isolating and cultivating TM7 strains

Cultivation of the first TM7x strain with its bacterial host XH001 has provided invaluable knowledge. The requirement of TM7x to only grow with a host bacterium and the discovery of the ability of TM7x to horizontally infect new host bacteria (Bor et al. 2018) has recently led to a novel host "baiting" methodology (http://www.homd.org/doc/Saccharibacteria Isolation and Cultivation.pdf). The efficacy of this isolation methodology in part prompted organization of the Inaugural Forsyth Institute's Symposium in October 2018, titled the "Uncultivable Bacteria". The conclusion of the symposium consisted of a hands-on workshop demonstrating TM7 bacteria isolation and cultivation from the human oral cavity. This symposium enabled exposure and dissemination of critical cultivation knowledge to the global research community. This cultivation methodology has resulted in stable cultures of several new TM7 strains of different species (unpublished data), greatly expanding the current isolated TM7 bacterial representatives. The addition and sequencing of new cultivated TM7 strains is pivotal to elucidating the molecular underpinnings of this novel parasitic mechanism as well as the universal TM7 bacterial ecology. It is anticipated that the attendees at this symposium and abroad will implement the validated method to isolate even more TM7 bacteria from diverse environments. This method removed a major roadblock and paved the way for cultivating and studying TM7 strains and may enable isolation of other oral candidate phyla that otherwise are difficult to cultivate, including 'yet-to-be cultivated' species from the GN02 and SR1 phyla in humans.

IV. Future Perspectives

The obligate, epiparasitic relationship between TM7x and XH001 represents a novel, yet presumably common and long established interspecies interaction in the oral microbiota, as suggested by the presence of CPR from ancient to modern humans (Camanocha et al. 2014, Weyrich et al. 2017, Baker et al. 2018). There is strong evidence that CPR organisms, particularly TM7, interact with the core members of the microbiome such as *Actinomyces* and play a critical, yet very poorly understood function in the development of the human community composition in health and disease (Abusleme et al. 2013, Costalonga et al. 2014, Baker et al. 2017). The distinct interactions between TM7 and their bacterial hosts may have a considerable impact on oral microbial ecology at various levels. Depending on local microenvironments, TM7 species could modulate the oral microbiome structure hierarchy and functionality through affecting their bacterial host's physiology, inhibiting host growth dynamics, or impacting the relative abundance of the host via direct killing. It is also possible that bacterial species carrying TM7 parasites could invade other hosts or host niches via parasite-mediated competition, effectively using the parasites as biological weapons, similar to how human intestinal bacteria, such as certain *Enterococcus faecalis* strain, use phage as a bioweapon to kill off competitors (Duerkop et al. 2012). Furthermore, the observed TM7x repression of the XH001-induced TNF-α mRNA expression in macrophages implies that interactions between TM7 species and their bacteria are likely to be more complex than a simple metabolic dependency, and may impact the human host responses (He et al. 2015), thus indirectly modulating human oral microbiome. While accumulating evidence has established enrichment and subsequent association of these ultra-small parasites of bacteria with disease states, the next critical step is to investigate the causation between TM7 and oral infectious diseases. As interest in the study of ultra-small bacteria increases, the isolation and investigation of additional TM7 strains and other CPR bacteria will provide much-needed

knowledge on the biology of this distinct bacterial lineage, as well as confirm if any of the findings

obtained from studies on the human associated TM7x/XH001 pair are generalizable.

Acknowledgements
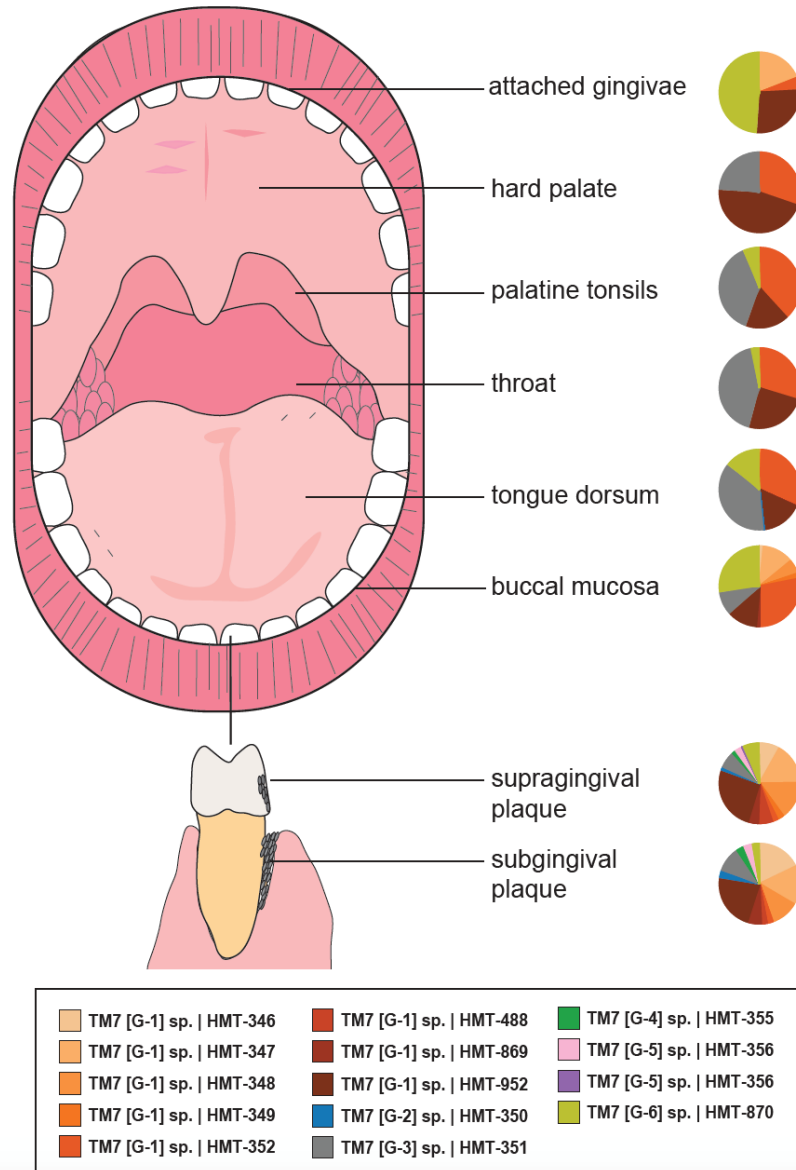
Figure 1. Saccharibacteria/TM7 biogeography in the oral cavity. With the accumulated availability of 16S rRNA gene databases, the phylogenetic diversity groups the phylum into at least 6 major groups which are detected at various levels in the oral cavity. Pie charts displaying the percentage distribution of the different groups within the phylum across oral cavity sites was derived from a re-analysis of the Human Microbiome Project data (https://hmpdacc.org/) using these new reference sequences from the different groups.
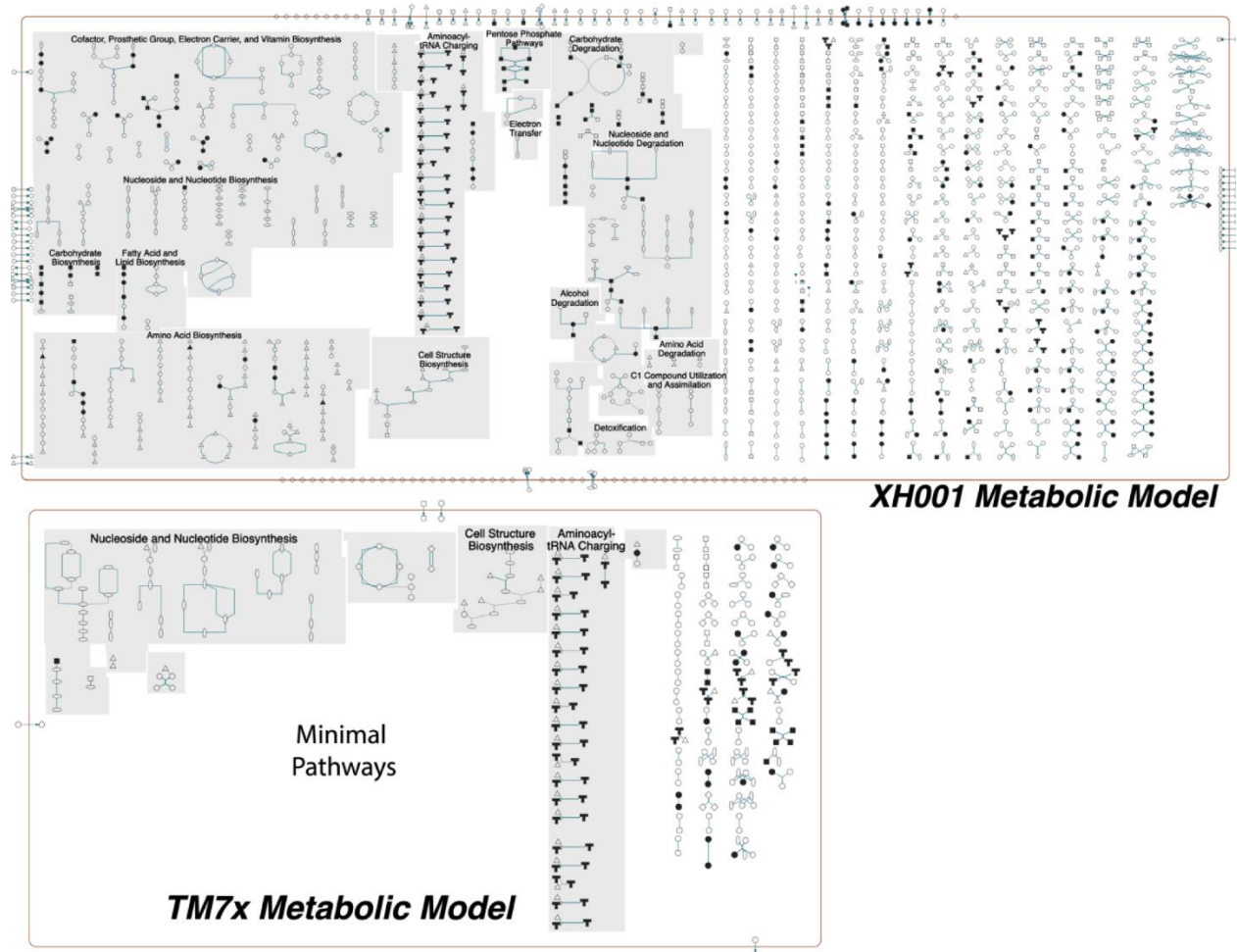
Figure 2. Genome scale metabolic maps of the XH001 and TM7x interaction. Curated, genome scale metabolic models of XH001 and TM7x derived from collaboration with the Biocyc team, which is publically available (https://biocyc.org/). There is a major contrast in the predicted functions for each of these bacteria. *Actinomyces odontolyticus* XH001 has 123 pathways and 774 reactions and 501 predicted enzymes. The reduced genome parasite TM7x is auxotrophic for all essential amino acids and in comparison has only 20 pathways and 151 reactions with 101 predicted enzymes. XH001: *Actinomyces odontolyticus* strain XH00; TM7x: Nanosynbacter lyticus type strain TM7x.
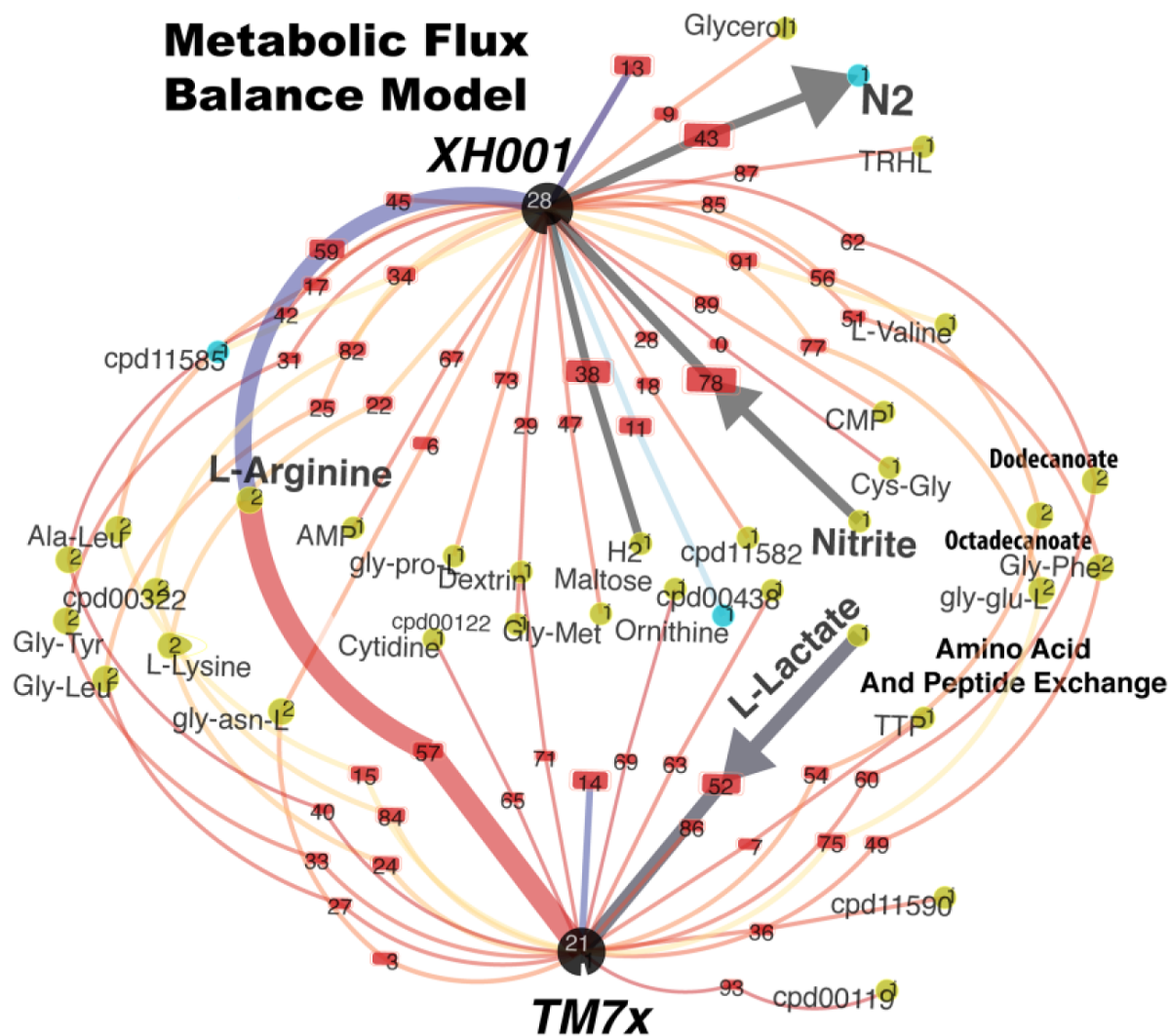
Figure 3. Flux balance analysis of the XH001 and TM7x interaction. Flux balance analysis using the Seed Model (http://modelseed.org/) enables a cursory prediction of the possible metabolic interaction between the two species in minimal media with glucose as the carbon source. Lactate under these conditions is the predicted substrate for TM7x metabolism. Colored nodes represent compounds and lines with numbers represent the predicted flux of metabolites. XH001: *Actinomyces odontolyticus* strain XH001; TM7x: *Nanosynbacter lyticus* type strain TM7x.
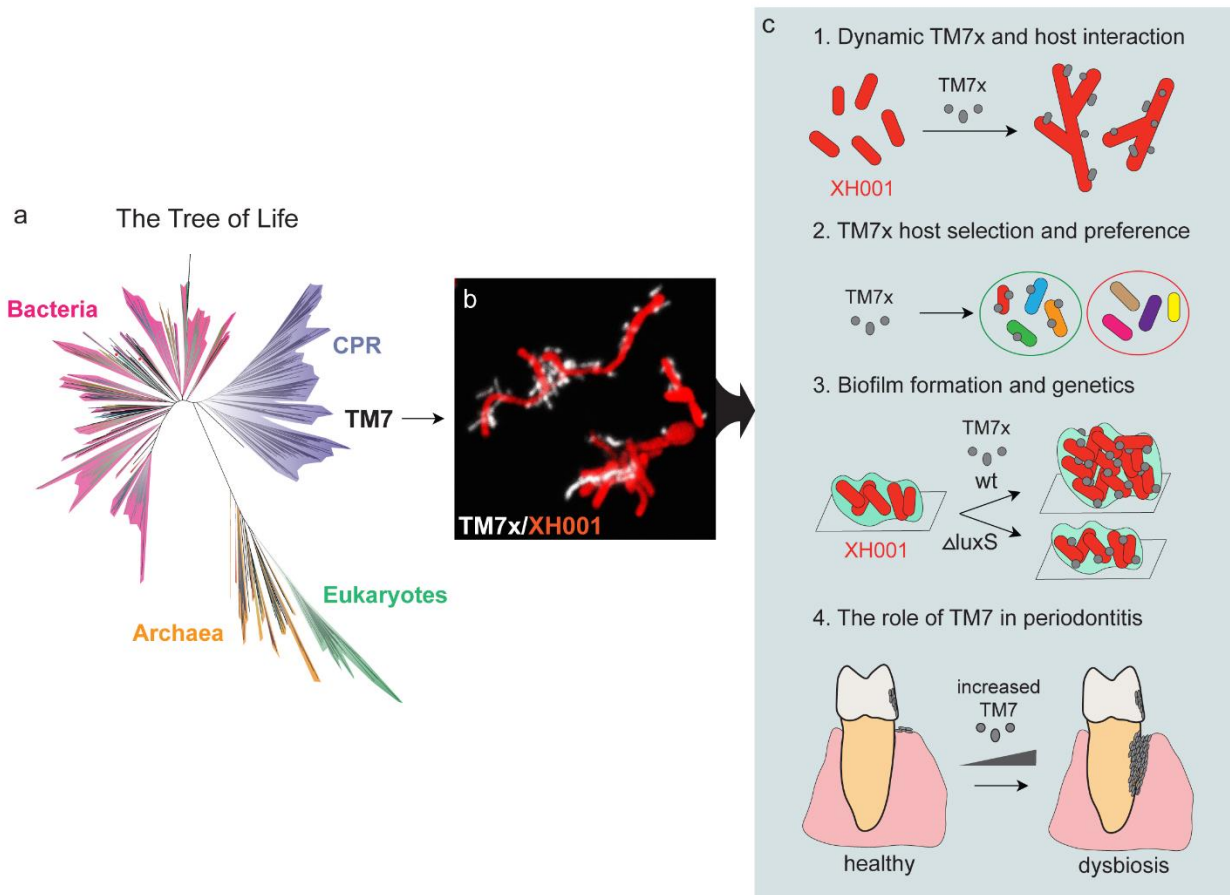
Figure 4: TM7x/XH001 represents a model system to understand human host-associated Saccharibacteria. A detailed mechanistic understanding of the parasitic relationship between TM7x and its host bacterium XH001(a); the host selection and host range of TM7x (b); the impact of interaction on bacterial physiology (c) and pathogenic potential (d), will provide a valuable prototype for understanding the unique lifestyle and reveal the hidden bio-physiological potential of human-associated Saccharibacteria as well as other CPR bacteria (e).

Chapter 2: Quorum Sensing Modulates the Epibiotic-Parasitic Relationship between *Actinomyces odontolyticus* and its Saccharibacteria epibiont, a *Nanosynbacter lyticus* strain, TM7x

Abstract

The ultra-small, obligate parasitic epibiont, TM7x, the first and only current member of the long-elusive Saccharibacteria (formerly the TM7 phylum) phylum to be cultivated, was isolated in co-culture with its bacterial host, *Actinomyces odontolyticus* subspecies *actinosynbacter*, XH001. Initial phenotypic characterization of the TM7x-associated XH001 co-culture revealed enhanced biofilm formation in the presence of TM7x compared to XH001 as monoculture. Genomic analysis and previously published transcriptomic profiling of XH001 also revealed the presence of a putative AI-2 quorum sensing (QS) operon, which was highly upregulated upon association of TM7x with XH001. This analysis revealed that the most highly induced gene in XH001 was an *lsrB* ortholog, which encodes a putative periplasmic binding protein for the auto inducer (AI)-2 QS signaling molecule. Further genomic analyses suggested the *lsrB* operon in XH001 is a putative hybrid AI-2/ribose transport operon as well as the existence of a *luxS* ortholog, which encodes the AI-2 synthase. In this study, the potential role of AI-2 QS in the epibiotic-parasitic relationship between XH001 and TM7x in the context of biofilm formation was investigated. A genetic system for XH001 was developed to generate *lsrB* and *luxS* gene deletion mutants in XH001. Phenotypic characterization demonstrated that deletion mutations in either *lsrB* or *luxS* did not affect XH001's growth dynamic, mono-species biofilm formation capability, nor its ability to associate with TM7x. TM7x association with XH001 induced *lsrB* gene expression in a *luxS*-dependent manner. Intriguingly, unlike wild type XH001, which displayed significantly increased biofilm formation upon establishing the epibiotic-parasitic relationship with TM7x, XH001Δ*lsrB*, and XH001Δ*luxS* mutants failed to achieve enhanced biofilm formation when associated with TM7x. In conclusion, we demonstrated a significant role for AI-2 QS in modulating dual-species biofilm formation when XH001 and TM7x establish their epibiotic-parasitic relationship.

29

Introduction

One of the greatest scientific revelations in recent history was the discovery of the enormous diversity and large abundance of microbes associated with the human body. These microbial communities co-evolve with humans and have important roles in health and disease. However, only a limited proportion of these microbial species can be cultured and studied *in vitro*, an observation known as the "Great Plate Anomaly," (Staley et al. 1985, Rappé et al. 2003). Recently, a unique and intimate association between two oral bacterial isolates from different phyla, a *Nanosynbacter lyticus* Type Strain TM7x HMT-952 (TM7x) , a member of the Saccharibacteria/TM7 phylum that has an ultra-small cell size (McLean et al. 2018), and an *Actinomyces odontolyticus* subspecies *actinosynbacter* strain "XH001", was discovered (He et al. 2015, McLean et al. 2016). Co-isolation of these strains revealed TM7x to be an obligate epibiotic parasite, which lives on the surface of its bacterial host, XH001. This interbacterial interaction represents a novel relationship in the bacterial kingdom yet to be characterized on a molecular level. Importantly, TM7x is the only cultivated member to date of the recently discovered Candidate Phyla Radiation (CPR) (Hug et al. 2016) organisms that could account for upwards of 26% of domain bacteria (Brown et al. 2015, Castelle et al. 2018). Overlapping characteristics between the phyla comprising of the CPR organisms include reduced genomes, lack of the biosynthetic capacity for most amino acids, as well as ultra-small cell morphological sizes inferred from representatives of the WWE3, OP11 and OD1 phyla, which are capable of passing through 0.2 μm sized filters (Luef et al. 2015). This suggests that a proportion of other CPR representatives may exist in epibiotic-parasitic relationships comparable to TM7x with XH001. Therefore, it is imperative to characterize this interaction on a molecular level to uncover important knowledge for studying other 'yet-to-be cultivated' CPR bacterial species.

As early colonizers, *Actinomyces* species contribute to oral microbial biofilm formation along with *Streptococci* (Nyvad et al. 1987, Nyvad et al. 1990, Diaz et al. 2006, Dige et al. 2007, Dige et al. 2009, Dige et al. 2009, Ding et al. 2010) and are associated with several human diseases including actinomycosis, periodontitis, oral carcinoma, and childhood caries (Nagy et al. 1998, Smego Jr et al. 1998, Becker et al. 2002, Aas et al. 2005, Colombo et al. 2006, Kanasi et al. 2010, Ling et al. 2010, Sato et al. 2012). Similarly, Saccharibacteria members are implicated in several human inflammatory-mucosal diseases, such as inflammatory bowel disease, periodontitis, and vaginosis (Paster et al. 2001, Fredricks et al. 2005, Kuehbacher et al. 2008, Kianoush et al. 2014, Soro et al. 2014). Saccharibacteria phylum members are particularly prevalent in the oral community in a low abundance of ~1% in the health-associated oral microbial community, with an increase up to 21% in patients with various types of periodontitis (Paster et al. 2002, Brinig et al. 2003, Kumar et al. 2003, Rylev et al. 2011, Liu et al. 2012). Furthermore, certain oral Saccharibacteria phylotypes are detected on or within mammalian host crevicular epithelial cells, a hallmark indicator of bacterial pathogenesis in periodontal disease (Paster et al. 2002). Our initial characterization allowed the first glimpse into the epibiotic-parasitic nature of TM7x when associated with XH001, which induces reciprocal morphological changes in XH001 and TM7x as well as differential gene expression patterns in XH001 (He et al. 2015, Bor et al. 2016). Interestingly, association with TM7x repressed the XH001-induced TNF-α mRNA expression in macrophages, implying that TM7x may either mask surface protein expression in XH001 required for induction of TNF-α by macrophages or directly suppress TNF-α expression in macrophages (He et al. 2015). This intriguing relationship provides an ideal model for unraveling the underpinnings of the epibiotic-parasitic relationship, and its ecological function in the oral microbiome, as well as the role in oral health and disease.

Our recent transcriptomic profiling (He et al. 2015) revealed that during association of XH001 with TM7x, the most highly induced XH001 gene is an *lsrB* ortholog, which encodes a putative

periplasmic binding protein for the auto inducer (AI)-2 quorum sensing (QS) signaling molecule. Despite numerous species identified to produce the AI-2 signal (Kolenbrander et al. 2010), only three types of AI-2 receptors have been characterized in detail. These include LuxP [*Vibrio harveyi*], LsrB [*Salmonella enterica* serovar Typhimurium str. 14028, *Escherichia coli* MG1655*, Sinorhizobium meliloti*, and *Aggregatibacter actinomycetecommitans* HK1651], and RbsB [*Aggregatibacter actinomycetecommitans* HK1651] (Bassler et al. 1994, Taga et al. 2001, Taga et al. 2003, Xavier et al. 2005, Shao et al. 2007, Shao et al. 2007, Pereira et al. 2008). AI-2 production has been reported in the literature to be regulated in a positive feedback loop: as AI-2 is transported into the cell in a cell density-depended manner, *luxS* expression is up-regulated, leading to increased production of AI-2 to achieve quorum followed by rapid internalization during stationary phase to activate the QS operon and downstream regulated genes (Taga et al. 2001, Taga et al. 2003, Wang et al. 2005). In addition to mediating multispecies biofilm formation (Bassler et al. 1997) in the oral cavity (Rickard et al. 2006, Periasamy et al. 2009, Kolenbrander et al. 2010), AI-2 QS has also been widely shown to regulate genes controlling virulence factor production, particularly in commensal and pathogenic bacteria, including oral representatives such as *Porphyromonas gingivalis* (Chung et al. 2001, Burgess et al. 2002), *A. actinomycetecommitans* (Fong et al. 2001, Fong et al. 2003), *Streptococcus intermedius* (Pecharki et al. 2008, Ahmed et al. 2009), *Streptococcus mutans* (Merritt et al. 2003, Merritt et al. 2005), and *Streptococcus gordonii* (McNab et al. 2003). In this study, the role of AI-2 QS in the epibiotic-parasitic relationship between TM7x and XH001 was investigated.

Materials and Methods

Bacterial Strains, Plasmids, and Media.

All bacterial strains and plasmids used in this study and their characteristics are listed in Table 1. TM7x associated *Actinomyces odontolyticus* subspecies *actinosynbacter* strain XH001, XH001*ΔlsrB*, and XH001*ΔluxS* and as monospecies were incubated in Brain-Heart Infusion (BHI) broth or agar (Difco laboratories, Detroit, Michigan) at 37°C in microaerophilic conditions (2% O_2, 5% CO_2, balanced with Nitrogen) using a Whitely Workstation A35 (Microbiology International). All monoculture XH001, XH001*ΔlsrB*, and XH001*ΔluxS* were infected with TM7x using an established protocol (He et al. 2015)**.** Media were supplemented with 150 μg/mL kanamycin sulfate (Fischer Bioreagents, Hampton, NH) for antibiotic selection when appropriate. Positive and negative *V. harveyi* control strains, BB152 and MM77, respectively, used in the GC-MS analysis of AI-2 were grown in Auto Inducer Bioassay medium (AB) for ~14 hours shaking (215 rpm) at 30°C as described in an established protocol (Greenberg et al. 1979, Taga et al. 2005).

Genetic and Molecular Phylogenetic Analyses of the LsrB and LuxS orthologs in XH001.

The closed annotated XH001 genome (accession no. LLVT00000000-the version described in this paper is version LLVT00000000.1.) was previously published (McLean et al. 2016) and provided the predicted protein sequences used in the NCBI-Blastp, NCBI Conserved Domain Database (Marchler-Bauer et al. 2010, Marchler-Bauer et al. 2014, Marchler-Bauer et al. 2016), and PHYRE2 (Kelley et al. 2009) analyses. Protein sequence alignment and phylogenetic analyses (construct via maximum-likelihood method) were conducted using the ClustalW Omega alignment method through MEGA7 software (Jones et al. 1992, Sievers et al. 2011,

Kumar et al. 2016). The LsrB, RbsB, and LuxS protein accession numbers are listed in Supplementary Table 2.

PCR, Cloning and Single Chromosomal Deletion Construct Development.

The shuttle vector, pJRD215 (Davison et al. 1987, Yeung et al. 1994) was isolated using QIAprep Spin Miniprep kit (Qiagen Cat. No./ID 27104). All primers were designed (Integrated DNA Technologies, Inc., Coralville, IA) based upon the sequence data from the published XH001 genome via Primer3 software (Koressaar et al. 2007, Untergasser et al. 2012) and are listed in Supplementary Table 1. The chromosomal gene deletion constructs were generated using a modified protocol of fusion PCR as described (Shevchuk et al. 2004):

The respective 0.8 kb up/downstream fragments of the *lsrB* and *luxS* genes, as well as the kanamycin gene resistance cassette of pJDR215, were PCR-amplified according to the schematic depicted in Supplementary Figure 2 using the corresponding primers listed in Supplementary Table 1. These fragments were combined in a subsequent fusion reaction in which the overlapping ends annealed. The resulting product was subjected to a final PCR amplification using the manufacturer's protocol for the Phusion Hi-Fidelity PCR Master Mix with GC Buffer (New England Biolabs) DNA polymerase generating a 2.8 kb construct.

After generating the linear gene deletion construct fragments, they were isolated via gel extraction using the QIAquick Gel Extraction kit (Qiagen, Hilden Germany) following the manufacturer's instructions and purified using DNA Clean Concentrator Kit (Zymo Research DNA Clean Concentrator Cat No./ID D4013). Using the manufacturer's protocol for the Phusion Hi-Fidelity PCR Master Mix with GC Buffer, PCR amplification of the resulting full *lsrB* and *luxS* gene deletion constructs were amplified using primers 1 and 6 and 7 and 12, respectively (Supplementary Figure 2) was used to generate sufficient product prior to transformation.

RNA Isolation and cDNA Synthesis.

RNA isolation and cDNA synthesis protocols were performed as previously reported (Bor et al. 2016) with the following modifications: cells were harvested from a 50 mL culture in BHI under 2% microaerophilic conditions after 18 hours of incubation. Cells were collected by centrifugation at 4600 rpm for 10 minutes. Prior to RNA isolation, cell pellets were treated for RNA stabilization with RNA protect Cell Reagent (Qiagen, Cat. No./ID 76526). Total RNA was isolated using RNeasy Protect Bacteria Mini Kit (Qiagen, Cat No./ID: 74524) following the manufacturers protocol. RNA Clean Concentrator Kit (Zymo Research RNA Clean Concentrator Cat. No./ID R1015) was applied for terminal purification of the RNA.

Quantitative Real Time PCR Analysis.

Quantitative real-time PCR (qRT-PCR) analysis was performed using an established protocol (Bor et al. 2016) with the following modifications: the GeneCopoeia All-in-One qPCR mix (GeneCopoeia, Inc., Rockville, MD) was used and the final qRT-PCR mixture (20 µL) contained 10XGeneCopoeia All in One mix, 1 µg cDNA, and 10 µM of the appropriate forward and reverse qRT-PCR primers designed for the *lsrB* gene (Supplementary Table 1). To calculate the relative *lsrB* expression, we used a previously developed protocol (Bor et al. 2016). qRT-PCR analysis of *lsrB* expression was evaluated using *lsrB* primers specific to XH001 (XH001 *lsrB* F and XH001 *lsrB* R) and the relative fold expression of *lsrB* was calculated in reference to the expression of the 16S gene in XH001 using primers specific to the XH001 16S rRNA gene (F5, R3) (Supplementary Table 1) described in a previous study (Bor et al. 2016). The sequence of the *lsrB* gene was verifiably absent in the TM7x genome as confirmed via PCR and sequencing (data not shown). Each assay was performed with at least two independent RNA samples in triplicate. One-way ANOVA analysis was used to compare all monoculture and co-culture

groups separately for differences in expression rates of *lsrB*. T-test statistical analysis was applied for pairwise comparisons between expression rates of *lsrB* between XH001 and TM7x-associated XH001, TM7x-associated XH001 and TM7x-associated XH001*ΔlsrB*, TM7x-associated XH001 and TM7x-associated XH001*ΔluxS*.

Electrocompetent Cell Preparation, Transformation Procedure, and Mutant Verification.

Fresh competent cells were prepared using a previously described protocol (Yeung et al. 1994) with the following modifications: Inoculation of 30 µL of XH001 stock into 2 mL of reduced BHI (2% 0_2). After overnight incubation, cell cultures were diluted 1:10 into 20 mL of fresh BHI. After an additional overnight incubation, cultures were inoculated into 100 mL of fresh BHI to a starting optical density of 0.1 OD_{600}. After incubation for 5-8 hours early exponential phase cells were harvested (between 0.2-0.3 OD_{600}). The 100 mL culture was split into 50 mL cultures, chilled for 1.5 hours, and centrifuged for 10 min at 4600 rpm in a 4°C refrigerated Sorvall Legend RT centrifuge (Sorvall (UK) Ltd., Thermo Fischer Scientific). Harvested cells were washed twice with ice cold $_{dd}H_20$ and once with 10% glycerol. The washed XH001 cells were resuspended in 10% glycerol (5 X 10^8 cells/mL) and were transformed with pJRD215 as described (Yeung et al. 1994) to demonstrate transformability and expression of the kanamycin cassette in the XH001 background. To generate *lsrB* and *luxS* gene deletion mutants, 1µg of *lsrB* and *luxS* gene deletion constructs (DNA) was separately added to different XH001 electrocompetent culture suspensions. Transformation was facilitated using chilled 0.2-mm Fischerbrand electroporation cuvettes (Fischer Scientific, Hampton, NH, Cat. No./ID FB102). The following electroporation settings were used: the electroporation was carried out using a Bio-Rad Gene Pulser II with the capacitance set to 25 µF, 2.5 kV, and resistance set to 400 ohms in parallel. The pulsed cells were diluted with reduced, 37°C BHI medium, and recovered for 3 hours by incubation in 1 mL of Brain-Heart Infusion (BHI) at 37°C in microaerophilic

conditions (2% O_2, 5% CO_2, balanced with Nitrogen) using a Whitely Workstation A35 (Microbiology International). After recovery, the 1.1 mL culture cells were centrifuged for 10 min at 4600 RPM and resuspended in 200 μL of fresh, reduced, 37°C BHI media, and plated. XH001 transformants were selected using 150 μg/mL kanamycin sulfate on BHI agar plates for up to 6 days. Un-pulsed electrocompetent cells or electrocompetent cells without transformable DNA were used as controls. No transformants were obtained without electric pulse or absence of transformable DNA.

XH001Δ*lsrB* and XH001Δ*luxS* mutants were confirmed via DNA sequencing (Laragen, Inc, Culver City, CA): briefly, in the putative XH001Δ*lsrB* and XH001Δ*luxS* mutant backgrounds and wild type XH001, PCR amplification of gDNA, upstream and downstream of the transcriptional start site in the target genes (approximately 500 bp amplicon), determined the presence or absence of the kanamycin resistance cassette in the correct locus. Primers 13/14 and 17/18 were used to amplify a ~500bp amplicon from XH001Δ*lsrB* and XH001Δ*luxS* gDNA, respectively using the manufacturer's protocol for the Phusion Hi-Fidelity PCR Master Mix with GC Buffer. Primers 15/16 and 19/20 were used to amplify a ~450-500 bp amplicon of overlapping sequences of the *lsrB* and *luxS* genes, respectively, from XH001 gDNA. XH001Δ*lsrB* and XH001Δ*luxS* were tested for lack of full mRNA transcript production to further verify true chromosomal deletion. Thus, primers 21/22 and 23/24 were designed to amplify the entire *lsrB* and *luxS* genes, respectively. Transcripts were absent in the XH001Δ*lsrB* and XH001Δ*luxS* background, but present in XH001. An annealing temperature of 58°C was used for all reactions and the PCR cycling parameters were identical except for the annealing temperature used to evaluate XH001Δ*luxS* transcript production, which was set to 57°C for primers 19/20.

Growth Kinetics and Generation time.

 XH001, XH001*ΔlsrB*, and XH001*ΔluxS* as monospecies and associated with TM7x were incubated at 37°C in microaerophilic conditions using a Whitely Workstation A35 (Microbiology International) for growth kinetics analyses using the BioSense Solutions (Farum, Demark) oCelloScope platform (CVR/VAT: 38602926). Wild type XH001, XH001*ΔlsrB*, and XH001*ΔluxS* were started at 0.05 OD_{600} in a final volume of 250µL in a Corning clear 96 well plate (Corning, Corning, NY). Three independent cultures were each grown in triplicate in two separate experiments. Time course measurements for Background Corrected Absorbance (BCA units), occurred every 30 min for 24 hrs. The BCA unit output was analyzed by growth kinetic algorithms based upon the measurement of light absorption, which is determined to be more robust and sensitive when compared to traditional optical density methods (Canali et al. 2018). The BCA value was calculated as $\mathrm{BCA\ value} = \log 10(\sum(object\ pixel\ intensities))$. Generation times and maximum optical density were calculated from these data. One-way ANOVA analysis was used to compare all monoculture groups separately for differences in generation time.

Phase Contrast Imaging and Confocal Laser Scanning Microscopy (CLSM) Imaging of Biofilm Formation.

After the established infection assay (He et al. 2015, Bor et al. 2016) was conducted to generate TM7x-associated XH001, XH001*ΔlsrB* and XH001*ΔluxS* co-cultures, representative phase contrast images were acquired using previously reported parameters (Bor et al. 2016) to capture the nascent TM7x infection of XH001, XH001*ΔlsrB* and XH001*ΔluxS* for evaluation of TM7x infectivity. TM7x-associated XH001, XH001*ΔlsrB* and XH001*ΔluxS* and as monospecies, were cultured associated with TM7x and without in sterile, µ-slide 4 well plastic bottom slide (Ibidi, Martinsried, Germany) for 24 hours with a starting OD_{600} of 0.25 prior to analysis. After removal of the supernatant and planktonic cells, the biofilms were stained with 600 µL of sterile

SYTO 9 (1:1000 diluted in PBS) solution and visualized with scanning confocal laser microscopy (Zeiss LSM 880, Oberkochen, Germany) using an Argon laser. The Zeiss parameters for image acquisition included a Z-slice thickness of 0.350-0.700µM and a plan-apochromat 63X (N.A = 1.4) objective under oil immersion. Z-stacks were imaged with a 488nm laser line, 488 nm beam splitter, and a wavelength detection range of 503-547 nm. Images were reconstructed using Bitplane: Imaris-Microscopy Image Analysis Software (Bitplane, an Oxford instruments company, Belfast, United Kingdom). Reconstructed images resulted in horizontal (xy) and sagittal (xz) views of the imaged biofilms.

Quantification of Biofilm Maximal Thickness (Height), Biovolume, Biofilm Roughness Correlation (Variance), and Biofilm Continuity Ratio.

Imaris (Bitplane, Belfast, United Kingdom) biofilm analysis XTension software was used to obtain maximal biovolume thickness (height), biovolume, biofilm roughness correlation (variance), and the biofilm continuity ratio. Biovolume thickness measures from the top of the surface to the base (substratum) and includes all gaps present in the reconstructed surface. Biovolume was obtained by measuring the volume of all surface objects (cubic micrometers). The compactness of the biofilm was assessed as total fluorescence per volume of biofilm (Ghafoor et al. 2011). Roughness coefficient (variance) was the measure of the variability of the localized thicknesses relative to the total mean thickness (defining the structured smoothness of the biofilm). The output data resulted from the roughness correlation formula:

$$roughness\ coefficient\ (variance) = \sqrt{\frac{sum((local\ thickness-overall\ thickness)2)}{Number\ of\ local\ thickness\ measurements}}.$$ Biofilm roughness

coefficient = 0, suggested a perfect uniformly thick surface. The larger this variance, the more uneven the surface object was considered. The larger the variance, the rougher a biofilm was considered. Biofilm continuity ratio was a dimensionless coefficient that measured the continuity of the reconstructed surface. It was measured by taking mean surface mask thickness divided

by the mean biovolume thickness. A value of "1" represented perfect continuity throughout the Z-stack. Values less than one were used to define how many gaps (holes) there were in the surface reconstruction. Surface mask thickness quantifies only those voxels in vertical column that lie inside the reconstructed 3D volume. If there were gaps in the rendering, they were not included in the thickness measure. One-way ANOVA analysis was used to compare all monoculture and co-culture groups separately applied for evaluating differences in maximal biovolume thickness (height), biovolume, biofilm roughness correlation (variance), and biofilm continuity ratio. One-way ANOVA analysis was used to compare all monoculture groups separately for differences in maximal biovolume thickness (height), biovolume, biofilm roughness correlation (variance), and biofilm continuity ratio. T-test statistical analysis was applied for pairwise comparisons of maximal biovolume thickness (height), biovolume, biofilm roughness correlation (variance), and biofilm continuity ratio between XH001 and TM7x-associated XH001, TM7x-associated XH001 and TM7x-associated XH001*ΔlsrB*, TM7x-associated XH001 and TM7x-associated XH001*ΔluxS*. Non-associated XH001, XH001*ΔlsrB,* and XH001*ΔluxS* were evaluated and compared via one-way ANOVA to ensure no intrinsic differences were attributed to the *lsrB* or *luxS* mutations.

Gas Chromatography-Mass Spectrometry Analysis of (S)-4,5-Dihydroxy-2,3-pentanedione (DPD), AI-2.

TM7x-associated XH001, XH001*ΔlsrB*, and XH001*ΔluxS* or the respective monocultures were grown as indicated above for 18 hours (starting at 0.1 OD_{600}) using 5 mL cultures. To prepare cultures for the (S)-4,5-Dihydroxy-2,3-pentandione (DPD, AI-2) analysis, a previous published protocol was used with the following modifications (Thiel et al. 2009): cultures were centrifuged at 4600xg for 10 min and the supernatant was harvested and filter-sterilized with Millipore Millex 0.22 µM sterile syringe filters. One mL aliquots of supernatant were added to 500 µL of 100 mM

Potassium Phosphate buffer (pH 7.2) in glass test tubes. Samples were exposed to solid, 2 mg of 1,2 phenylenediamine (in excess) incubated at room temperature for two hours (vortexing every 20 min) derivatizing DPD to quinoxalinediol. After derivatization, quinoxalinediol-d4 (deuterated-quinoxalinediol) serving as the internal standard, was added to a final concentration of 250 ng/mL using a Hamilton 5 µL Model 75 glass syringe-32 gauge, 2 inch, point style 3 (Hamilton, Reno, NV). Samples were manually homogenized using sterile, disposable, Fischer brand borosilicate glass (Fischer Scientific, Hampton, NH) Pasteur pipets (Cat. No 22-183632). One mL of dichloromethane (DCM) was added and homogenized. Samples were centrifuged at 4600xg for 5 minutes to fully separate DCM and H_2O layer. The DCM layer was harvested through manual liquid/liquid extraction. Samples were then dried under soft flow of nitrogen gas for 1 hour at room temperature. 80 µL of N-Methyl-N-(trimethylsilyl)trifuoroacetamide (Cat. No. M7891 CAS No. 24589-78-4) was added to dried samples and incubated in a 65°C water bath for 30 min. After this silylation and terminal derivatization, the samples were analyzed for S-DPD concentration. In addition, the positive and negative controls, BB152 and MM77, respectively, were prepared similarly. Each sample was vortex GC-MS measurements were carried out using an Agilent Model 7683 Autosampler (Agilent Technologies, Inc., Santa Clara, CA), 6890 Gas Chromatograph, and 5975 Inert Mass Selective Detector in the Electron Impact (EI) mode. Sample injection was carried out in splitless mode with a 2 min purge, and inlet temperature set to 280°C. Separation was carried out on an Agilent HP5-MS column with dimensions 30m x 250 µm x 0.25 µm. Ultra High Purity Grade He (Airgas, Radnor, PA) was used as carrier gas with the flow set to 0.9 mL/min in constant flow mode. The initial oven temperature was set to 100°C for 3 min followed by a 25°C/min ramp to a final temperature of 300°C which was maintained for 4 min. A 3.2 min solvent delay was used. EI energy was set to 70 eV. The MSD Enhanced Chemstation software (Agilent) was set to scan the 40 - 600 m/z range. Data collection and analysis were performed using GC/MSD Chemstation Software

41

(Agilent). S-DPD abundance was determined by measuring the area under the extracted ion traces for m/z 245 and 348 for the derivatized S-DPD, and m/z 249 and 352 for the deuterated standard. Measured S-DPD abundance values were normalized to those of the deuterated internal standard in each sample and OD_{600}. Absolute concentration values were determined using an external standard calibration curve in the range 25-250μg/mL. No carryover was detected using MSTFA-TMCS blanks. Interpolation of DPD, AI-2 concentration was confirmed via reproducibility in derivatization of DPD external standards used in absolute quantification (Supplementary Figure 4 and 5). T-test statistical analysis was applied for pairwise comparisons of differences in DPD, AI-2 production between XH001 and TM7x-associated XH001, TM7x-associated XH001 and TM7x-associated XH001*ΔlsrB*, TM7x-associated XH001 and TM7x-associated XH001*ΔluxS*.

Results

XH001 Encodes a *lsrB* and a *luxS* Ortholog.

Our recent transcriptomic analysis revealed the upregulation of more than 70 XH001 genes in excess of threefold when XH001 was physically associated with TM7x (He et al. 2015). APY09_02520, the first gene in a six-gene operon (Supplementary Figure 1), was most highly upregulated (~20-fold), while the remaining genes in the same operon ranged from two to fivefold increase in transcription. NCBI-Blastp analysis annotated the predicted APY09_02520-encoded protein as an ortholog of LsrB, the receptor for binding the AI-2 QS molecule. Additionally, PHYRE 3-D structure folding analyses indicated the best hit in functional prediction of APY09_02520 as a putative AI-2 receptor (Supplementary Document 1). Thus, gene APY09_02520 was annotated as *lsrB* ortholog. However, contrary to the PHYRE analysis, protein sequence alignment revealed that XH001 LsrB shared low sequence identity to known representative LsrB species in *S. typhimurium* 14028 (23%), *E. coli* K-12 (26%), and *A. actinomycetecomitans* HK1651 (25%). Among the six proposed conserved amino acid residues (K35, D116, D166, Q167, P220, and A222) for identifying LsrB-like orthologs (Pereira et al. 2009), which are predicted to form hydrogen bonds with [(2*R*,4*S*)-2-methyl-2,3,3,4-tetrahydroxytetrahydrofuran (*R*THMF)], the AI-2 signaling molecule bound by the LsrB periplasmic binding protein in *S. typhimurium* (Miller et al. 2004), only Lysine at position 35 was identified in XH001 via protein sequence alignment (Figure 1A). To reconcile predictions from the two analysis methods, phylogenetic analyses, however, showed that XH001 LsrB is more evolutionarily related to AI-2 binding proteins, including LuxP, LsrB and RbsB, identified in *V. harveyi, S. typhimurium* 14028 as well as *E. coli*, and *A. actinomycetecommitans*, respectively (Figure 1B). Downstream of *lsrB*, the order of predicted genes within the same operon

43

(Supplementary Figure 1) is as follows: *rbsA* (encoding Ribose ABC Transporter, ATP binding cassette), two *rbsC* (encoding Ribose ABC Transporter, permease protein) structural genes, and *dak1* gene that form a functional putative dihydroxy acetone kinase. Upstream of the putative *lsrB* ortholog, in the reverse direction, is annotated as a putative DeoR family transcriptional regulator for rhamnose utilization.

In addition to identifying the *lsrB* ortholog, genome analyses revealed that the XH001 genome also contains an ortholog of the AI-2 synthase encoding *luxS*. Protein sequence analysis was employed to locate and confirm the previously determined requisite conserved amino acid residues (H, H, and C) that constitute the catalytic center of the LuxS protein and coordinate the Zn^{2+} ion (Figure 1C) (Hilgers et al. 2001). Phylogenetic analyses also determined its evolutionary relationship to other representative LuxS protein species (Figure 1D).

Genetic System Development in XH001.

Prior to this study, no genetic tools have been developed for either XH001 or TM7x. Since TM7x can currently not be cultivated in the absence of its XH001 host, which presents a major obstacle for genetic system development, we focused on XH001 instead. A genetic system was established for XH001 by adapting previous work by Yeung and colleagues on transformation of *Actinomyces* species (Yeung et al. 1994, Yeung 1995, Yeung et al. 1997, Kolenbrander 2000). To demonstrate transformability of XH001, pJRD215, a known broad-host range expression vector used in genetic studies of other closely-related *Actinomyces* species, was electroporated into XH001 with similar transformation efficiencies previously reported in other *Actinomyces* species (Yeung et al. 1994, Yeung 1995). Utilizing the Km^R cassette, present in the pJRD215 plasmid, a chromosomal gene deletion construct was generated (see methods) to inactivate the *lsrB* and *luxS* genes in XH001 via homologous recombination (Supplementary Figure 2). Using a

modified electroporation protocol, *lsrB (*XH001*ΔlsrB)* and *luxS (*XH001*ΔluxS)* gene deletion mutants were generated, albeit with low efficiencies compared to previous reports in other *Actinomyces* species (Yeung 1995), which demonstrated that XH001 is genetically tractable. Gene deletion mutants were plated on kanamycin selective plates and were confirmed through sequencing. No growth defect was detected in either of the XH001*ΔlsrB* and XH001*ΔluxS* mutant backgrounds compared to wild type XH001 (Figure 2). Furthermore, neither XH001*ΔlsrB* nor XH001*ΔluxS* mutants displayed a discernable defect in TM7x association (Supplementary Figure 3) when tested using the established TM7x infection assay (He et al. 2015)

TM7x Association Upregulates the Expression of *lsrB* in XH001 in a *luxS*-Dependent Manner.

qRT-PCR analysis was used to quantify *lsrB* expression in the newly constructed mutant strains. TM7-associated XH001*ΔlsrB* and XH001*ΔlsrB* monoculture produced no *lsrB* transcripts as expected (Figure 3). Moreover, these results validated the initial transcriptomic profile, which revealed a statistically significant, 4.7-fold increase in *lsrB* expression in the TM7x-associated XH001 background compared to XH001 monoculture. Interestingly, while XH001*ΔluxS* displayed similar *lsrB* expression level as the XH001, the association of TM7x failed to induce enhanced *lsrB* expression, suggesting that TM7x-induced *lsrB* upregulation required the presence of *luxS* in XH001.

Quantification of the AI-2 signaling Molecule via GC-MS

It was of high interest to determine if XH001 indeed produces the AI-2 signaling molecule in a *luxS* dependent manner. GC-MS was employed to quantify DPD (Thiel et al. 2009), the precursor that randomly cyclizes into the group of equilibrium-connected isomers exclusively known as AI-

45

2 autoinducers (Chen et al. 2002, Xavier et al. 2007), in the cell-free supernatants of XH001,

XH001*ΔlsrB* and XH001*ΔluxS* as monoculture, as well as their respective cocultures associated

with TM7x. GC-MS quantification revealed that similar concentrations (~1.1 µm) of DPD, were

detected in the supernatant of both XH001 and XH001*ΔlsrB*, in monoculture and in TM7x-

associated states, in quantities lower than an AI-2 signal-producing positive control, BB157, a

Vibrio harveyi strain (Figure 4). Meanwhile, the *luxS* deletion resulted in abrogated DPD

production independent of TM7x-association (Figure 4).

Association of TM7x Enhances XH001 Biofilm Formation in a *lsrB* and *luxS*-Dependent Manner.

AI-2 QS is widely studied and implicated as a universal signaling molecule in interspecies

communication during multispecies oral biofilm development and in relation to the oral cavity

influencing dental caries formation and periodontitis (Kolenbrander 1997, Frias et al. 2001,

Palmer Jr et al. 2003, Kolenbrander et al. 2010). To testwhether the XH001 encoded AI-2 QS

system is involved in dual-species biofilm formation comprising of XH001 and its parasitic

epibiont, TM7x, CLSM was utilized to visualize biofilm formation of XH001 wildtype, *ΔlsrB* and

ΔluxS mutant monocultures, as well as their respective co-cultures with TM7x. Confocal analyis

showed that TM7x-associated XH001 formed a significantly thicker biofilm in height (31.79 µm)

relative to XH001 (19.31 µm) as monospecies. Moreover, while XH001*ΔlsrB* (18.77 µm) and

XH001*ΔluxS* (20.11 µm) did not display a biofilm deficit relative to XH001 wildtype (19.31 µm)

as monoculture, the association with TM7x failed to enhance biofilm formation in the *lsrB* (22.01

µm) and *luxS* (20.28 µm) mutant background (Figure 5, Figure 6A). Quantitative measurement

further evaluated the biovolume, biofilm roughness correlation, and biofilm continuity ratio to

demonstrated that TM7x induction of biofilm formation enhancement was present in the XH001

background, but not in the *lsrB* and *luxS* mutant backgrounds (Figure 6B-D). Specifically, TM7x-associated XH001 showed consistently an apparent higher biovolume (12.74 µm^3), albeit this was not-statistically significant (p=0.076), than XH001 monoculture (6.25 µm^3) (Figure 6B). Meanwhile, biofilm of TM7x-associated XH001 displayed significantly higher biovolume compared to that of TM7x-assocated *lsrB* or *luxS* mutant (Figure B). Furthermore, we observed a statistically significant increase in roughness correlation (structured smoothness of the biofilm) (p<0.0001) in the TM7x-associated XH001 coculture background compared with XH001 as monoculture, while no such increase was observed in *lsrB* and *luxS* mutant backgrounds (Figure 6A and C). No statistically significant change in biofilm continuity ratio between any of the groups was observed (Figure 6D).

Discussion

Epibiotic-parasitic lifestyles are predicted to be widespread among the recently discovered CPR group of ultra-small bacteria. The co-isolation and co-cultivation of TM7x, with its bacterial host, *Actinomyces odontolytics* subspecies *actinosynbacter* strain, XH001, has enabled the first characterization of a living TM7 organism, as well as the relationship between the two bacterial species Our genetic and phenotypic analyses presented here strongly indicate an important role for the XH001 AI-2 QS system in modulating the epibiotic-parasitic relationship between XH001 and TM7x. Targeted transcriptional analysis via qRT-PCR in this study confirmed our prior findings that TM7x association triggered significant induction of gene APY09_02520 in XH001. Despite sharing low amino acid sequence identity to known LsrB species, NCBI Conserved Domain Structure Search, PHYRE2 as well as phylogenetic analysis all predicted that APY09_02520 encodes a putative LsrB ortholog which likely functions as receptor for the AI-2 signaling molecule. Thus, gene APY09_02520 was designated as a *lsrB* ortholog. NCBI-Blastp and protein sequence alignment analyses also revealed the presence of a *luxS* ortholog (Figure 1), the AI-2 QS signaling molecule synthase, in the XH001 genome. The *luxS* in XH001 was confirmed as an AI-2 synthase by GC-MS quantification, when a *luxS* deletion resulted in abrogated AI-2 signal production (Figure 4). These data, along with the observation that TM7x association induced up-regulation of *lsrB* was dependent on *luxS* (Figure 3), strongly suggested that AI-2 QS is involved in XH001 and TM7x association. Furthermore, deletion of *luxS* significantly reduced the TM7x-association induced biofilm enhancement in XH001, suggesting that AI-2 QS is involved in regulating dual-species biofilm formation between XH001 and TM7x (Figure 5 and 6). Additional data supporting that *lsrB* is an AI-2 receptor and part of the AI-2 QS system was indicated by the requirement of both *lsrB* and *luxS* genes for TM7x association induced biofilm enhancement in wildtype (Figure 6).

48

AI-2 signaling is well documented in regulating many bacterial interspecies interactions during biofilm formation, particularly in the oral cavity (Cuadra-Saenz et al. 2012). The development of these multispecies biofilms involves close physical interactions between bacteria and results in an intricate structural hierarchy enabling a complex avenue of bacterial communication, ultimately affecting the diffusible signal exchange efficiency (Kolenbrander et al. 2010). For example, oral *Streptococci* and *Actinomyces* are known to co-aggregate *in vitro* and in the natural environment being among the first to colonize the enamel by binding to the salivary pellicle. *Streptococcus oralis 34* and *Actinomyces naeslundii* T14V are incapable of forming monoculture biofilms, but form robust dual species biofilms when coaggregated (Palmer Jr et al. 2003), which are mediated through *luxS* expression encoded in *S. oralis* (Rickard et al. 2006). Thus, the abolished increased dual-species biofilm formation observed in TM7x-associated XH001Δ*luxS* relative to TM7x-associated XH001 is consistent with previous reports.

Our bioinformatic analysis suggested that the QS system in XH001 is unlikely a canonical AI-2 signaling system. Previously, organisms with *lsrB*-like orthologs have been organized into two groups: >60% *lsrB* protein sequence identity, a complete set of orthologs to the *lsr* genes, and presence of the six conserved amino acid residues in the binding pocket were considered a Group I member. If organisms are missing two or more orthologs to the *lsr* genes as well as at least two of the 6 residues of the AI-2 binding pocket, and exhibit <60% protein sequence identity to LsrB in *S. typhimurium*, they were placed in Group II and not considered to have true AI-2 receptors (Pereira et al. 2009). The following bioinformatic criteria were established for determining potential *lsrB*-like orthologs: six conserved amino acid residues (K35, D116, D166, Q167, P220, and A222) were predicted to form hydrogen bonds with the AI-2 signaling molecule bound by the LsrB periplasmic binding protein in *S. typhimurium* (Miller et al. 2004, Pereira et al.

2009). Specifically, of the six residues (K35, D116, D166, Q167, P220, and A222), aspartate 166 and alanine 222 residues were determined to be required for AI-2 binding (Pereira et al. 2009). The LsrB protein in XH001 lacks aspartate 166 and alanine 222, but the K35, Lysine, is conserved.

Importantly, within the top 10 hits generated by PHYRE 3-D structure folding analysis of LsrB, the second was listed as putative ribose receptor, RbsB (Supplementary Document 1) and coupled with the presence of an intact ribose ABC transporter machinery downstream of *lsrB* in XH001 indicated that the XH001 *lsrB* operon could also be involved in ribose transport. Interestingly, it has been shown that the ribose substrate binding protein, RbsB in *A. actinomycetecomitans* HK1651 has binding affinity, albeit lower than LsrB, for AI-2 (James et al. 2006) and may facilitate the internalization of AI-2 (Shao et al. 2007). Furthermore, ribose has also been shown to inhibit AI-2 internalization by competitive inhibition of AI-2 binding, thereby may dictate the binding preference for ribose or AI-2, and consequently affecting biofilm formation (James et al. 2006, Liu et al. 2017). While *A. actinomycetecomitans* HK1651 has two separate *lsr* and *rbs* operons, it is conceivable that the data summarized demonstrates that the identified XH001 *lsrB* operon could encode dual functionality for importing AI-2 and ribose, an interesting feature that warrants further investigation.

Overall, the data from this study reveals that TM7x association with XH001 augments biofilm formation via AI-2 QS. To our knowledge, this is the first time it has been demonstrated that a CPR bacterial species can promote biofilm formation capability of its bacterial host. However, the current available methods enabling visualization of the biofilm formation does not distinguish between the two species nor quantify the ratio of TM7x to XH001, or any potential biofilm matrix components involved in the observed biofilm enhancement. While there is no change in initial

attachment and infectivity of TM7x (Supplementary Figure 3), the captured biofilm formation data suggests disrupted regulation of genes required for biofilm development in TM7x-associated XH001*ΔlsrB* and XH001*ΔluxS* backgrounds. It is also worthwhile to discuss the relative fitness advantage of TM7x induced biofilm formation relative to the oral cavity and fundamental clinical ramifications of their interaction. One possible advantage for inducing biofilm formation in XH001 via QS would be to hinder the inflammation response *in vivo*. Previously, TM7x-associated XH001 relative to XH001 as monoculture was shown to decrease TNF-α expression in macrophages (He et al. 2015). This observation is consistent with previous literature demonstrating that biofilm forming bacteria hinder recognition of the immune system (Donlan et al. 2002, Domenech et al. 2012, Domenech et al. 2013). Other literature suggests that the biofilm matrix production is associated with a decrease in the pro-inflammatory response by decreasing TNF-α production (Thurlow et al. 2011). Although the biofilm promoting genes in TM7x-associated XH001 are not currently elucidated, our previous transcriptomic analysis provided insight by revealing an expression increase of a gene set, including those which encode choline binding proteins (CPBs) in XH001 (He et al. 2015). CBPs have been associated with biofilm formation, adherence, phagocytosis, evasion of the innate immunity, and invasion of eukaryotic host cells (Rosenow et al. 1997, Luo et al. 2005, Moscoso et al. 2006, Schommer et al. 2011, Agarwal et al. 2013). TM7x induction of these genes could provide evolutionary fitness, enabling better survival of its host, XH001, in the oral cavity. The involvement of AI-2 QS in XH001 regulating these genes warrants further investigation.

In summary, a newly developed genetic system generated gene deletion mutants in key AI-2 QS related genes which revealed the important role of AI-2 QS in augmenting the biofilm formation of XH001 when it was associated with its epibiont, TM7x. As evidence accumulates that a massive scale of uncultured bacteria may be obligate participants in relationships like that of TM7x and

XH001, it is imperative to understand their interaction and provide basic knowledge for the study of other uncultivated bacterial species. In-depth characterization of AI-2 signaling between XH001 and TM7x, particularly in the context of biofilm formation and the development in periodontitis, could yield great insight into CPR bacteria, as well as their role in the microbial communities that so drastically influence human health and disease.

Acknowledgements

Figure 1. Protein Sequence Alignment and Molecular Phylogenetic Analyses of the LsrB and LuxS in XH001. Figure 1A protein sequence alignment of the XH001 LsrB and representative LsrB species: 1, XH001; 2, *S. typhimurium* 14028; 3, *E. coli* MG1655; 4, *A. actinomycetecomitans* HK1651; 5, and *Bacillus anthracis*. Alignment was conducted using MEGA7 (Kumar et al. 2016) via ClustalW Omega alignment method (Sievers et al. 2011). The conserved AA residues required for AI-2 binding are highlighted in bold, purple (K35, D116, D166, Q167, P220, and A222) and the corresponding XH001 conserved residue in bold, red. Figure 1B, the evolutionary relationship of the LsrB protein among the representative taxa. The evolutionary history was inferred by using the Maximum Likelihood method based on the JTT matrix-based model (Jones et al. 1992). The tree with the highest log likelihood (-7027.33) is shown. Initial tree(s) for the heuristic search were obtained automatically by applying Neighbor-Join and BioNJ algorithms to a matrix of pairwise distances estimated using a JTT model, and then selecting the topology with superior log likelihood value. The tree is drawn to scale, with branch lengths measured in the number of substitutions per site. The analysis involved 26

54

amino acid sequences. All positions containing gaps and missing data were masked. There was

a total of 284 positions in the final dataset. Evolutionary analyses were conducted in MEGA7

(Kumar et al. (2016). Figure 1C, protein sequence alignment of the XH001 LuxS protein and

representative species. Marked in bold, yellow are the requisite amino acid residues (H,H, and

C) that constitute the catalytic center of LuxS (Hilgers et al. 2001) and coordinate the Zn^{2+} ion:

1, XH001; 2, *S. typhimurium* 14028; 3, *E. coli* MG1655; 4, *A. actinomycetecomitans* HK1651; 5,

S. mutans UA159. Figure 1D, the evolutionary relationship of the luxS protein among the

representative taxa. The tree was generated using the same method parameters as 1B. The

tree with the highest log likelihood (-1292.94) is shown. The analysis involved 5 amino acid

sequences and there was a total of 157 positions in the final dataset.
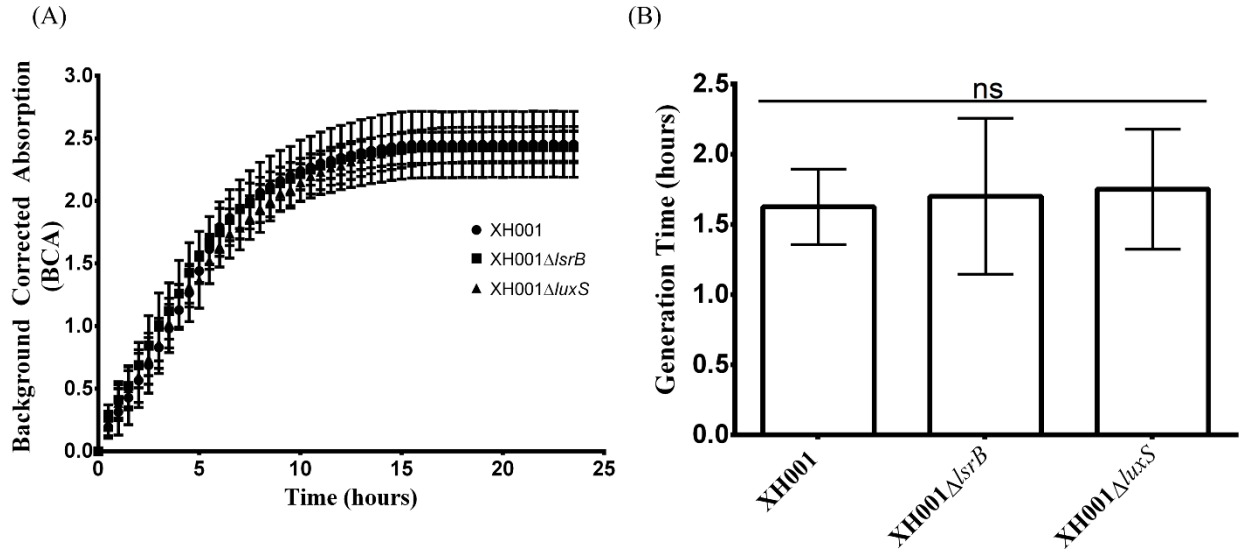
Figure 2. Representative Growth Kinetics and Generation Time Analyses Comparing Wild Type XH001, XH001*ΔlsrB*, and XH001*ΔluxS*. Wild type XH001, XH001*ΔlsrB*, and XH001*ΔluxS* were grown as indicated in methods for 24 hours, acquiring measurements (in the form of Background Corrected Absorption Units) every 30 minutes which produced a growth kinetic curve (A) and enabled quantification of generation time (B). Each bar represents the average of three independent cultures performed in triplicate (*error bars*, SD) in two separate experiments. Statistical analysis was performed using one-way ANOVA.
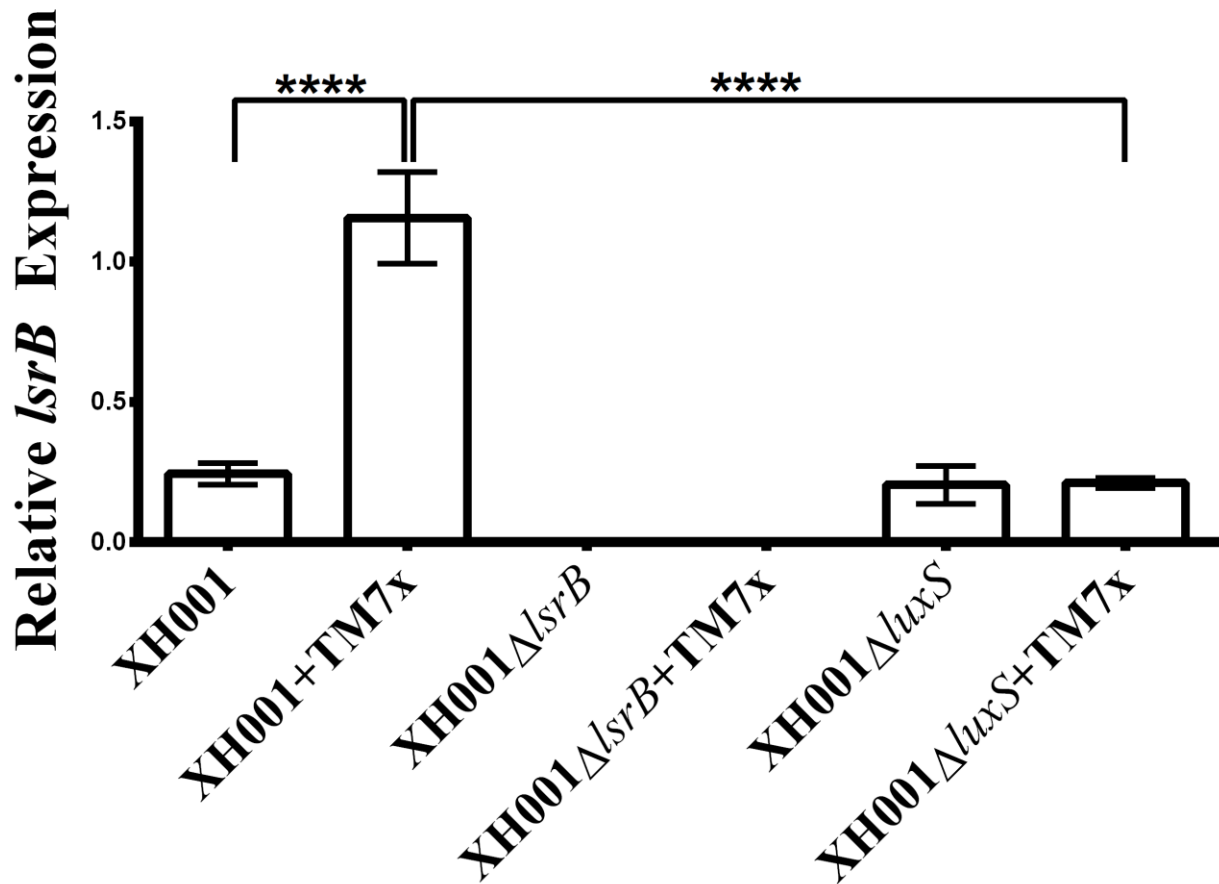
Figure 3. Quantification of *lsrB* expression. *lsrB* expression levels were monitored and each bar represents the average of two independent cultures performed in triplicate (*error bars*, SD). Significance is indicated when p<0.0001 with four asterisks. Statistical analysis was performed using the Student t-test (two tailed).
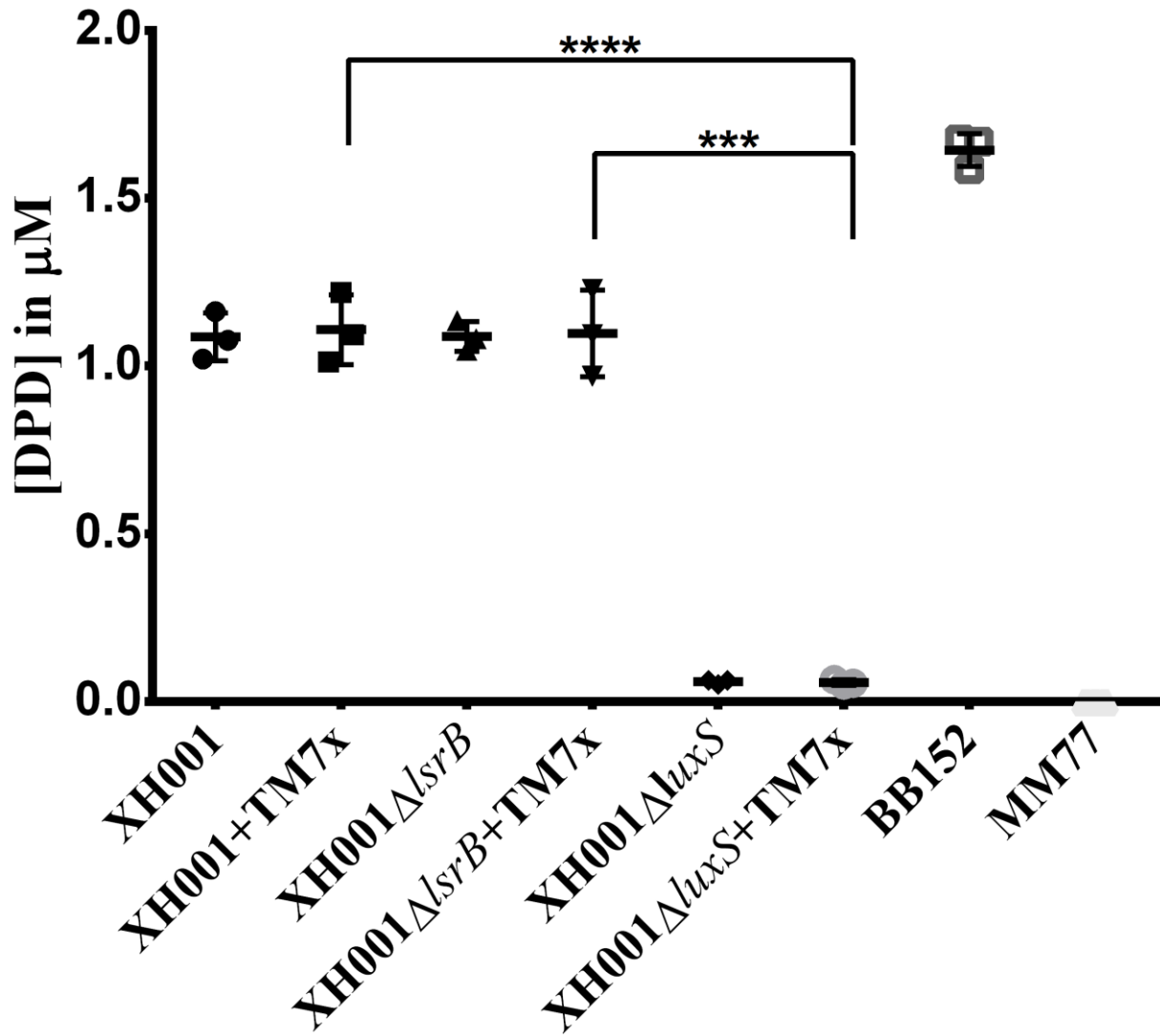
Figure 4. Quantification of the AI-2 signaling molecule via GC-MS. DPD concentration in media was evaluated. Each bar represents the average of one independent culture performed in triplicate (*error bars*, SD). Significance is indicated when p=0.0002 with three asterisks and when p<0.0001 with four asterisks. Statistical analysis was performed using the Student t-test (two tailed) using Graph Pad Prism 6 software.
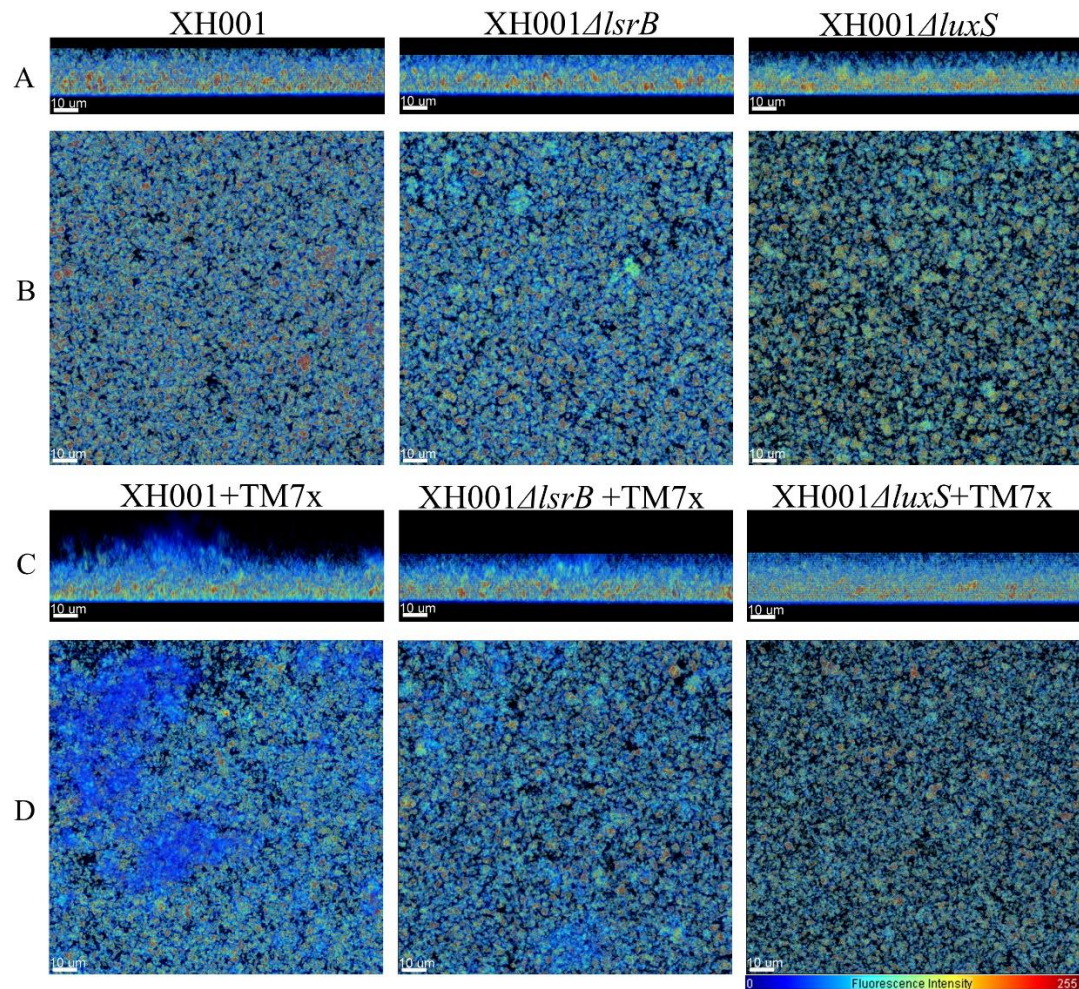
Figure 5. Representative three-dimensional reconstructions of biofilms. Biofilms of wild

type TM7x associated XH001, XH001*ΔlsrB, and* XH001*ΔluxS* monoculture as well as co-culture

when they were associated with TM7x were grown (biological triplicate) as described in the

methods. Images were obtained by CLSM and reconstructed using Bitplane: Imaris-Microscopy

Image Analysis Software (Bitplane). Reconstructed images led to a view of the same biofilms

revealing a significant increase in overall biofilm thickness (height) in the TM7x-associated

XH001 relative to XH001. (A and C) and (B and D) represent saggital (xz) and horizontal (xy)

projected images, respectively. The relative fluorescence intensity of the pseudo-colored

images is reflected by the scale located in the lower right corner. All scale bars are 10μm in

length.
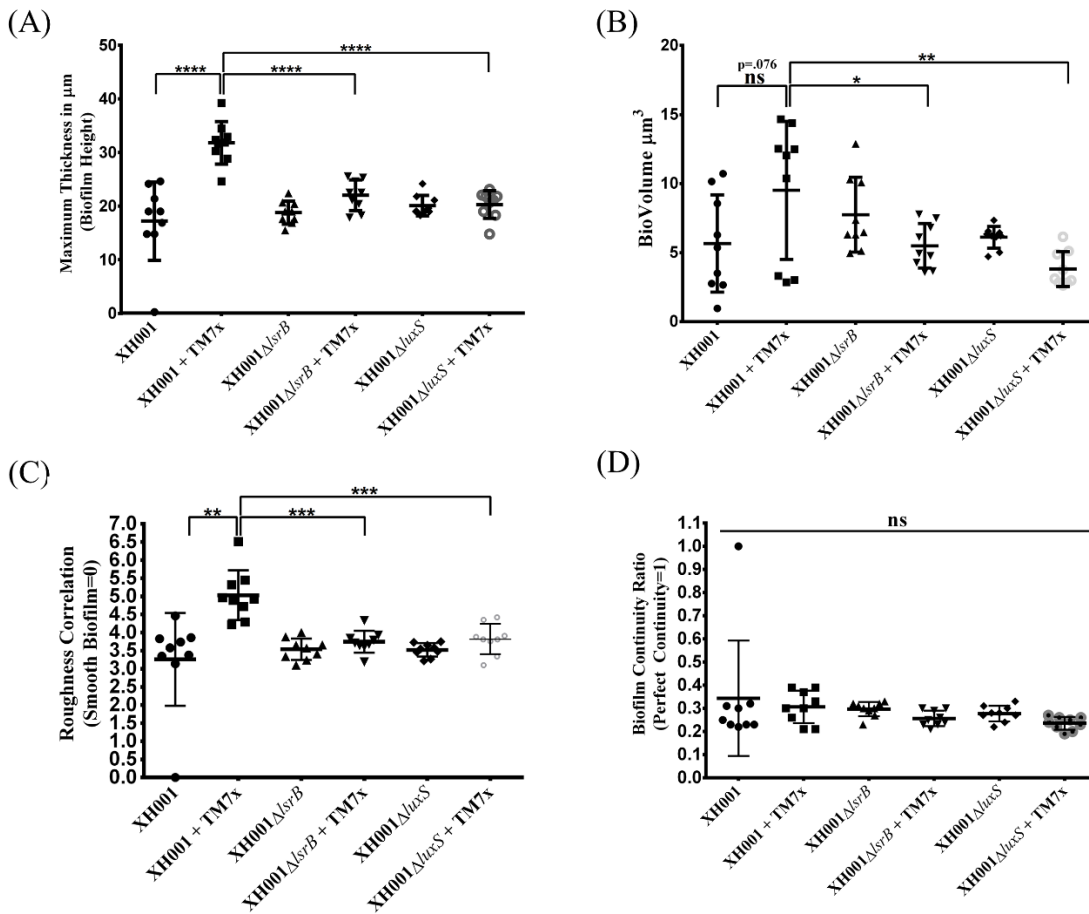
Figure 6. Quantification of total maximal biofilm thickness (height), biovolume, biofilm roughness correlation and biofilm continuity ratio. Histograms represents (A) Maximum Biofilm Thickness (Height), (B) Biovolume, (C) Biofilm Roughness Correlation, and (D) Biofilm Continuity Ratio, comparing wild type XH001, XH001*ΔlsrB, and* XH001*ΔluxS* monoculture as well as co-culture when they were associated with TM7x. The images analyzed were acquired with the same settings as indicated in Figure 6 and in the methods. Three independent cultures for each group were selected with 3 representative images between each culture. Each bar represents the average of two independent cultures performed in triplicate (*error bars*, SD). Significance is indicated when p<0.05, p<0.01, p<0.001, p<0.0001 with one, two, three, and four asterisks, respectively. Statistical analysis was performed using the Student t-test (two tailed) and 1-way ANOVA analysis using Graph Pad Prism 6 software.
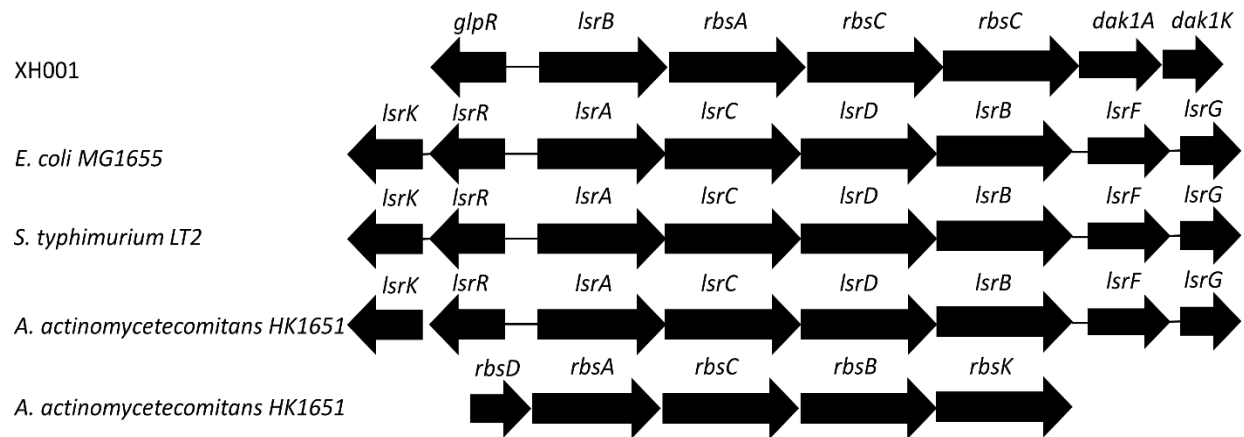
Supplementary Figure 1. The Hybrid AI-2/Ribose operon in XH001. Supplementary figure 1 represents a schematic comparing the hybrid AI-2/Ribose operon in XH001 relative to the annotated *lsr* operon in *Escherichia coli* MG1655, *Salmonella enterica serovar typhimurium* str. 14028, *Aggregatibacter actinomycetecommitans* HK1651, and *rbs* operon in *Aggregatibacter actinomycetecommitans* HK1651.
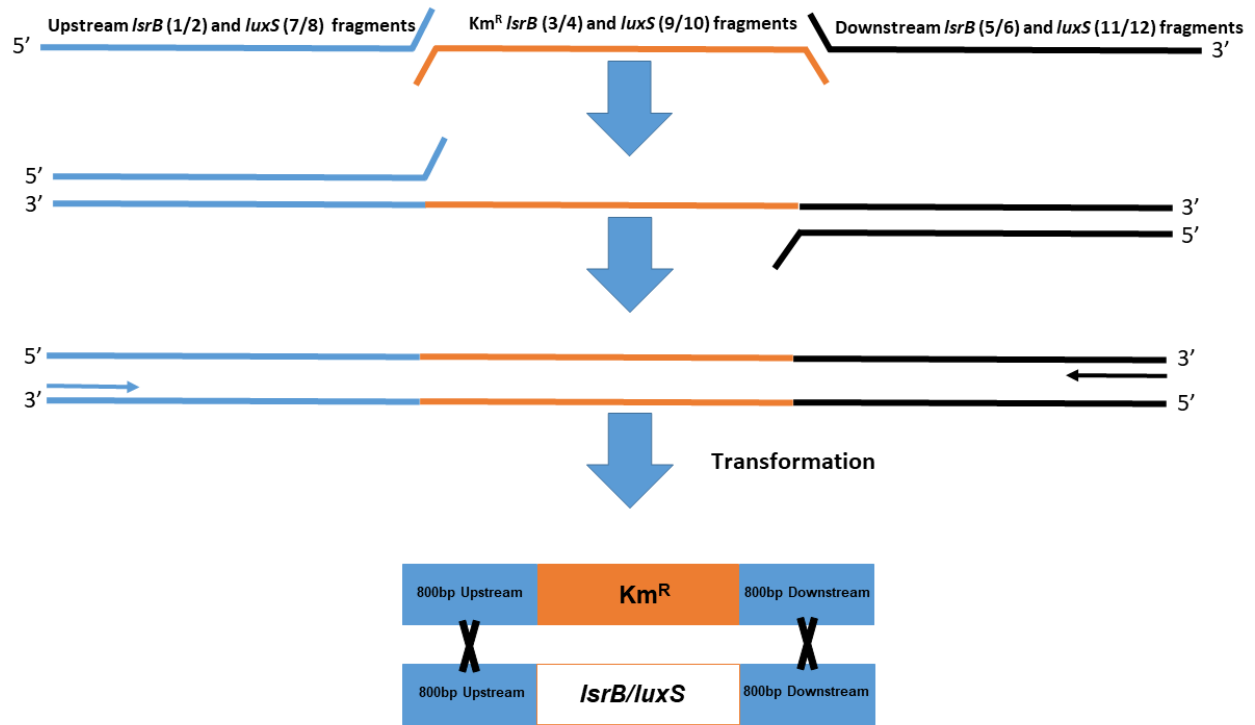
Supplementary Figure 2. The Genetic Construct Design for Chromosomal Gene Deletion.

Supplementary figure 2 is a representative schematic of the generated chromosomal gene

deletion constructs used to create single deletions in the XH001 genetic background for *lsrB*

and *luxS*. Schematic adapted from Shevchuk et al. 2004.

XH001+TM7x   XH001*ΔlsrB* +TM7x   XH001*ΔluxS*+TM7x

A   B   C

10 µm   10 µm   10 µm
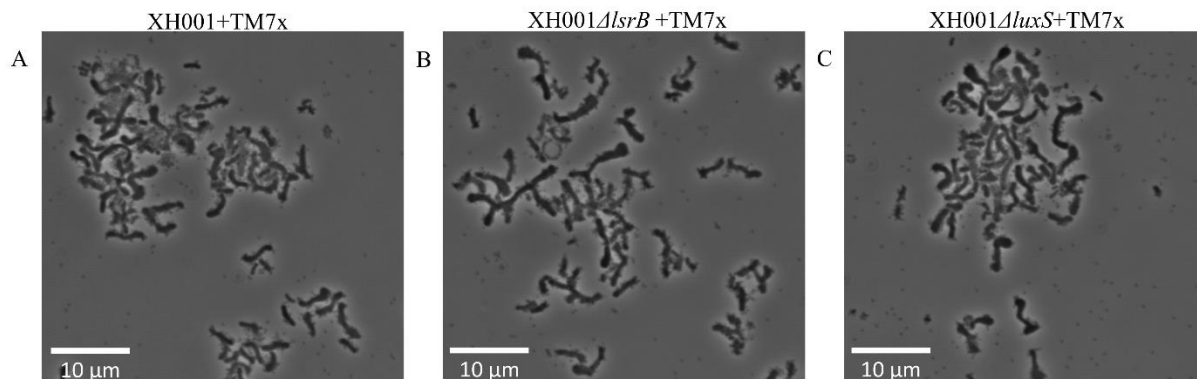
Supplementary Figure 3. Representative phase contrast microscopy images of cellular morphology in the XH001, XH001*ΔlsrB*, and XH001*ΔluxS* backgrounds when infected with TM7x. Cellular morphology was qualitatively assessed via phase contrast microscopy. No differences in initial TM7x infectivity were observed between XH001 (A), XH001*ΔlsrB* (B), and XH001*ΔluxS* (C). All scale bars are 10µm in length.

The graph shows a plot of Instrument Response (eV) versus ng/mL DPD Detected with the equation $y = .01673x - .2167$ and $R^2 = .9977$.
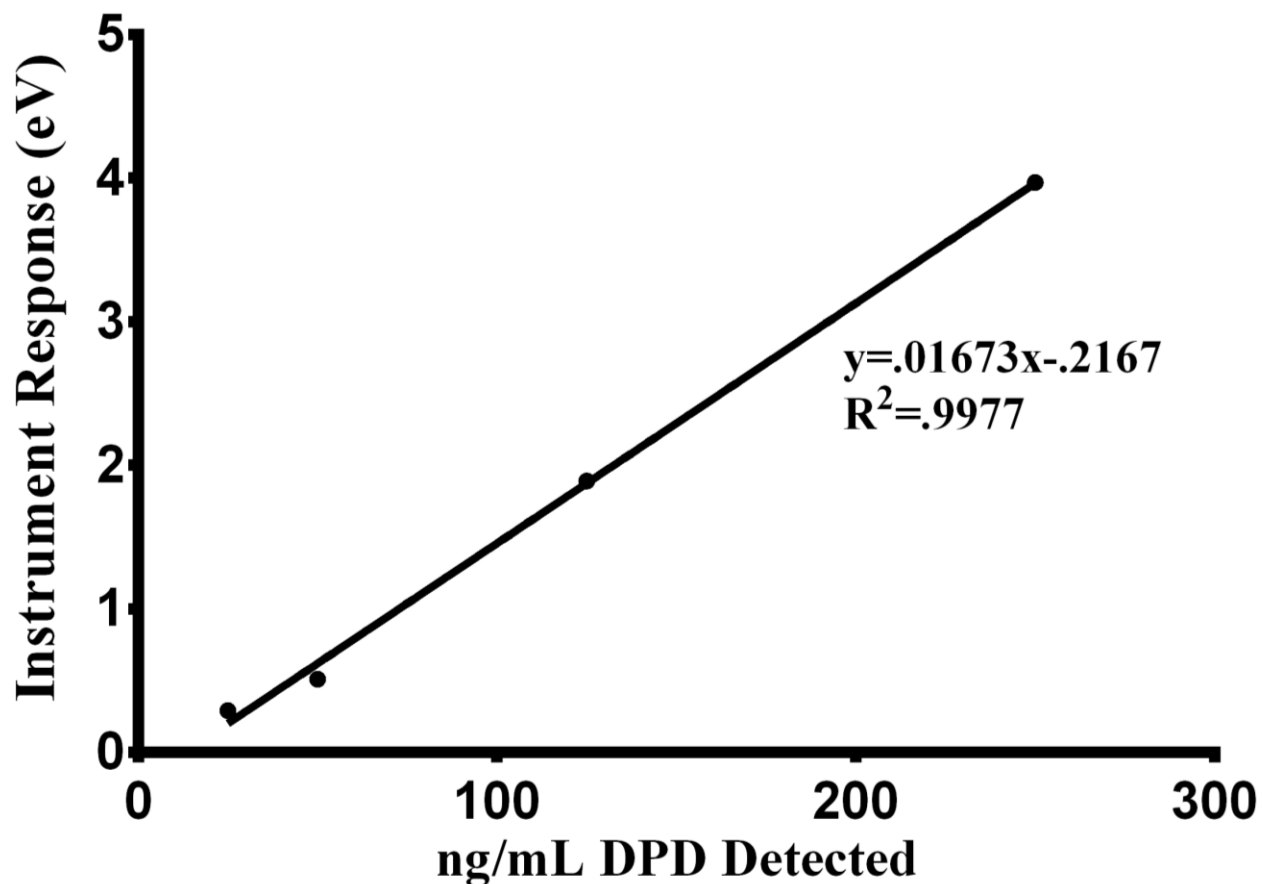
Supplementary Figure 4. Standard curve used for interpolation of GC-MS Quantification of DPD, AI-2. Linearity Testing: External Standards were produced in concentrations of 250 µg/mL, 125 µg/mL, 50 µg/mL, and 25 µg/mL. The correlation coefficient was determined by plotting the calculated amount of DPD (ng/mL) in solution against the instrument response (eV) resulting in a $R^2 = .9977$ value. Quantification of the instrument response (eV) for DPD was normalized to the instrument response (eV) deuterated-DPD internal standard throughout each sample. The resulting standard curve was used to interpolate AI-2 concentration in TM7x-associated XH001 and XH001 as mono species, TM7x-associated XH001Δ*lsrB* and XH001Δ*lsrB*, TM7x-associatedXH001Δ*luxS* and XH001Δ*luxS*, BB152, and MM77.

The chart shows a plot of Instrument Response (eV) on the y-axis (ranging 0 to 6) versus Calculated DPD Concentration ng/mL on the x-axis (ranging 0 to 300), with a linear fit:

$$y = .02010x - .02674$$
$$R^2 = .9957$$
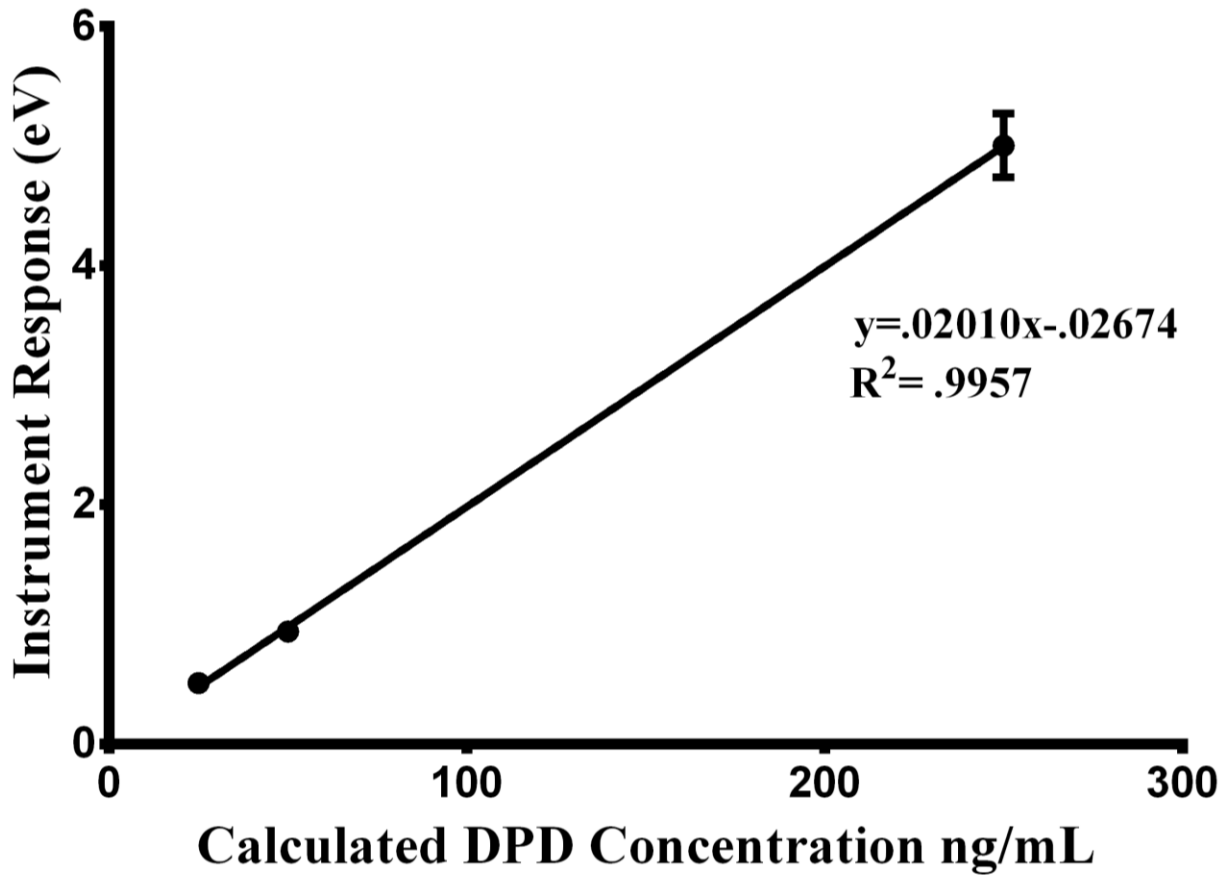
Supplementary Figure 5. DPD Derivatization Reproducibility of External Standards for AI-2 Absolute Quantification. AI-2 Derivatization Reproducibility and linearity testing: external standards were produced in concentrations of 250 µg/mL, 50 µg/mL, and 25 µg/mL in triplicate. Quantification of the instrument response (eV) for DPD was normalized to the instrument response (eV) of the deuterated-DPD internal standard throughout each sample. The correlation coefficient was determined by plotting the calculated amount of DPD (ng/mL) in solution against the instrument response (eV) resulting in a R^2=0.9957 value.

Table 1. Bacterial Strains and Plasmids used in This Study

Strain/Plasmid	Relevant Characteristics	References(s)
pJRD215	Broad-host range expression vector, Km^R Sm^R Mob^+, 10.2 kb	(Davison et al., 1987)
XH001	WT, *A. odontolyticus* subspecies *actinosynbacter* strain, Km^s	(He et al., 2015)
XH001+TM7x	WT, TM7x-associated *A. odontolyticus* subspecies *actinosynbacter* strain, Km^S	(He et al., 2015)
XH001*ΔlsrB*	*ΔlsrB* Km^R in XH001 background	This Study
XH001*ΔlsrB*+TM7x	TM7x-associated XH001*ΔlsrB*	This Study
XH001*ΔluxS*	*ΔluxS* Km^R in XH001 background	This Study
XH001*ΔluxS*+TM7x	TM7x-associated XH001*ΔluxS*	This Study
BB152	*luxLM*::Tn5 in *Vibrio harveyi* strain	(Bassler et al., 1994)
MM77	*luxLM*::Tn*5*, *luxS*::Cm^R in *Vibrio harveyi* strain	(Mok et al., 2003)

Supplementary Table 1. Primer sequences used in this Study

Primer Name/No.	Primer Sequence	Reference(s)
XH001 *lsrB* F:	5'-GGACGTCTCGCCGGAAAA-3'	This Study
XH001 *lsrB* R:	5'-CCTGTTCAAGGACGGAGGAA-3'	This Study
F5	5'-GCGGAGCATGCGGATTA-3'	(Bor et al., 2016)
R3	5'-AACGTGCTGGCAACATAGGG-3'	(Bor et al., 2016)
1	5'-CGAACACCAGGTTCAGGGAAGG-3'	This Study
2	5'-TGAGCGGGACTCTGGGGTTCGCGTCGTCACTTCCTCGTGATCTAG-3'	This Study
3	5'-CTAGATCACGAGGAAGTGACGACGCGAACCCCAGAGTCCCGCTCAG-3'	This Study
4	5'-GGCCGGGGCTGCGCGACCTGCAGCCAAGCTAGCTTCACG-3'	This Study
5	5'-GTGAAGCTAGCTTGGCTGCAGGTCGCGCAGCCCCGGCC-3'	This Study
6	5'-GTCCCGATCGCATGATGGTGA-3'	This Study
7	5'-TCCGCTCGGTCCTGTCTCAGAT-3'	This Study
8	5'-TGAGCGGGACTCTGGGGTTCGCCGGTTAGTCCCTTTCGGTGTAGTTTT-3'	This Study
9	5'-AAAACTACACCGAAAGGGACTAACCGGCGAACCCCAGAGTCCCGCTCA-3'	This Study
10	5'-CCAGGCGAACGCCCAGAACCTGCAGCCAAGCTAGCTTCAC-3'	This Study
11	5'-GTGAAGCTAGCTTGGCTGCAGGTTCTGGGCGTTCGCCTGG-3'	This Study
12	5'-TGGTTTTTCACAAATATGAGGCCAGA-3'	This Study
13	5'-CCTAAATCGCCAGTCCACAG-3'	This Study
14	5'-GCTTGCCGAATATCATGGTG-3'	This Study
15	5'-CCTAAATCGCCAGTCCACAG-3'	This Study
16	5'-GTCCTCGTGTCGTATCCATTCT-3'	This Study
17	5'-CACTTCGTCCAGGTGGTCCT-3'	This Study
18	5'-CGAATATCATGGTGGAAAATGG-3'	This Study
19	5'-CTGGCTTCGAGGAGCTTGAC-3'	This Study
20	5'- GTTAATGAGGCGCACGTAGG-3'	This Study
21	5'-ATGAAGATCGGAAGACTGACGGC-3'	This Study
22	5'-TCAGAAGTCGTAGTTCTTCGCTTGC-3'	This Study
23	5'-GAGCTTTACCCTGGACCACA-3'	This Study
24	5'-AGTGGATGACGTCGACACG-3'	This Study
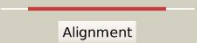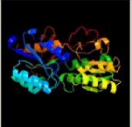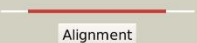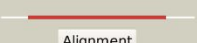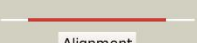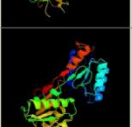
Supplementary Table 2. Gene Accession Numbers/Versions for the Proteins Analyzed in This Study

Bacterial and Protein Species Name	Gene Accession No.	Version
XH001 LsrB	KSW13249	KSW13249.1
Escherichia coli MG1655 LsrB	WP_000172465	WP_000172465.1
Salmonella enterica serovar Typhimurium ATCC 14028 LsrB	WP_000090737	WP_000090737.1
Aggregatibacter actinomycetecommitans HK1651 LsrB	AHN72389	AHN72389.1
Bacillus anthracis Strain Sterne	AJH47018	AJH47018.1
Vibrio harveyi LuxP	WP_012129029	WP_012129029.1
Escherichia coli MG1655 RbsB	WP_001056271	WP_001056271.1
Salmonella enterica serovar Typhimurium ATCC 14028 RbsB	WP_001056260	WP_001056260.1
Aggregatibacter actinomycetecommitans HK1651 RbsB	WP_005567919	WP_005567919.1
XH001 LuxS	WP_060566748	WP_060566748.1
Escherichia coli MG1655 LuxS	WP_001130211	WP_001130211.1
Salmonella enterica serovar Typhimurium ATCC 14028 LuxS	WP_001130194	WP_001130194.1
Aggregatibacter actinomycetecommitans HK1651 LuxS	WP_005548120	WP_005548120.1
Streptococcus mutans UA159 LuxS	WP_002263047	WP_002263047.1

Phyre²

Detailed template information

#	Template	Alignment Coverage	3D Model	Confidence	% i.d.	Template Information
1	c4pz0A_	Alignment		100.0	21	**PDB header:**sugar binding protein **Chain: A: PDB Molecule:**sugar abc transporter, sugar-binding protein; **PDBTitle:** the crystal structure of a solute binding protein from bacillus2 anthracis str. ames in complex with quorum-sensing signal3 autoinducer-2 (ai-2)
2	c5braA_	Alignment		100.0	39	**PDB header:**solute-binding protein **Chain: A: PDB Molecule:**putative periplasmic binding protein with substrate ribose; **PDBTitle:** crystal structure of a putative periplasmic solute binding protein2 (ipr025997) from ochrobactrum anthropi atcc49188 (oant_2843, target3 efi-511085)
3	d1tjva_	Alignment		100.0	22	**Fold:**Periplasmic binding protein-like I **Superfamily:**Periplasmic binding protein-like I **Family:**L-arabinose binding protein-like
4	c4kvfA_	Alignment		100.0	19	**PDB header:**transport protein **Chain: A: PDB Molecule:**rhamnose abc transporter, periplasmic rhamnose-binding **PDBTitle:** the crystal structure of a rhamnose abc transporter, periplasmic2 rhamnose-binding protein from kribbella flavida dsm 17836
5	c3d02A_	Alignment		100.0	30	**PDB header:**sugar binding protein **Chain: A: PDB Molecule:**putative laci-type transcriptional regulator; **PDBTitle:** crystal structure of periplasmic sugar-binding protein2 (yp_001338366.1) from klebsiella pneumoniae subsp. pneumoniae mgh3 78578 at 1.30 a resolution
6	c4wzzA_	Alignment		100.0	19	**PDB header:**transport protein **Chain: A: PDB Molecule:**putative sugar abc transporter, substrate-binding protein; **PDBTitle:** crystal structure of an abc transporter solute binding protein2 (ipr025997) from clostridium phytofermentas (cphy_0583, target efi-3 511148) with bound l-rhamnose
7	c5bq3A_	Alignment		100.0	18	**PDB header:**transport protein **Chain: A: PDB Molecule:**rhamnose abc transporter, rhamnose-binding protein; **PDBTitle:** crystal structure of a sugar abc transporter (actodo_00688) from2 actinomyces odontolyticus atcc 17982 at 2.60 a resolution
8	c4y9tA_	Alignment		100.0	17	**PDB header:**solute-binding protein **Chain: A: PDB Molecule:**abc transporter, solute binding protein; **PDBTitle:** crystal structure of an abc transporter solute binding protein2 (ipr025997) from agrobacterium vitis s4 (avi_5305, target efi-511224)3 with bound alpha-d-glucosamine
9	c2rjoA_	Alignment		100.0	16	**PDB header:**signaling protein **Chain: A: PDB Molecule:**twin-arginine translocation pathway signal protein; **PDBTitle:** crystal structure of twin-arginine translocation pathway signal2 protein from burkholderia phytofirmans
10	c4wwhA_	Alignment		100.0	19	**PDB header:**transport protein **Chain: A: PDB Molecule:**abc transporter; **PDBTitle:** crystal structure of an abc transporter solute binding protein2 (ipr025997) from mycobacterium smegmatis (msmeg_1704, target efi-3 510967) with bound d-galactose
11	c3g1wB_	Alignment		100.0	16	**PDB header:**transport protein **Chain: B: PDB Molecule:**sugar abc transporter; **PDBTitle:** crystal structure of sugar abc transporter (sugar-binding protein)2 from bacillus halodurans

69

Chapter 3: Optimized Genetic Tool Development in XH001 for Gene Essentiality and Fitness under TM7x Parasitism

Abstract

The unique, epibiotic-parasitic relationship between TM7x and *Schaalia odontolytica* (formerly *Actinomyces odontolyticus subsp. actinosynbacter*) strain, XH001, warrants a deep understanding of the genetic mediators of their interaction, which will provide insight into their relationship, but perhaps, broadly for members of the Candidate Phyla Radiation. Recent work demonstrated differential expression of genes in XH001 when associated with TM7x, leading to the first genetic study elucidating the role of quorum sensing and biofilm formation. The study herein, builds upon this genetic capacity to study TM7x and XH001 in a high throughput (Tn-seq) and real time manner. Tn-seq was employed to screen for XH001 mutants positively and negatively selected against TM7x infection, revealing several gene mutants (85 candidate gene coding sequences and 188 intergenic regions) involved in diverse functions, such as sugar transport of biosynthesis of essential compounds, which could be putatively essential for their interaction as previously described and involved in quorum sensing corroborating previous studies.

Introduction

Recently, there have been new isolations of Saccharibacteria members with their hosts (Bor et al. 2020, Murugkar et al. 2020), but the *Nanosynbacter lyticus* type strain, TM7x (HMT_952), and *Schaalia odontolytica* (formerly *Actinomyces odontolyticus subsp. actinosynbacter*) strain (Nouioui et al. 2018), XH001 co-culture is the first and most well studied (He et al. 2015, Bor et al. 2016, McLean et al. 2016, Bedree et al. 2018, Bor et al. 2018, McLean et al. 2020, Utter et al. 2020). As such, to acquire insight into the tantalizing relationship between TM7x and XH001, a robust genetic system would be needed for both TM7x and XH001. However, to date, no genetic system has been developed for any Saccharibacteria member, such as TM7x. This could be due to Saccharibacteria's dependence on their host preventing the utility of standard genetic mutant selection in independent culture. Thus, to indirectly study TM7x's biology, development of a genetic toolset (site-specific mutagenesis) for its bacterial basibiont, XH001, was initially constructed (Bedree et al. 2018). This initial genetic system in XH001 was in-part influenced by previous work by Maria Yeung and colleagues, who are largely credited with the pioneering the foundation for genetic system development in *Actinomyces spp.* (closely related to *Schaalia spp.*) through the study of fimbrial biogenesis in *Actinomyces naeslundi* as a model system (Yeung 1999, Kolenbrander 2000), evaluation of a the transformability of a broad-host-range vector (Yeung et al. 1994), pJRD215 (Davison et al. 1987), as well as the construction of integration vectors for allelic replacement to study type 1 and type 2 fimbrial biogenesis in *Actinomyces naeslundi* T14V (Yeung 1995, Yeung et al. 1997, Yeung et al. 1998). Genetic systems to induce in-frame fimbrial deletion mutants (Mishra et al. 2007) or marker-less, in-frame deletion mutants via GalK counterselection (Mishra et al. 2010) are available for *Actinomyces naeslundi* MG-1. Additionally, lytic and temperate bacteriophage were used for transfection, however, interestingly none were found to infect *Actinomyces odontolyticus* (Yeung et al. 1997). Most recently, newer genetic systems have been built for *Actinomyces oris* MG-1 through marker-less, in-frame

mutations using fluorescence (mCherry) counterselection (Wu et al. 2010) or transposon mutagenesis (Wu et al. 2014) to study sortase and fimbrial function (Wu et al. 2016). The accumulation of this knowledge laid the groundwork for a crucial, high-throughput mutagenesis tool enhancing the current genetic system developed in XH001 (Bedree et al. 2018) to elucidate genetic mediators in the epibiotic-parasitic relationship between XH001 and TM7x described in this study. To date, there no known high-throughput genetic toolsets, such as Tn-seq (Van Opijnen et al. 2009), developed for *Actinomyces* (or *Schaalia*) *spp.* prior to this study. Furthermore, no gene essentiality study (conditionally essential in any growth condition) exists, but a few studies have been completed for most of the major oral pathogens, *Aggregibacter Actinomycetecomitans* (Lewin et al. 2019), *Porphorymonas gingivalis (Klein et al. 2012)*, and *Streptococcus mutans* (Shields et al. 2018, Shields et al. 2020). A classic and robust technique, Tn-seq (Van Opijnen et al. 2009), whereby high-throughput transposon mutagenesis achieves an insertional saturation threshold for elucidating the essential genes of any organism in a probabilistic manner based upon relative gene size and insertion rate (Klein et al. 2012, Molina-Quiroz et al. 2016). Therefore, construction of an XH001 Tn-seq library to elucidate conditionally essential genes along-side specifically applied evolutionary selection pressure, such as TM7x parasitism, the most prudent approach for elucidating the genetic mediators of XH001 predation was warranted, as previously modeled in another bacterial-bacterial predation system (Duncan et al. 2018). In totality, this chapter represents the completion and crucial advancements of the XH001 genetic toolset to investigate the interesting relationship between TM7x and XH001.

Materials and Methods

Bacterial Strains, Plasmids, and Media

Initial description of XH001 and used in this study are described in the materials and methods and listed in Table 1 of Chapter 2. All remaining bacterial strains, plasmids and media are listed in Table 1 of Chapter 3, most relevant to this work. All growth conditions used followed previous protocols (Bedree et al. 2018), except XH001::Tn5 mutants were selected on Brain-Heart Infusion (BHI) broth or agar (Difco Laboratories, Detroit, Michigan) with 500 µg/mL of kanamycin sulfate (Fischer Bioreagents, Hampton, NH, United States), XH001 harboring pJB1 or pJB2 plasmid with 250 µg/mL, to ensure no background satellite cells given the close proximity of cells resulting from high transformation efficiency and were incubated for 7 days. TM7x reinfection of all XH001::Tn5 and XH001 harboring pJB1 or pJB2 plasmids followed published protocols (Utter et al. 2020).

Transposon Mutagenesis and Mutant Library Collection

XH001 underwent electrocompetent cell preparation and transposition with the EZ-Tn5 transposon as previously described (Wu et al. 2014, Wu et al. 2016) with the following modifications: selection on BHI with 500 µg/mL of kanamycin sulfate for 7 days using growth conditions previously stated (Bedree et al. 2018) and a starting electrocompetent culture of 50mL to optimize cell spread. Post mutant growth, colonies from each library were individually collected as described (Freed et al. 2016) aggregated into 10 mL of fresh media supplemented with 500 µg/mL of kanamycin sulfate, aliquoted (~2.0 X 10^8 CFUs/mL), and stored at -80 °C for future use in 30 % glycerol.

Tn-seq Library Construction, Sequencing and Bioinformatic Analysis for Gene Essentiality and TM7x Selection

DNA isolation was performed using Epicentre MasterPure™ Complete DNA and RNA Purification Kit (Lucigen) following the manufacturer's protocol with the following modifications: pre-lysis incubation of samples with Lysozyme (50mg/mL) and Mutanolysin (2 mg/mL) at 37°C and included an RNAase step for 30 minutes at 37°C. Library preparation was performed as previously described (Klein et al. 2012, Lazinski et al. 2013) with the following modifications: during the barcode adapting PCR step, primer 1 was added with a mixture of truncated primer 2, primer 1, was added at a 10:1 volume ratio (primer 1: primer 2) to enhance amplification and avoid primer dimer formation. The second PCR step, barcode addition, was completed using primer 5 and barcode primers (BC1-12) listed in Table 7. All PCR reactions were completed using Q5® Hot Start High-Fidelity DNA Polymerase (New England Biolabs, Ipswich, MA) following the manufacture's protocol. For sequencing on Illumina's HiSeq 2500 platform, a custom sequencing primer (Table 7) was created.

Bioinformatic analysis of the Tn-seq library sequencing datasets were performed as described (Molina-Quiroz et al. 2016, Duncan et al. 2018) trimmed all reads of the 3' poly-C adapter and 5' EzTn5 ME using stringent parameters for cutadapt.py (Martin 2011). All trimmed reads from each of six libraries were ultimately concatenated. To determine aggregate insertional density from all six library was completed using parameters previously established (Molina-Quiroz et al. 2016). The aggregate hopcount analysis was performed with the following parameters: (1) minimum read positional cutoff of 15 (15 reads at a given position needed for analysis); (2) when aggregating EZ-Tn5 hops into the genome, did not count reads in the first or last 5% of the CDS; (3) Only count reads that align perfectly to the reference across the entire read (no mismatches or gaps). For conditionally essential gene analysis, the following criteria were used: Dval genome value (defined as the number of reads of each gene divided by predicted number of reads) <= 0.01 ((Molina-Quiroz et al. 2016) and minimum region length = 100 base pairs generating a putatively

essential gene list (Table 2). All designated CDS Gene loci was then assigned to Clusters of Orthologous Groups as previously described (Angiuoli et al. 2011).

TM7x Selection of XH001::Tn5 Assay

To perform TM7x selection of XH001::Tn5, the re-attachment of TM7x and titer inoculum followed previous protocols (Utter et al. 2020) except with the following modifications: XH001::Tn5 received 4-fold higher amount of TM7x (Figure 4) to maximize TM7x:XH001::Tn5 MOI ratio (~1.1 X 10^9:2.0 X 10^6) and minimize stochastic effects of TM7x infection, where as XH001 received the maximum titer as previously published (Utter et al. 2020). Optical Density (OD_{600}) and Colony Forming Units were used to assess TM7x infection rates. Every XH001::Tn5 culture passage was under selection of 250 µg/mL kanamycin sulfate, except for the XH001 and TM7x-associated infection control group (Figure 4). However, critically, at Passage 1, the volume for the experimental group, TM7x-associated XH001::Tn5, was normalized to the control as the TM7x addition prior to selection was extremely turbid artificially skewing the OD_{600} measurement, no normalization occurred in Passage 2 and Passage 3. At each passage, 1 mL aliquots were taken for DNA extraction as previously described.

Bioinformatic Analysis of Tn-seq Selection of XH001::Tn5

Assumptions for analysis**:** (1) with each successive passage, more TM7x replicates thereby maintaining selective pressure in the experimental arm. Therefore, at passage 3, XH001::Tn5 mutants with beneficial or detrimental insertions should be successively enriched or lost, respectively, with each passage. Previous bacterial-bacterial interaction aggregate hopcount studies (Duncan et al. 2018) were performed and applied to TM7x selection of XH001::Tn5 along with the hopcount thresholds described above. Identification of genetic loci candidates required calculating the fitness for each individual passage and selection sample, where fitness =

DvalGenome_Output / DvalGenome_Input (Molina-Quiroz et al. 2016). Next, averaging the fitness data across individual selections for each passage 1, 2, and 3 for the experimental (TM7x+) and control (TM7x-), elimination of entries where the number of unique insertions in the input is less than 4 (DvalGenome) and entries where the fitness of TM7x+ Passage 3 is between 0.4 and 2.5 (eliminates entries in which the insertion is relatively neutral in the experimental arc), and finally eliminate entries where the ratio of (TM7x+ Passage 3 fitness / Control Passage 3 fitness) is between 0.6 and 1.5 (eliminates entries in which the control behaved rather similarly to the experimental). All parameters described generated the candidate list (Table 5) and truncated list based upon biological relevance to TM7x-XH001 interaction (Table 6).

Construction of Constitutive and Inducible Florescent Markers in XH001

Two plasmids, pJB1 and pJB2, were constructed by using Gibson Assembly (Gibson et al. 2008) to clone either an RpsL-mCherry gene block (native promoter in XH001) or Plac-LacI/PlacO-mCherry gene blocks into progenitor plasmid, pCWU1 (Wu et al. 2010). All gene blocks sequences were derived from previously published studies (Lutz et al. 1997, Wu et al. 2010, McLean et al. 2016). RpsL-mCherry was amplified using primers 5 and 6 and Plac-LacI/PlacO-mCherry using primers 7/8 and 9/10. pJB1 and pJB2 backbone was amplified using primer 11 and 12. All PCR reactions were completed using Q5® Hot Start High-Fidelity DNA Polymerase (New England Biolabs, Ipswich, MA) following the manufacture's protocol. Transformation of XH001 with pJB1 or pJB2 as previously described (Bedree et al. 2018). Gibson Assembly was performed using NEBuilder® HiFi DNA Assembly Master Mix (New England Biolabs, Ipswich, MA) using the manufacturer's protocol with the following modifications: using insert to backbone ratio (1:1) with a maximum volume of 3 µL combined with3 µL of NEB HiFi master mix for a reaction volume of 6 µL. 1 hour was used for the thermocycling event instead of 15 minutes.

TM7x Infection Selection of XH001 harboring pJB1 and pJB2 and Confocal Imaging

TM7x was re-attached to XH001 harboring pJB1 or pJB2 (n=3) using the highest MOI ratio (TM7x:XH001) from the previously established protocol (Utter et al. 2020) and selected with 250 μg/mL kanamycin sulfate. pJB2 was induced with 1 mM IPTG (Teknova) for 24 hours prior to imaging. XH001 harboring pJB1 or pJB2 cultures were incubated at 37°C in aerobic conditions for 1 hour to aerate and induce mCherry protein folding. XH001 harboring pJB1 or pJB2 was then re-suspended in 4% paraformaldehyde Phosphate Buffered Saline (PBS) to concentrate cells to OD_{600} 5. 1 μL aliquots were then visualized under differential interference contrast transmission and confocal microscopy imaging (Zeiss LSM 880) using objective plan-apochromat 63x 1.4 oil. Representative images (.czi files) were processed via Fiji/ImageJ (Schindelin et al. 2012, Rueden et al. 2017) (Figure 6).

Results

Mutant Library Construction and Conditionally Essential Gene Analysis by Tn-seq in XH001

To construct a highly saturated Tn-seq library, the Tn5 transposon was ultimately selected for its stable, 'cut and paste' insertion mechanisms and random insertion bias (Goryshin et al. 1998), relative to the Himar1-mariner transposon, which has an AT-nucleotide insertional bias (Van Opijnen et al. 2009, Picardeau 2010) and unsuitable for high GC% organisms, albeit at low efficiency (Hoffman et al. 2002) normally. However, a combination of a hyperactive triple mutation of the Tn5 transposase (Goryshin et al. 1998) and inverted repeat ends containing a mosaic end (ME) sequences (Zhou et al. 1998), increased the Tn5 insertion efficacy by several orders of magnitude (Hoffman et al. 2002). Therefore, in addition to its use in several bacterial organisms (Vidal et al. 2009, Khatiwara et al. 2012, Wu et al. 2014, Molina-Quiroz et al. 2016), the EZ-Tn5 commercially available transposon was selected, which contains both a hyperactive transposase and transposon with hyperactive ME's, that forms a transposome (Goryshin et al. 2000) directly used for mutagenesis of XH001. Furthermore, the commercial EZ-Tn5 pMOD vector modified with the kanamycin resistant cassette from pJRD215 (Davison et al. 1987), which has been used in XH001 previously (Bedree et al. 2018), generating a custom EZ-Tn5 transposon with high rates of transposition in a closely related *Actinomyces spp.* (Wu et al. 2014) and utilized for development of a highly saturated Tn-seq library in XH001 (Figure 1). A total of six separate mutant libraries were generated (Wu et al. 2014) and collected (Freed et al. 2016) using established protocols with modifications (see methods). Each mutant library was subsequently processed for DNA, underwent library preparation, and sequenced individually as previously described (Klein et al. 2012, Lazinski et al. 2013). Analysis was performed on the resulting Tn-seq library sequencing reads after concatenation in a single aggregate data set, which followed

previously described essential gene parameters cutoffs (Klein et al. 2012) and revealed 203 (10.5%) conditionally essential genes of the 1,936 gene coding sequences (CDS) in XH001 (McLean et al. 2016), consistent with previous reports (Akerley et al. 2002, Sassetti et al. 2003, Gallagher et al. 2007, De Berardinis et al. 2008, Chaudhuri et al. 2009, Goodman et al. 2009, Khatiwara et al. 2012, Klein et al. 2012), for growing on solid Brain-Heart Infusion (BHI) media with no insertions in two intergenic regions and ~660,000 unique insertions (Figure 1, Data Table 2). Validation of consistent and unbiased insertional mutagenesis was validated as represented by Spearman's rank correlation coefficient, demonstrating consistent transposon mutagenesis and mutant library collection through sequencing (Figure 2). BlastP analysis revealed 193/203 putatively essential genes with homologues within the Database of Essential Genes (Zhang et al. 2004, Zhang et al. 2009). To validate both the essential gene functional assignment and distribution, all essential genes that could be assigned to Clusters of Orthologous Groups (COGs) was performed as described (Angiuoli et al. 2011), albeit some non-essential genes could not be assigned, thereby artificially increasing the gene essentiality percentage to 12.2% (Figure 3A, Table 3). As expected, significant enrichment of 'H' (coenzyme metabolism and metabolism), 'I' (lipid metabolism and metabolism), 'J' (Translation ribosomal structure and biogenesis), 'L' (replication, recombination, and repair), 'M' (cell wall/membrane/envelop biogenesis), 'O' (post-translational modification, protein turnover, chaperone functions, 'U' (intracellular trafficking, secretion, and vesicular transport). However, unexpectedly, 'V' (defense mechanisms), was enriched, potentially suggestive of essential stress responses to microaerophilic conditions that XH001 is cultured. Interestingly, approximately ~20% (~350) of the total CDS within XH001's genome are assigned to category 'S' (function unknown).

XH001 Genetic Fitness During TM7x Parasitism revealed by Tn-seq

Previously studies analyzing genetic mediators in XH001 when re-infected with TM7x as compared to uninfected conditions demonstrated differential expression (RNA-seq) of a variety of genes (He et al. 2015) as well as acquisition of single nucleotide polymorphisms during serial passage (Bor et al. 2018). Furthermore, the most upregulated gene, *lsrB*, the receptor of the Auto-Inducer 2 signaling (AI-2) molecule involved bacterial quorum sensing and the AI-2 synthase, *luxS*, were demonstrated to induce biofilm deficiencies in XH001Δ*lsrB* or XH001Δ*luxS* when associated with TM7x likely through indirect mechanisms (Bedree et al. 2018). Thus, a powerful genetic screen, such as Tn-seq (Van Opijnen et al. 2009), was warranted to elucidate factors during the TM7x parasitic event. Recently, the TM7x parasitic event has been captured over serial passage (Bor et al. 2018) in a TM7x titer dependent manner (Utter et al. 2020). Therefore, this established TM7x infection assay was used to hyper infect the XH001::Tn5 mutant library host to screen for genetic constituents involved in the nascent TM7x infection cycle (Figure 4a) that replicated the XH001 crash cycles (Figure 4b, 4c) as previously described (Utter et al. 2020). We expected that by passage 3, as wild-type starts to recover from infection, the positively selected and negatively selected XH001::Tn5 mutants would most enriched or lost, respectively (Figure 4b, 4c, Table 4). After sequencing each passage and using Tn-seq analysis parameters recently described for bacterial-bacterial predation (Duncan et al. 2018), an initial candidate gene/intergenic list of 273 targets that comprised of 85 CDS and 188 intergenic regions (Table 5), was ascertained when comparing TM7x-associated XH001::Tn5 compared to XH001::Tn5 alone and ultimately narrowed to a select list of 25 candidates, of which 9 where mutants with insertions in intergenic regions (Table 6). Interestingly, insertional mutants in two intergenic regions just upstream of *lsrB* and *luxS*, APY09_02515--APY09_02520_ig and APY09_06105--APY09_06110_ig, were positively selected, albeit APY09_02520 (*lsrB*) and APY09_06105 (*luxS*) remained neutral selected genes throughout the selection when compared to the control (Figure 4). Most of the remaining candidates are involved with transport of sugars

or biosynthetic pathways putatively purported to be required for TM7x survival as previously described (He et al. 2015, Bor et al. 2020, McLean et al. 2020).

Real-Time Monitoring of XH001 of TM7x Parasitism

TM7x has a reduced genome and lacks all major biosynthetic pathways suggestive of a completely reliant relationship on its host XH001 (He et al. 2015) for nutrition. Thus, it was hypothesized a transfer of cytoplasmic contents might occur between the two organisms. To qualitatively assess this transfer a constitutive, pJB1, and inducible fluorescent marker system, pJB2, that is rpsL (native promoter) driven or lac inducible, using mCherry was constructed (Figure 5) and transformed into XH001 as previously described (Bedree et al. 2018). To capture the parasitic event, XH001 harboring the constitutively expressed mCherry construct were infected as described (Figure 4) and imaged at passage 1 via confocal microscopy for cytoplasmic content transfer. However, no mCherry signal was detected in free-floating or attached TM7x (Figure 6).

Discussion

Conditionally essential gene studies are extremely important for both understanding bacterial physiology and growth requires to validate transcriptomic profiling and genetic fitness (Tn-seq) data sets in natural biological contexts. Here we demonstrate the first conditionally essential gene study ever completed in *Schaalia spp*. 203 putatively essential genes, ~10.5% of the XH001 genome were elucidated to be necessary for growth on BHI agar (solid media) by generating a robust and highly saturated Tn-seq library (Figure 1) as demonstrated in previous studies from the oral cavity (Klein et al. 2012). Unsurprisingly, significant enrichment of COGs involving coenzyme metabolism, lipid metabolism, translation ribosomal structure and biogenesis, replication, recombination, and repair, cell wall/membrane/envelop biogenesis, post-translational modification, protein turnover, chaperone functions, secretion, and vesicular transport. Approximately ~20% (~350) of the total CDS within XH001's genome are assigned to unknown function (Figure 3).

As previously described, quorum sensing has been shown to influence the TM7x and XH001 relationship in biofilm (Bedree et al. 2018) and batch-culture conditions (He et al. 2015). Thus, a Tn-seq screen was implemented to determine genetic factors involved in the epibiotic-parasitic relationship for the first time, which reveled 273 candidate loci that were consequently selected. Insertional mutants in two intergenic regions just upstream of *lsrB* and *luxS*, APY09_02515--APY09_02520_ig and APY09_06105--APY09_06110_ig, were selected during this screen, albeit APY09_02520 (*lsrB*) and APY09_06105 (*luxS)* were not enriched, which suggests that regulation of these genes is more important than the genes themselves. This is consistent with the indirect regulation of quorums sensing genes and downstream biological processes (Sperandio et al. 1999) particularly within oral bacterial pathogens (Burgess et al. 2002, Merritt et al. 2005). Furthermore, the vast majority of CDS that were positively selected in XH001::Tn5 when associated with TM7x were involved in sugar transport or biosynthetic pathways validating

83

previous hypotheses regarding TM7x nutritional requirements and its co-association with XH001 (He et al. 2015, McLean et al. 2020). Lastly, Tn-seq (Van Opijnen et al. 2009) can be used to assess genetic fitness conditionally essential *in vitro* and *in vivo* (Ibberson et al. 2017). Additionally, the validated XH001 Tn-seq library presented in this study can be used for a variety of evolutionary screens including *in vivo* colonization experiments and evaluate changes in immune function with or without TM7x. This platform will lay more ground work to ultimately determine the putative pathogenicity and relevance of TM7x's clinical associations (Paster et al. 2001, Fredricks et al. 2005, Kuehbacher et al. 2008, Kianoush et al. 2014, Soro et al. 2014, He et al. 2015). Finally, the aggregations of these genetic tools derived from Chapter 2 and 3, could elevated the TM7x and XH001 relationship to a model system for understanding their role in oral health and disease, but also CPR biology.

Acknowledgements
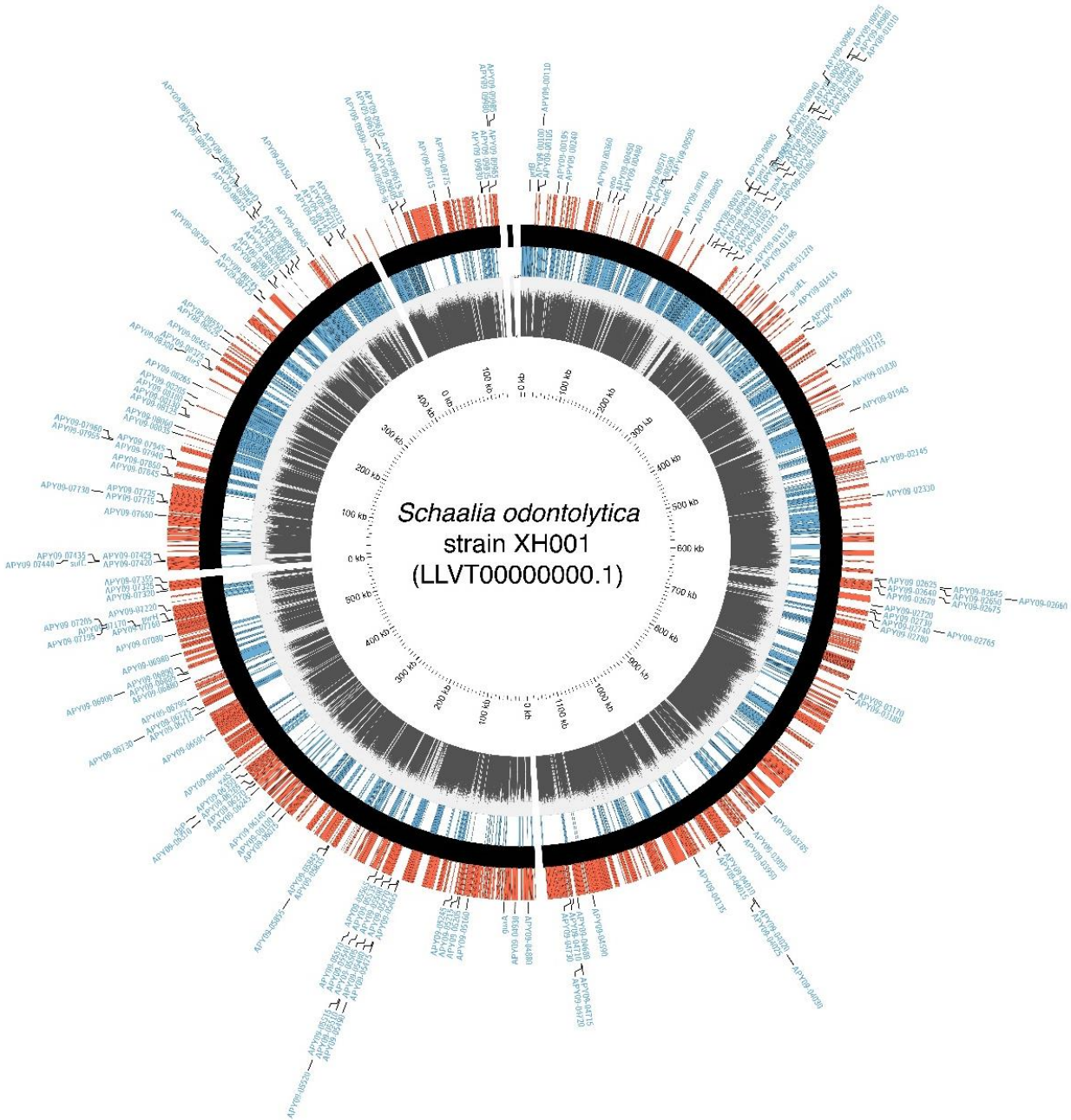
Figure 1. The Conditionally Essential Genes in XH001 for Growth on Solid Media. Fig. 1 represents all 203 conditionally essential genes, the most outer ring in light blue, designated by APY gene loci tags or designated gene name. The distribution of all Tn5 insertion density, + (red) and − (dark blue) strand insertions, across the genome is quantified as scaled from 10^0-10^5 (inner most grey ring).

Spearman Correlation Matrix - All Regions

A

	Lib1	Lib2	Lib3	Lib4	Lib5	Lib6
Lib1	1.000	0.881	0.879	0.864	0.895	0.866
Lib2	0.881	1.000	0.917	0.900	0.913	0.898
Lib3	0.879	0.917	1.000	0.898	0.927	0.910
Lib4	0.864	0.900	0.898	1.000	0.906	0.884
Lib5	0.895	0.913	0.927	0.906	1.000	0.903
Lib6	0.866	0.898	0.910	0.884	0.903	1.000

Spearman Correlation Matrix - CDS Only

B

	Lib1	Lib2	Lib3	Lib4	Lib5	Lib6
Lib1	1.000	0.963	0.956	0.955	0.960	0.959
Lib2	0.963	1.000	0.969	0.969	0.976	0.972
Lib3	0.956	0.969	1.000	0.964	0.971	0.968
Lib4	0.955	0.969	0.964	1.000	0.970	0.970
Lib5	0.960	0.976	0.971	0.970	1.000	0.971
Lib6	0.959	0.972	0.968	0.970	0.971	1.000

84

Figure 2. Robust Tn5 mutagenesis of the XH001 genome. Fig 1A represents the Spearman correlation matrix comparing the robustness of 6 individual Tn5 mutagenesis experiments assessing all of regions within the XH001 genome (intergenic and CDS). Fig 1B represents the Spearman correlation matrix comparing the robustness of 6 individual Tn5 mutagenesis experiments assessing all CDS regions within the XH001 genome. Only significant correlations (>0.8) are plotted.
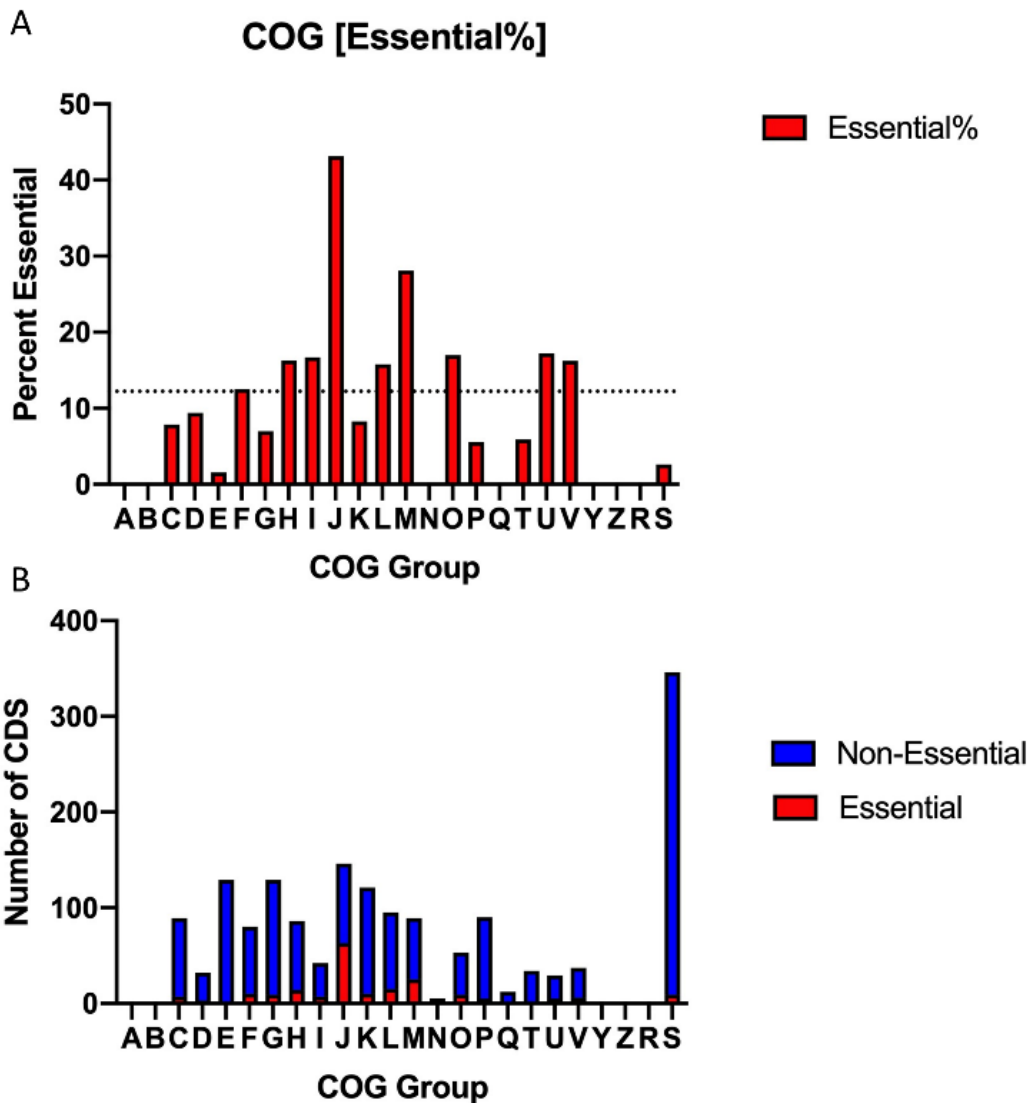
Figure 3. Clusters of Orthologous Groups in XH001. Fig. 1A represents the relative distribution of Clusters of Orthologous Groups (COGs) within the 12.2% conditionally essentials genes of XH001. Fig. 1B represents the relative non-essential to conditionally essential gene coding sequences (CDS). Both Figs. 1 and B utilize the following X-axis key as described (Angiuoli et al. 2011): [A = RNA processing and modification; B = Chromatin structure and dynamics; C = Energy production and conversion; D = Cell cycle control, cell division, and chromosome partitioning, E = Amino acid metabolism and transport, F = Nucleotide transport

and metabolism, G = Carbohydrate transport and metabolism, H = Coenzyme metabolism and metabolism, I = Lipid metabolism and metabolism, J = Translation ribosomal structure and biogenesis, K = Transcription, L = Replication, recombination, and repair, M = Cell wall/membrane/envelop biogenesis, N = Cell motility, O = Post-translational modification, protein turnover, chaperone functions; P = Inorganic ion transport and metabolism; Q = Secondary metabolites biosynthesis, transport, and catabolism; T = Signal transduction mechanisms; U = Intracellular trafficking, secretion, and vesicular transport; V = Defense Mechanisms; W = Extracellular structures; Y = Nuclear structure; Z = Cytoskeleton; R = General functional prediction only; S = Function unknown].
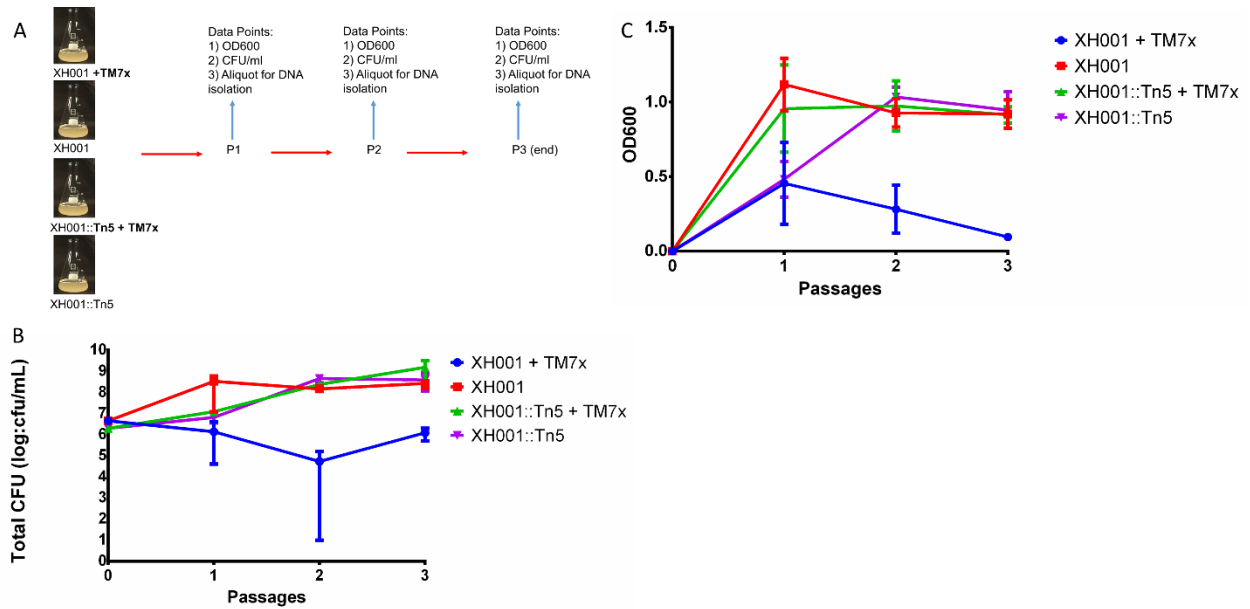
Figure 4. Tn-seq selection of XH001::Tn5 with TM7x during the Parasitic Event. Fig 1A

represents the work flow for TM7x selection against XH001::Tn5. Figure 1B and 1C represent

the Optical Density (OD600) and Total Colony Forming Units (CFUs/mL) captured during the

parasitic selection event as previously described in *Bor et al.* 2020. Each bar represents the

average of three independent culture performed in triplicate (*error bars*, range) for fig. 1B, and

for fig. 1C (*error bars*, *SD*).
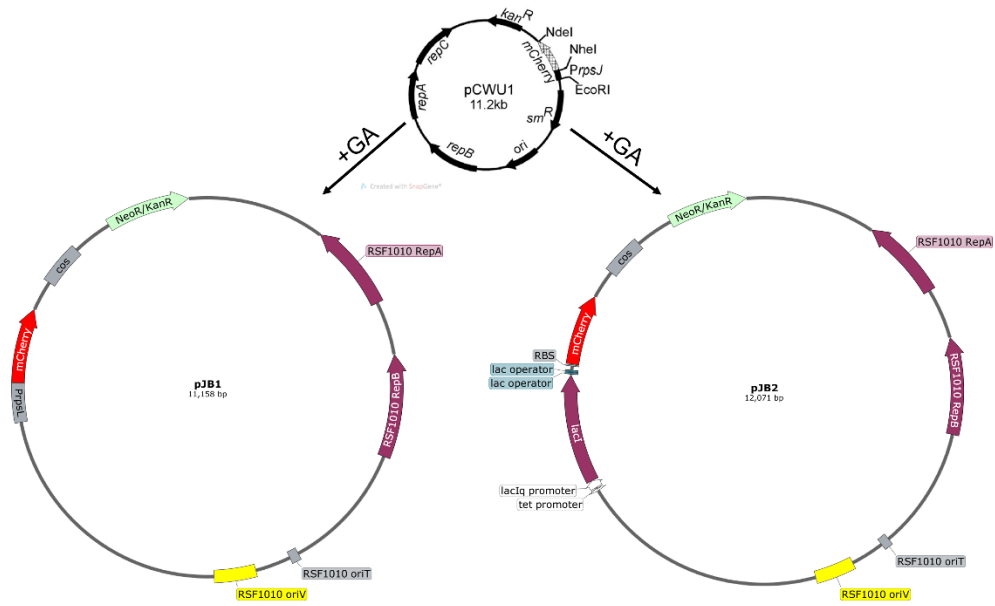
Figure 5. Gibson Assembly of pJB1 and pJB2. Schematic represents the Gibson Assembly

of PrpsL-mCherry or Plac-LacI/PlacO-mCherry gene blocks into pCWU1, the progenitor

plasmid. pCWU1 plasmid was adapted from (Wu et al. 2010).

rpsL-mCherry (pJB1)　　　　　　　　Plac-mCherry (pJB2)
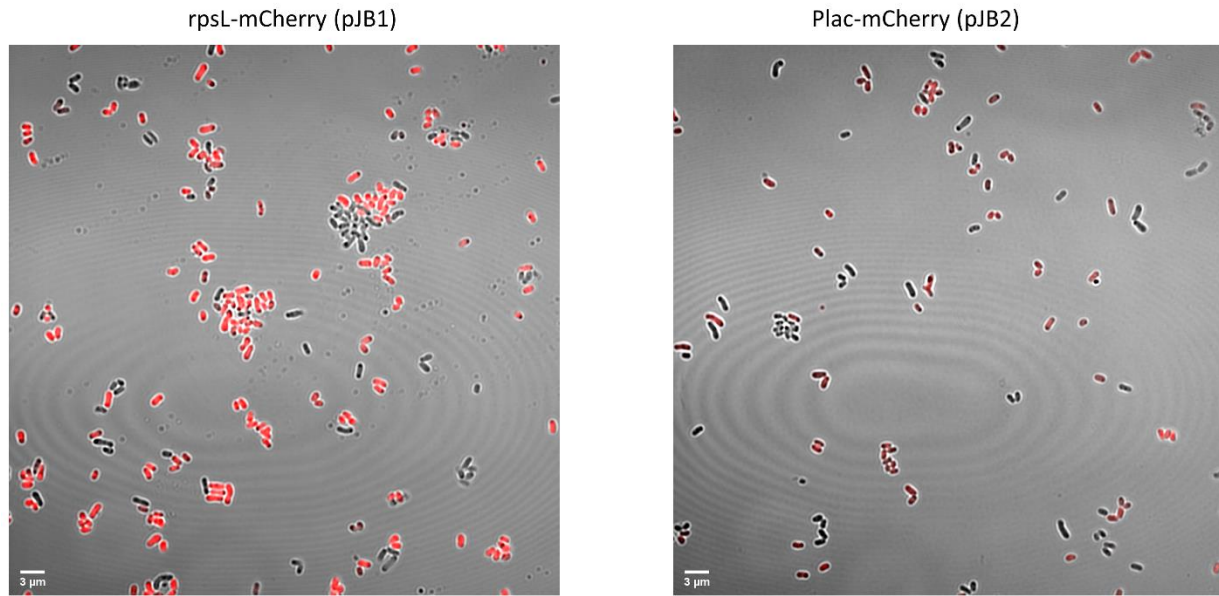
Figure 6. Representative Images of mCherry expression in XH001 harboring pJB1 or pJB2 via Confocal Microscopy. XH001 harboring pJB1 (n=3) or pJB2 (n=3) was treated with paraformaldehyde after overnight growth and visualized via Differential Contrast Transmission and Confocal Microscopy (Zeiss LSM 880) with objective Plan-Apochromat 63X/1.4 Oil.

rpsL-mCherry (pJB1)
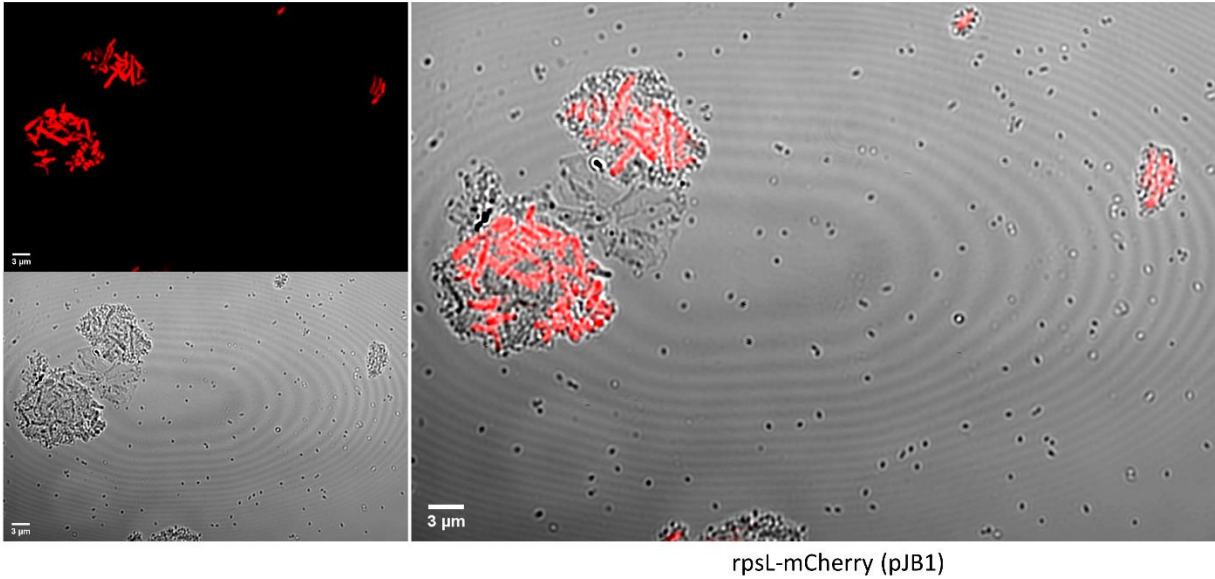
Figure 7. Representative Images of mCherry expression in TM7x-associated XH001 harboring pJB1 or pJB2 via Confocal Microscopy. TM7x-associatied XH001 harboring pJB1 (n=3) or pJB2 (n=3) was treated with paraformaldehyde after overnight growth and visualized via Differential Contrast Transmission and Confocal Microscopy (Zeiss LSM 880) with objective Plan-Apochromat 63X/1.4 Oil.

Table 1. Bacterial Strains and Media used in this study

Table 1 is attached as an excel file (.xslx)

Table 2. Conditionally Essential Genes in XH001

Table 2 is attached as an excel file (.xslx)

Table 3. XH001 COG Master List

Table 3 is attached as an excel file (.xslx)

Table 4. Master Gene List from Tn-Seq Selection of XH001::Tn5 with TM7x

Table 4 is attached as an excel file (.xslx)

Table 5. Passage 3 Candidate Gene List from Tn-Seq Selection of XH001::Tn5 with TM7x

Table 5 is attached as an excel file (.xslx)

Table 6. Viable Validation Gene List from Tn-Seq Selection of XH001::Tn5 with TM7x

Table 6 is attached as an excel file (.xslx)

Table 7. Fluorescent Plasmids and Primers Used in This Study

Table 7 is attached as an excel file (.xslx)

Table 8. pJB1 Plasmid Sequence

Table 8 is attached as a word file (.docx)

Table 9. pJB2 Plasmid Sequence

Table 9 is attached as a word file (.docx)

Chapter 4:   The Impact of Low-Earth Orbit Space Travel on The Rodent Microbiome

Abstract

Mankind's exploration into the cosmos, one of the remaining biological frontiers, coincides with increasing space travel durations and demands upon the human body. Yet, there is insufficient data related to the impact of microgravity on the human microbiome, the complex commensal microbial ecosystem intrinsically implicated in health and disease homeostasis, to inform safety health measure protocols to successfully navigate deep-space travel. The two human astronaut and Rodent Research 1 (RR1) studies demonstrated increases in alpha and beta diversity of gut microbiome associated with microgravity exposure. However, the RR1 study did not characterize the longitudinal effects on the gut or oral microbiome Post-Flight Return and the present RR5 study described herein provides a profound initial insight into bridging this knowledge gap. Here we demonstrate these data corroborate the previously observed changes in bacterial diversity of gut microbiome in the smaller RR1 study resulting from microgravity exposure and elucidates the effect of microgravity exposure on the first live-return rodent (LAR) flight study in the US. Furthermore, the increase in alpha and beta diversity associated with microgravity is the longest exposure to date for a rodent model and found enrichments of enzymes in the butanoate pathway functionally assigned to *Lactobacillus murinus* and *Dorea spp* in the International Space Station Terminal group (ISS) versus the terrestrial control (ISS_G). The reduction of the gut microbial diversity upon returning to Earth in the LAR group relative to terminal flight group (ISS) is corroborated by previous human studies. The LAR maintained persistent community structure alterations longitudinally Post-Flight Return, but stabilized relative to its terrestrial control (LAR_G). These data encourage higher resolution analyses of microgravity exposure via genomic, transcriptomic, and metabolomic studies aimed to elucidate the benefits and consequences of these microbial compositional shifts upon safely returning to earth, traversing past the Van Allen radiation belt, and beyond.

Introduction

Space travel delivers great stress to the human body, including cosmic radiation, sleep deprivation, psychological stress, and microgravity (Voorhies et al. 2016). The physical elements greatly alter the homeostasis of human physiology normally experienced on Earth. Microgravity has also been reported to alter the human microbiome, though the effects of this environmental stress remain underexplored (Garrett-Bakelman et al. 2019, Voorhies et al. 2019). Understanding the dynamic interactions between these commensal organisms will be important for developing therapies to maintain healthy homeostasis for future long-duration space travel (Voorhies et al. 2016). Innovations in genomic science and technology have enabled vast improvements in understanding the effect of the microbiome on both health and disease-associated states. Bacterial dysbiosis of the commensal microbiota is correlated with multiple diseases ranging from irritable bowel syndrome (Saulnier et al. 2011), bone homeostasis (Ali et al. 2009, Sjögren et al. 2012), various types of cancer (Giongo et al. 2011), and diabetes (Schwabe et al. 2013) to depression(Luna et al. 2015). Most recently, the NASA Twin study (Garrett-Bakelman et al. 2019), in addition to other long term studies (Voorhies et al. 2019), have repeatedly shown an increases in gut bacterial diversity in-flight relative to terrestrial conditions and in rodents from the NASA's Rodent Research 1 mission (Jiang et al. 2019). Lastly, while future studies with greater sampling sizes and temporal durations, such as the Rodent Research 7 mission and the NASA Astronaut Microbiome project already underway (Voorhies et al. 2016), there remains no reliable or well established rodent research model to test hypotheses generated from observational studies in humans.

As part of a large interdepartmental collaboration, the recent NASA's Rodent Research 5 mission (RR-5) provided a unique opportunity to test the use of BALB/c rodent as a potential *in vivo* rodent model system for evaluating the effects of microgravity on the host's microbiome. Using fecal samples obtained from non-treatment control groups, ISS Flight group (ISS) and a

Live Return Group (LAR), as part of a larger research study (Shi 2019), we sought to characterize the effects of these different gravitational environments in relationship to the gut and oral microbiome for BALB/c rodent. This study is the first live-return rodent research study conducted in the United States and provides our first look into the longitudinal effects of microgravity on the rodent oral and gut microbiomes in space and upon return to Earth.

Materials and Methods

Experimental Design and Timeline

All animals were handled in accordance with the institutional guidelines of the Institutional

Animal Care and Use Committee (IACUC) of the National Aeronautics and Space

Administration (NASA) and the University of California, Los Angeles (UCLA). Animals were

housed in a light- and temperature-controlled environment and given moisturized food or food

and water *ad libitum*. The animals used in this study are from the Rodent Research 5 (RR-5)

mission with its primary objective to test an osteoporosis therapy, BP-NELL-PEG (Shi 2019). In

this study, only animals that received control PBS therapy were used, and thus only control

animals and procedures are described in the methods below.

32-week-old BALB/c female mice were obtained from Taconic Biosciences (New York, U.S.A.)

and acclimated at NASA Kennedy Space Center in Florida, U.S.A. for 2 weeks in vivarium

cages and provided with water and standard chow. Baseline animals (n=20) were examined

and euthanized immediately before rocket launch. Experimental animals were randomly

assigned to the following groups (n=10/group): Live-Animal Return group (LAR), Full-Term

Flight group (ISS), Ground control group for LAR (LAR_G), and Ground control group for ISS

(ISS_G). Flight groups (LAR and ISS) were flown to space via SpaceX Dragon (CRS-11) and

housed onboard the International Space Station. Matching ground control groups (LAR_G and

ISS_G) were housed at the Kennedy Space Center, where light/dark cycles, CO_2, temperature,

and humidity were matched to that of ISS. At 5 weeks post-flight, LAR group was returned live

to Earth (UCLA) from space, and LAR_G group mice were shipped to UCLA from KSC. LAR

and LAR_G groups were both kept at UCLA to examine the effects of recovery for 4 additional

weeks. ISS and ISS_G groups remained in the Space Station and the Kennedy Space Center, respectively, for the 4 weeks. All animals were euthanized at termination (9 weeks post-launch).

Animal Husbandry:

All Flight and Ground groups were housed in the Rodent Habitat(Ronca et al. 2019, Choi et al. 2020), the next generation of NASA's Animal Enclosure Module (AEM), and provided with NASA Rodent Food Bar until delivery to UCLA, where they were placed in standard vivarium cages and provided with water and standard chow. All rodents continued with the same diet (NASA Rodent Food Bar) throughout the entire study (Supplementary Table 1). Throughout the duration of the experiment (9 weeks), animals received phosphate-buffered saline (PBS) injection peritoneally every 2 weeks. LAR and LAR_G groups were sampled pre-flight and post-flight return immediately upon live-return (at 5 weeks post-flight), and at terminal time-point (at 9 weeks post-flight). Individual fresh fecal samples and oral swabs were acquired Pre-Flight from each mouse, Post-Flight Return (24 hours post-earth arrival), and at termination (week 9 post-launch) for time-point microbiome analysis. ISS and ISS_G groups were euthanized in the Space Station and the Kennedy Space Center, respectively, and delivered to UCLA as frozen carcasses (at -80 °C). Thus, samples were acquired after carcasses were thawed for tissue harvest for all collaborating teams at termination during necropsy (Figure 2).

Fecal Sample Acquisition and Harvesting

Nominally, two freshly harvested fecal samples or more per mouse (in individual, autoclaved cages) were collected and placed in 2.0 mL sterile, nuclease free (RNAase/DNAase), non-pyrogenic, polypropylene Corning Cyrogenic vials. Samples were promptly "flash frozen" with liquid nitrogen for 15 minutes – one hour (within 2-5 hours of collection) and stored in a -80°C freezer. One fecal pellet (equivalent in mass) was used per mouse for DNA extraction and

sequencing of the 16S ribosomal RNA gene was then performed as previously described(Tong et al. 2014). Briefly, bacterial DNA was isolated using the QIAGEN Power Fecal DNA isolation kit (QIAGEN, Cat. No. 12955-4) with bead beating. All procedures were approved under IACUC Protocol Number: NAS-16-001-Y1.

Oral Sample Acquisition and Harvesting

The molars, cheeks and tongue (lingual and buccal) regions of the LAR and LAR_G rodents (3 swabs per mouse within each cage) were used as a consistent anatomical position for oral microbiome sampling. The rodents were anesthetized via ketamine and sampled. Specifically, Plasdent Maxaplicator Super fine (2 mm) swabs were used for collection (MPN# 600-R-2). DNA samples were processed using the Lucigen - Master Pure DNA isolation kit (Ca. No. MC85200). The experimental PBS controls and baseline, avoiding influence of the NELL-1 treatment. All procedures were approved under IACUC Protocol Number: NAS-16-001-Y1.

Sequence Quality Control and Noise Reduction of Fecal Microbiome Samples

The V4 region of the 16S rRNA gene was amplified and barcoded using 515f/806r primers then 2x150bp (paired-end) sequencing was performed on an Illumina HiSeq 2500 platform(Caporaso et al. 2012). The reads of amplicons from the V4 region of 16S rRNA were processed using the DADA2 package (Callahan et al. 2016) following a standard workflow of quality trimming, de-replicating, DADA2 denoising, read-pair merging and chimera removal steps with the following parameter settings: For quality trimming, truncLen=c(151, 144), maxEE=c(Inf, Inf), minQ=c(0, 0); for error rate learning and DADA2 denoising, selfConsist = TRUE, pool=TRUE; for chimera removal, method = "pooled". A total of 454 distinct amplicon sequence variants (ASVs) were identified by DADA2 among all samples. The distinct sequences were sorted according to their total counts in all samples in descending order and assigned a numeric sequence ID, e.g. seq1,

seq2, …, seq454, representing from the most abundant sequence to the least abundant sequence in terms of total read count in all samples.

Taxonomy Assignment of Fecal Microbiome Samples

Fecal ASV sequences were searched against a reference sequence set containing 16S rRNA sequences from all named prokaryotes downloaded from the SILVA high quality ribosomal RNA database(v132)(Quast et al. 2012) using "blastn". The best hit covering >= 95% of the query length was identified for each sequence. If the best hit shares >= 98% identity with query sequence, the query sequence is assigned the taxonomy of the hit to the species level. If the sequence identity between the query and the hit is greater than 97% but less than 98%, the query sequence is assigned taxonomy of the hit to the genus level. If a sequence does not have any hit with >= 97% identify, the taxonomy was not assigned. The genus level read count data, generated by the "tax_glom" function of Phyloseq (see methods) were used in this analysis.

Sequencing Noise Reduction and Sequence Quantification of Oral Samples

The sequencing of the V1-V3 region(Allen et al. 2016) of 16S rRNA was completed using a custom protocol(F. Escapa et al. 2020) and on the Illumina Mi-Seq platform. The 100x401 uneven paired-end reads of amplicons from the V1-V3 region of 16S rRNA were processed using the DADA2 package (Callahan et al. 2016) for quality trimming, de-replicating, and DADA2 denoising with default settings and following parameters: truncLen=c(100,200), maxN=0, maxEE=c(2,2), truncQ=2. Due to the sequencing gap between the two reads, the read pairs were concatenated by inserting 10 Ns in between two reads with the "justConcatenate=TRUE" option in the DADA2 "mergePairs" function. Chimera were then removed with the "removeBimeraDenovo" function using the "consensus" method. A total of 1,708 ASVs were identified and were subject to taxonomy assignment.

Taxonomy Assignment of Oral Samples

Oral ASV sequences were searched against a collection of species level full length 16S rRNA reference sequences consisting of the HOMD RefSeq V15.1, HOMD RefSeq Extended V1.11, GreenGene Gold and NCBI 16S rRNA Reference collections, based on a specie-level taxonomy assignment algorithm(Al-Hebshi et al. 2015) (Detailed algorithm and reference sequences available online at http://www.homd.org/ftp/NGS_Pipeline/Species_Level_BLASTN/).

Bacterial Diversity and Statistical Analyses

Samples that were obtained for oral and gut microbial community analysis assessed for the microbiome composition resulting from microgravity exposure. We profiled the microbial abundance and diversity of the flight groups ISS and LAR, as well as ground controls, ISS_G and LAR_G, avoiding influence of the NELL-1 treatment. All diversity and statistical analyses were done under the R statistical environment (version 3.6.1)(Team 2013). ASV count data, along with taxonomy assignment and sample meta information (Supplemental Tables 2-4), were imported into R using the *PhyloSeq* package(McMurdie et al. 2013). Count data were sub-sampled into various comparison groups (for example, to compare ISS and ISS_G ground control only relevant samples were included). After sub-sampling, ASVs with fewer than 10 reads in at least 2 samples, or fewer than 100 reads across all samples, were excluded, using the "filter_taxa" function. Count data were then rarefied to the same sampling depth based on the minimal sample sum among the comparison group using the "rarefy_even_depth" with the parameters "sample.size=minimal_sample_sum" and "replace=F" (where minimal_sample_sum = 56,000, 40,400 and 18,000 for ISS group, LAR Fecal and Oral group, respectively, as well as their controls).

Alpha diversity analysis was conducted by using the mean ASV counts (or species or genus counts) for each group as input to calculate Hill Numbers (or effective number of ASVs, species,

or genera) using the R package, *iNEXT*(Hsieh et al. 2016). The "iNEXT" function was used with the parameters "q=c(0,1,2),datatype='abundance', nboot=100". In this function, the Hill Number numerical equivalents were generated for interpolation of sample based rarefaction (solid line segment) and extrapolation curves with 95% confidence intervals (shaded region) and the "ggiNEXT" function was used to generate plots to illustrate a) q=0 (genera or species richness), q=1 (Shannon index), q=2 (Simpson index), and sample completeness curves (Hsieh et al. 2016). To assess the statistical significance of the difference in alpha diversity between two groups of samples, read count data of individual samples were subject to iNEXT to calculate the Hill Numbers. Hill Numbers at a fixed read count depth of 56,000, 18,000 for oral samples, were then extracted from the iNEXT results, so that all samples would have a Hill Number at the same sampling depth for fecal samples. Three groups (Preflight LAR, Preflight LAR_G, and Post-Flight Return LAR_G) lost one sample with the 56,000 cutoff and only have 9 samples for fecal microbiome analysis, the remainder contain all ten. Hill numbers between two groups of samples were then statistically assessed for their difference using the R functions to perform unpaired two-sample statistical tests either by 1) "t.text" function for Student's T-test, or 2) "wilcox.test" function for Wilcoxon ranksum test.

Beta diversity was assessed by non-metric multidimensional scaling (NMDS) - rarefied count data of the comparison group were subject to the "ordinate" R function specifying "NMDS" as the ordination method and "bray" specifying Bray-Curtis as the distance calculating function. To assess whether the variation in distances can be explained by the test groups, the "adonis" R function (analysis of variance using distance matrices, a form of nonparametric multivariate analysis of variance) were used to partition sums of squares and calculate the R^2 and *p* values (R^2 is the portion of the variants that can be explained, and *p* value indicating the possibility of the result by chance). To identify and illustrate differentially abundant microbes at various taxonomic ranks (i.e., from ASV to domain) the "compare_group" function in the R package

metacoder(Foster et al. 2017) was used to determine the differences in median abundances between two groups of samples. The *p* values were measured using the Wilcoxon Rank-Sum test, followed with adjustment for multiple comparisons using the "fdr" method. Abundance ratios of taxa with non-significant *p* value (>0.05) were set to zero so that they will not show in the final differential abundance taxonomy tree, which was compiled with the "heat_tree" function in the *metacoder*. Firmicutes/Bacteroidetes ratios were calculated by agglomerating the read count data to the phylum level using the "tax_glom" function provided by the R *PhyloSeq* and *ggplot2* packages (McMurdie et al. 2013), and the log2 count ratios between the two phyla were calculated for each sample. Wilcoxon Rank-Sum test was then performed to evaluate the difference between the test groups.

Metagenome Analysis of ISS vs ISS_G Groups

Whole genome shotgun (WGS) sequencing was performed at the University of Washington's Northwest Genomics Center (NWGC) on 10 biological replicates for both ISS and ISS_G rodents respectively (N=20). Sequencing libraries were generated using KAPA HTP Library Preparation Kits (07961901001, Roche) and sequenced on an Illumina NovaSeq 6000 System using a S Prime flow cell configured for 300 cycles which resulted in a total of 1,342,813,654 reads with an average of 70,674,403 reads per sample. Raw paired-end reads were then filtered, trimmed for quality, and screened against a mouse (C57BL) reference database using kneadData(McIver et al. 2018). Filtered reads were then analyzed using the Metagenomic Intra-Species Diversity Analysis System (MIDAS) (database v.1.2, Species Coverage Cutoff 0.01, Merge Sample Depth Cutoff 1.0) (kkerns85/midas_nextflow.git). Species, gene, and single nucleotide polymorphism (SNP) analysis were performed (database v.1.2, Species Coverage Cutoff 0.01, Merge Sample Depth Cutoff 1.0). Species were identified by clustered sub-species (>95% ANI) and assigned by a reference genome for that cluster. A total of 67 species clusters were identified. Genes were identified and mapped to pangenomes of these sub-species clusters and then annotated using

an in-house annotation pipeline utilizing the Pathosystems Resource Integration Center (PATRIC) Database (v. 3.6.5). Differential species abundance was determined using mean relative abundance between ISS and ISS_G after imposing a cutoff of a row-summed relative abundance ≥ 0.0001 and prevalence ≥ 20% of the total samples (4/20): resulting in a total of 50 species clusters that were then plotted using R (v. 15.6.0; Clustvis(Metsalu et al. 2015)). Differential gene abundance was analyzed using counts per million (CPM) normalized gene counts using the online web server Degust(Powell 2015) which calculated differential abundance by Voom/Limma (Min Gene Read Count 1.0, Min Gen CPM 1.0). Out of 396,080 total genes identified by MIDAS, 64,574 genes were determined to be differentially abundant. Use of a cutoff allowed for more stringent analysis of differentially abundant genes between ISS and ISS_G rodents (FDR P-value > 0.001, abs Log Fold Change = 3, > 8X Coverage), which resulted in 651 highly differentially abundant genes. Using the midas_merge function we were able to determine the coverage of genes by taxonomic group. In order to better investigate this, we utilized RNASeq2G (unpaired, group 0, min read count 10, normalized using trimmed mean of M values (TMM), and log normalized using local polynomial regression, Loess(Zhang et al. 2017)) within R. TMM normalized gene counts were then used to determine differences in Enzyme Commission numbers (EC's) for various KEGG annotations. Heatmaps were generated using Clustvis(Metsalu et al. 2015) in R. TMM normalized gene counts were then converted to using a row z score $(x - (mean(x)) / std(x))$. Statistical analysis of these differences in EC's was determined using non-parametric Kruskal-Wallis anova (p values adjusted by FDR). For statistically significant groups, the non-parametric Wilcoxon Ranked Sum test was applied (p values adjusted by FDR). EC pathways were mapped using Kyoto encyclopedia of genes and genomes (KEGG) and Metacyc. An Rmarkdown will be made available if this is integrated into the publication and made publicly available and linked to the manuscript. Supplemental tables will be provided for raw reads, species and gene counts, normalization methods, and statistics.

Results

Longitudinal assessment of the LAR microbiome post-flight return reveals similar microbiome diversity to LAR_G. The landmark RR-5 mission enabled the first live-return rodent experiment in the United States and the opportunity to assess the gut and oral microbiome composition resulting from post of microgravity exposure as well as longitudinal evaluation. Half the rodents (LAR) from the International Space Station returned alive and were analyzed post-flight return (week 5) to assess any longitudinal changes in the gut microbiome as a result from microgravity exposure until termination (week 9). Corresponding microbiome samples were analyzed using 16S rRNA amplicon sequencing. To assess biodiversity of these communities, taxonomically assigned reads were converted to Hill Numbers (Hill 1973) or 'Effective Number of Species/Genera', which are a mathematically unified set of diversity measures and obey *the replication principle or doubling property*, as previously described (Jost 2007, Chao et al. 2010, Chao et al. 2014, Hsieh et al. 2016), that enabled the most reliable analysis of 16S rRNA phylogenetic data throughout the study by factoring in relative abundance and phylogenetic diversity accordingly. Post-flight return (week 5) analysis demonstrated the LAR flight group was comparable in alpha and beta diversity as well as Firmicutes/Bacteroidetes ratio in the gut (Fig. 2) and oral (Supplementary Fig. 1) microbiome composition relative to LAR_G. This observation held true until termination, indicating a stabilization of the gut microbiome, when assessing fresh fecal samples (Fig. 1, Supplementary Data Tables 1-3) or at necropsy (Supplementary Fig. 2a, Supplementary Data Tables 4), and the oral microbiome (Supplementary Fig. 1, Supplementary Data tables 5-7). Additionally, post-flight return analysis also revealed enrichment of genera *Lactobacillus, Ruminiclostridum 9, Shuttleworthia,* and *Acetatifactor* with loss of *Escherichia-Shigella*, *Hungatella*, and *Acetatifactor*, that were not differently abundant by termination (Fig. 1).

107

Microgravity influences microbial diversity of the ISS flight group. The most recent assessment of the rodent gut microbiome exposed to microgravity was of modest sample size and involved only a short duration exposure to microgravity (Jiang et al. 2019). To gain insights into the effects of longer term exposure to microgravity, the gut microbiome of the ISS group, which remained in the International Space Station until termination, was compared to its terrestrial corresponding ground control, ISS_G. Fecal samples were acquired at necropsy after euthanasia at termination (week 9). Evaluation of the microbiome diversity of the ISS group and its corresponding ground control, ISS_G, revealed statistically significant increases in overall alpha and beta diversity compared to the ISS_G control group as previously observed (Jiang et al. 2019), albeit with no change in genera richness, that were correlated with microgravity exposure (Fig. 1). Hill number analysis determined a mean total of 72 genera, genera richness (q=0), that were detected in the ISS group relative to 73 genera in the ISS_G (Fig. 2a, 2b, 2c). However, the observed Hill numbers from the Shannon (q=1), 7.4 , and Simpson (q=2), 3.7, alpha diversity indices were modestly increased in the ISS group relative to ISS_G with 4.63 (q=1), and 2.29 (q=2) respectively. Community structure analysis revealed increases in beta diversity between ISS and ISS_G (p=0.016) (Fig. 1d). Furthermore, the ISS group showed a significant increase in the relative abundance of the phylum *Firmicutes* relative to *Bacteroidetes* (Fig. 2e) compared to ISS_G. A comprehensive analysis of differential genera abundance was carried out using *metacoder* (Foster et al. 2017). This analysis revealed several enriched genera within the ISS group relative to ISS_G, including: *Ruminiclostridium 9*, *Romboustia*, *Clostridium Sensu Stricto 1*, and *Shuttleworthia* as well as loss of *Hungatella* and *Lachnospiraceae UCG-001* (Figure 2f, Supplementary Data Table 1). These data suggest a dramatic shift in gut microbiome composition consistent with the previous reports in both human astronauts (Garrett-Bakelman et al. 2019, Voorhies et al. 2019) and rodents (Jiang et al. 2019).

Significant microbiome compositional structure alterations detected between the ISS and LAR group at termination. To determine the microbiome diversity of the ISS group relative to LAR at termination, fecal samples from necropsy (LAR) were additionally processed, sequenced, and analyzed as stated above and in the methods. We observed statistically significant increases in alpha (Fig. 3a, 3b, 3c) and beta (Fig. 3d) diversity measures of the ISS grouped compared to LAR. The observed Hill numbers from genera richness analysis (q=0) demonstrated a mean total of 69 genera that were detected in the ISS group relative to 61 genera in the LAR, (p=1.0e-3). The Shannon (q=1), 7.4 , and Simpson (q=2), 3.7, indices were significantly increased in the ISS relative to the LAR group with a Shannon index, 2.9, and Simpson index, 2.2. Community structure analysis observations revealed increases in beta diversity, between ISS and LAR. Furthermore, there was a statistically significant increase in the relative abundance of the phyla Firmicutes relative to Bacteroidetes (Fig. 3e) in the ISS relative to the LAR group. Additionally, differential genus abundance comparisons of genera(Foster et al. 2017) using metacoder (Foster et al. 2017) revealed several enriched genera in the ISS group relative to LAR (Fig. 3f, Supplementary Table 8) Intriguingly, ISS vs LAR comparisons at termination showed enrichment of *Lactobacillus* akin to LAR and LAR_G at post-flight return. However, this effect was not found when comparing ISS vs ISS_G.

Metagenome analysis of the ISS flight and ISS_G ground control groups reveals gene cluster enrichment of short chain fatty acid production.

In addition to applying amplicon sequencing strategies to investigate taxonomic differences between the ISS and ISS_G, whole genome shotgun (WGS) metagenomic sequencing was also performed in order to help elucidate the functional capacity and differential gene abundance between these groups. Using the Metagenomic Intra-Species Diversity Analysis System (MIDAS)

we carried out a robust species and gene level metagenomic analysis of fecal microbiome obtained from ISS_G/ISS rodents. MIDAS utilizes a universal set of single copy marker genes to determine relative abundance of species level assignments. Here we identified several differentially abundant species between ISS_G and ISS (Figure 4a) as well as determined that beta diversity between samples was significantly different between groups (Figure 4f). A total of 65 species clusters was identified within this WGS analysis, with 51 species being shared between the ISS_G and ISS group and 7 unique species within each group respectively. Some of the most differential abundant species between ISS_G and ISS included *Lactobacillus murinus* and *Dorea sp.* (Figure 4c). Species clusters assigned by MIDAS were compiled to generate pangenomes and used to map the remaining unassigned reads. A total of 396,080 genes were identified with 65,547 of those differentially abundant when compared by EdgeR differential analysis using weighted trimmed mean of the log abundance ratios (TMM). Due to the large number of differentially abundant genes, a strict cutoff was applied to isolate the most significantly different genes between ISS_G and ISS rodent and to identify associated metabolic functions. We used gene assigned enzyme commission numbers (EC's) to compare gene differences between the ISS_G and ISS groups. Multiple metabolic pathways were greatly enriched within the ISS group when compared to the ISS_G, even though the ISS group had 4,762 fewer genes per sample on average (Figure 4e). Butanoate metabolism (BM) was significantly enriched within the ISS group. Thu, we pulled all of the EC's associated with BM from all 396,080 genes and aimed to identify differentially abundant BM associated EC's as well as the taxonomic contribution to those EC's within each group (Figure 4b). Of the 5 identified differentially abundant EC's associated with BM, 60% were only found in one species – *Lactobacillus murinus*. We mapped the differentially abundant EC's for the BM pathway using the Kyoto Encyclopedia of Genes and Genomes (KEGG) and Metacyc. This result indicated that *L. murinus* provides a unique function within the ISS gut microbiome community in which it converts Pyruvate to either meso-(R,S) 2,3-

110

butanediol or para (R,R) 2,3-butanediol under aerobic and/or anaerobic conditions (Figure 4d). The product, 2,3-butanediol, and its role in gut health and gut microbiome research is not well understood or discussed in the literature. This is a novel observation and warrants further investigation.

Discussion

To our knowledge, this is the first live animal return study in the United States ever conducted to evaluate how microgravity is affecting the microbiome in a rodent model system. Furthermore, this study used the largest rodent cohort and longest temporal duration of microgravity exposure to date. Importantly, there are limitations to this study and interpreted outcomes: cosmic radiation is known to negatively disrupt the GI epithelial integrity (Kumar et al. 2018) and previous work during the shuttle era (Space Shuttle Atlantis mission STS-135) studied dietary regimens to mitigate radiation induced effects (Ritchie et al. 2015). Therefore, it is an important variable to consider when interpreting low-earth orbit microbiome data, though *Jiang et al*. 2019 demonstrated microbiome diversity shifts observed were markedly different from that of spaceflight effect (STS-135) . Additionally, it is now well established that iatrogenic effects such as transportation (Ma et al. 2012, Bidot et al. 2018, Montonye et al. 2018), vendor source (Ivanov et al. 2008, Hufeldt et al. 2010, Denning et al. 2011, Ericsson et al. 2015, Hart et al. 2018), as well as environmental, stress, caging, bedding, ventilation, and husbandry effects can affect the rodent microbiome composition (Franklin et al. 2017, Bidot et al. 2018, Ericsson et al. 2018). To circumvent these stressors for the ISS and ISS_G groups (LAR and LAR_G returned to standard vivarium cages post-flight return to UCLA), NASA utilizes the Rodent Habitat (Ronca et al. 2019, Choi et al. 2020), the next generation of the Animal Enclosure Module (AEM) that is a sophisticated rodent housing unit (with a built in air-particle filter more selective than HEPA-0.1 micron) to conduct rodent spaceflight research and has been successfully used in over 26 rodent spaceflights (Moyer et al. 2016). A recent study performed robust analyses assessing animal health and wellness, including animal growth and body masses, organ masses, rodent food bar consumption (Supplementary Data Table 9), water consumption, and blood contents and found AEM housed rodents to be in normal biological ranges when compared to traditional vivarium housed rodent (Moyer et al. 2016). Furthermore, due to the

112

NASA biosafety concerns, IACUC regulations, and constrain of the experimental setup, no data are available for the gut or oral microbiome composition for these LAR rodents on International Space Station before return to earth. However, considering the consistent genetic background, and well-controlled design, the gut microbiome of ISS group rodents at week 5 is plausibly similar as the LAR group at post-flight return. Thus, the argument could be made that microgravity exposed rodents are sensitive to microbial disturbance, for example, resulting in the rapid loss or enrichment of certain existing species compared to humans (Garrett-Bakelman et al. 2019, Voorhies et al. 2019), leading to a quick reverse in microbial diversity to a level comparable to the ground control group. Furthermore, the microbial shift post-flight was far from a total recovery. However, despite the significant microgravity correlation, as well as new housing environment effects on the microbiome composition observed (Supplementary Fig. 2), these data indicate a persistent microbiome shift in the post-flight until termination. Despite experiencing the same diet, it is difficult to directly conclude its influence other than the observation of a persistent microbiome shift longitudinally. Additionally, the LAR and LAR_G groups in this study allowed us to monitor any further gut and oral microbiome longitudinal changes after returning to earth for the first time in a rodent model. Based on the recent human observation of reduction in alpha diversity in human astronauts (Garrett-Bakelman et al. 2019, Voorhies et al. 2019) after returning to earth, we hypothesized that alpha and beta diversity changes in the rodent gut microbiome would also reduce in the LAR group post-flight or at termination relative to the ISS group (Fig. 3), albeit with no change compared to the LAR_G (Supplementary Fig. 2a). Further, we demonstrated persistent community structure alterations when comparing the LAR to the ISS terminal group (Fig. 3).

Intriguingly, we also found statistically significant increases in overall alpha (Shannon and Simpson indices, but not richness) and beta diversity (Bray-Curtis Dissimilarity), within the gut microbiome of the ISS Flight group when compared with the ISS_G ground control, associated

with microgravity exposure and is partially corroborated by previous human (Garrett-Bakelman et al. 2019, Voorhies et al. 2019) and rodent studies (Jiang et al. 2019). Further, our study did not observe the increases in richness as observed in the RR1 study despite recapitulating the increase in the Shannon index and beta diversity. Additionally, there is some contradiction between the *Garret-Bakelman et al.* 2019 and *Voorhies et al*, which did not find an increase in alpha diversity associated with microgravity, but did find a correlated increase in beta diversity. *Voorhies et al.* 2019 did find increases in richness and the Shannon index associated with microgravity and reduced upon returning to Earth, which was recapitulated in the LAR group post flight return until termination (Fig. 2). Interestingly, the LAR did not show any changes in the oral microbiome diversity when assessed for biodiversity (Supplementary Fig. 1), corroborating the human astronaut tongue microbiome analysis when comparing pre and post-flight timepoints (Voorhies et al. 2019). A potential explanation for the minor differences observed in all of these studies would be the varying use of different DNA extraction methods (Hart et al. 2015), next generation sequencing, as well as phylogenetic markers used in the pipeline analysis, as well as the different reference databases used.

Under these notions, our findings, along with previous studies (Garrett-Bakelman et al. 2019, Jiang et al. 2019, Voorhies et al. 2019), of increased microbial diversity in ISS group is partially surprising considering that microgravity, along with other flight factors such as radiation. Despite susceptibility to these space-flight stressors in rodents and humans alike, it is unclear how these data can be reconciled. Terrestrially speaking, the well-accepted concept in ecological gut microbiome dynamics, which is the positive correlation between biodiversity and ecosystem stability, associates decreases in gut microbial diversity as one of the hallmarks of gastrointestinal inflammatory diseased states, such as Inflammatory Bowel disease or Crohn's disease (Mosca et al. 2016). However, the opposite association is found in oral disease states when evaluating the microbiome (Zheng et al. 2015, Lee et al. 2017, Gao et al. 2018, Tsai et al. 2018). Thus, these

paradigms may not hold true in the absence of terrestrial gravitational forces or excess radiation exposure normally deflected by the earth's electromagnetic field. Nonetheless, long-term exposure to microgravity and low-earth orbit/beyond could impose significant adverse effects, such as systematic and local microenvironment changes that are likely to impact host-microbiomes, and induce adaptive and pathophysiological changes in digestive structures and physiology (Rabot et al. 2000). Naturally, assessing causal outcomes of dysbiosis, such as inflammation in the colonic epithelial layer, in the ISS group relative to ISS_G was of high priority, but impossible due to the primary objective of RR5, which required freezing the carcasses prior to flight return for assessment and co-variables such as cosmic radiation exposure (Kumar et al. 2018). Thus, the tissue was compromised from the freeze-thaw event and could not be reliably assessed (data not shown). However, increasing evidence suggests that an increased *Firmicutes*/*Bacteroidetes* ratio change has been widely considered a signature of gut dysbiosis (Mariat et al. 2009, Sanz et al. 2014, Strati et al. 2017). In this study, an increase relative abundance in Firmicutes, as well as decrease in *Bacteroidetes* (F/B ratio), was associated with microgravity exposure (Fig. 1) and is consistent with the pattern of microbiome flux observed in the RR1 microgravity related rodent study (Jiang et al. 2019). When comparing the ISS vs LAR groups, we found the F/B ratio in the LAR group to decrease relative to the ISS group (Fig. 3e) as seen in the NASA Twin study (Garrett-Bakelman et al. 2019). Furthermore, a recent study in a mouse colitis model found increases of many genera, including *Romboutsia* and *Clostridium_Sensu_stricto_1* in the colitis disease group relative to the control (de Bruyn et al. 2018), which was found to be increased in the ISS group relative to ISS_G.

Here for the first time we show that *Lactobacillus murinus*, a commensal rodent gut bacterium, is enriched in the ISS rodents in comparison to the ISS_G cohort. This differentially abundant species seems to provide a unique metabolic function within the butanoate metabolic pathway within ISS rodents (Figure 4). Interestingly, *Dorea* sp. was also found to be enriched within the

ISS cohort. Notably, *Dorea* sp. was only observed in 10% of the ISS_G cohort, and at very low relative abundance, 0.00124%. Yet *Dorea* sp. was found within 100% of the samples from the ISS group with increased relative abundance of 0.48% on average. There has been recent work linking the gut microbiome to bone formation and maintenance (Ali et al. 2009, Sjögren et al. 2012, Hernandez et al. 2016, Yan et al. 2016) and this study has enabled insight into these phenomena. Interestingly, in terrestrial rodent models, it has been shown that administration of SCFAs, as well as microbial metabolites, increased serum levels of insulin growth factor-1, IGF-1, a hormone that directly affects and leads to skeletal growth (Yan et al. 2016) and decreased CTX-1, P1NP, and NF-Kβ factors responsible for osteoclastic activity (Yan et al. 2016, Lucas et al. 2018). Moreover, SCFAs, primarily produced by GI anaerobes, are known immunomodulators and regulate systemic bone mass as well as prevent bone loss (Lucas et al. 2018). Our results showed an increase in functional enrichment of C4 SCFA gene pathways directly associated with *L. murinus* and *Dorea spp.* and elucidating any potential role of these bacterial-encoded SCFA related pathways in rodent bone homeostasis warrants further investigation.

Acknowledgements

Fig. 1 | Longitudinal Analysis of the Fecal Microbiome in the LAR Flight Group versus LAR_G Ground Control. a. Longitudinal differences in alpha diversity using richness (q=0), Shannon (q=1), and Simpson (q=2) diversity orders based upon sample-based rarefaction and extrapolation as previously described(Hsieh et al. 2016) for Pre-Flight, Post-Flight Return, and the Termination of the study (See methods). The Wilcoxon Rank-Sum statistical test was employed to compare LAR vs LAR_G groups for alpha diversity analysis. Non-statistical significance is not indicated. **b,** Beta diversity analysis between LAR and LAR_G groups showing a statistically significant difference between the LAR and LAR_G. Nonparametric multivariate analysis of variance (PERMANOVA) was used to indicate with p value for statistical comparison of variance using distance matrices between LAR and LAR_G groupings. **c,** Analysis of Firmicutes to Bacteroidetes ratios between the LAR and LAR_G groups. The Wilcoxon Rank-Sum statistical test was employed to compare LAR vs LAR_G where significance is indicated with p value. **d**, Analysis of genera enriched or lost in the LAR

compared with LAR control group. Taxa enriched or lost in the ISS group at a threshold of

p<0.05 compared to taxa present in the LAR group are represented in the *metacoder* heat tree

by a color intensity Log_2 median ratio scale.
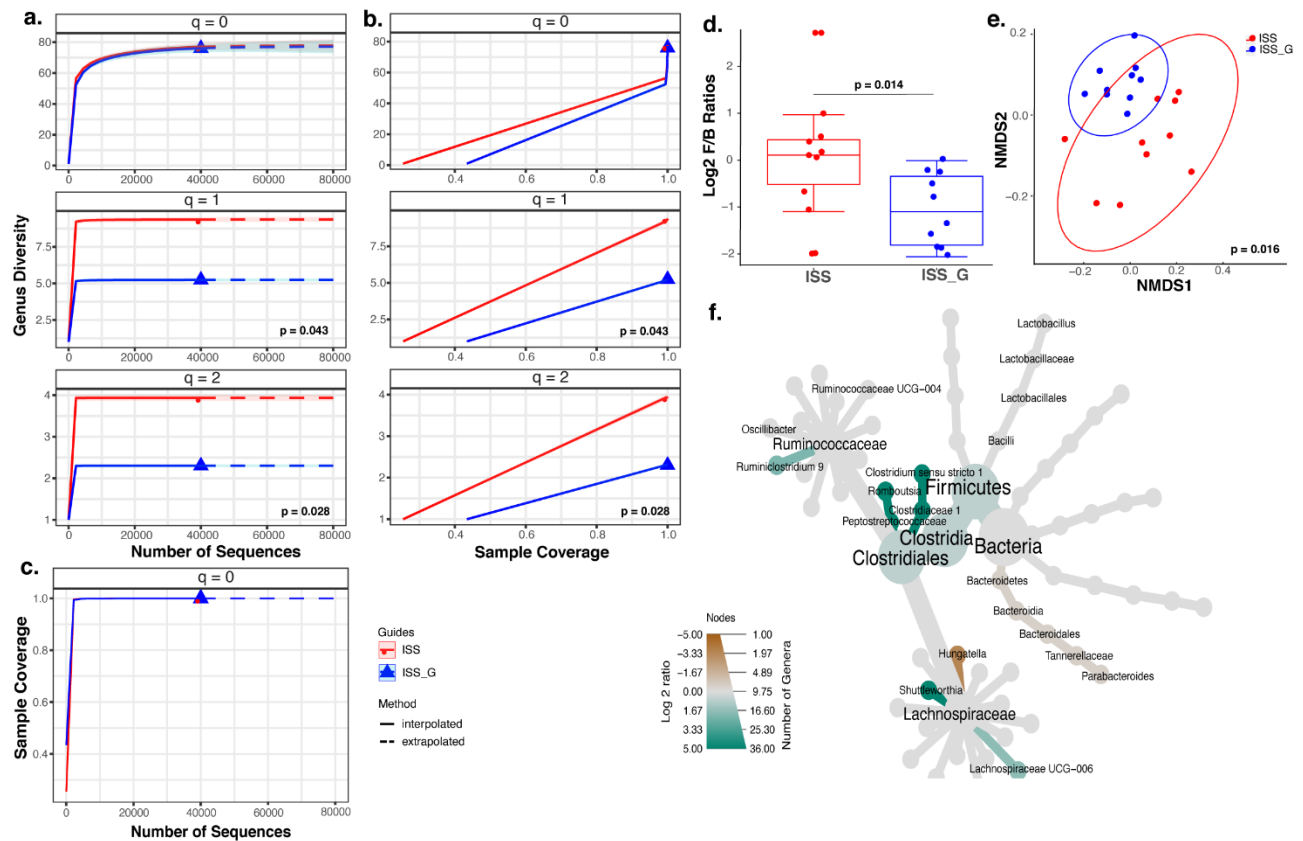
Fig. 2 | Alpha Diversity, Beta Diversity, and Comparative Compositional Shift Analysis in the of the Fecal Microbiome in the ISS Flight group versus ISS_G Ground Control. a, bacterial genera richness (q=0), Shannon (q=1), and Simpson (q=2) diversity orders based upon sample-based rarefaction and extrapolation as described(Hsieh et al. 2016). The Wilcoxon Rank-Sum statistical test was employed to compare ISS vs ISS_G groups for alpha diversity analysis and statistical significance is designated with p value**. b** and **c**, coverage-based rarefaction and extrapolation. **d**, Beta diversity analysis between ISS and ISS_G groups showing a statistically significant difference between the ISS and ISS_G groups. Nonparametric multivariate analysis of variance (PERMANOVA) was used to calculate a statistical comparison (p-value) between the ISS and ISS_G groupings using distance matrices. **e**, *Firmicutes* to *Bacteroidetes* ratios between the ISS and ISS_G groups. The Wilcoxon Rank-Sum statistical test was employed to compare ISS vs ISS_G groups where significance is indicated with p

value. **f**, analysis of genera enriched or lost in the ISS compared with ISS_G control group.

Taxa enriched or lost in the ISS group at a threshold of $p<0.05$ compared to taxa present in the

ISS_G group are represented in the *metacoder* heat tree by a color intensity Log_2 median ratio

scale.
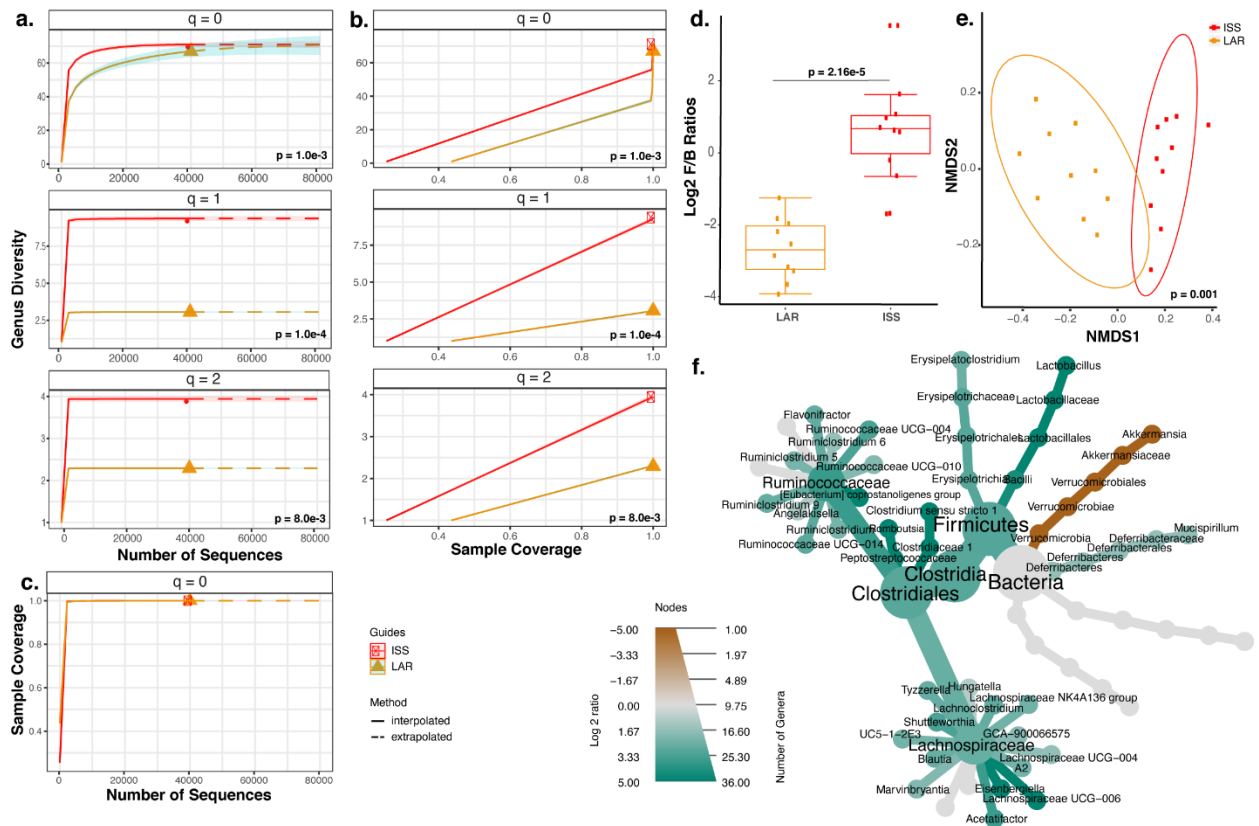
Fig. 3 | Alpha Diversity, Beta Diversity, and Comparative Compositional Shift Analysis in the of the Fecal Microbiome in the ISS Flight Group versus LAR Flight Return Group. a, statistically significant differences found in bacterial genera richness (q=0), Shannon (q=1), and Simpson (q=2) diversity orders based upon sample-based or coverage-based as in **b** and **c**, rarefaction and extrapolation as described(Hsieh et al. 2016). The Wilcoxon Rank-Sum statistical test was employed to compare ISS vs LAR groups for alpha diversity analysis and statistical significance is designated with p value. **d**, represents Beta diversity analysis between ISS and LAR groups showing a statistically significant difference between the ISS and LAR groups. Nonparametric multivariate analysis of variance (PERMANOVA) was used to indicate with p value for statistical comparison of variance using distance matrices between ISS and LAR groupings. **e**, represents analysis of Firmicutes to Bacteroidetes ratios between the ISS and LAR groups. The Wilcoxon Rank-Sum statistical test was employed to compare ISS vs LAR

groups where significance is indicated with p value. **f**, represents analysis of genera enriched or

lost in the ISS compared with LAR control group. Taxa enriched or lost in the ISS group at a

threshold of $p<0.05$ compared to taxa present in the LAR group are represented in the

metacoder heat tree by a color intensity Log_2 median ratio scale.
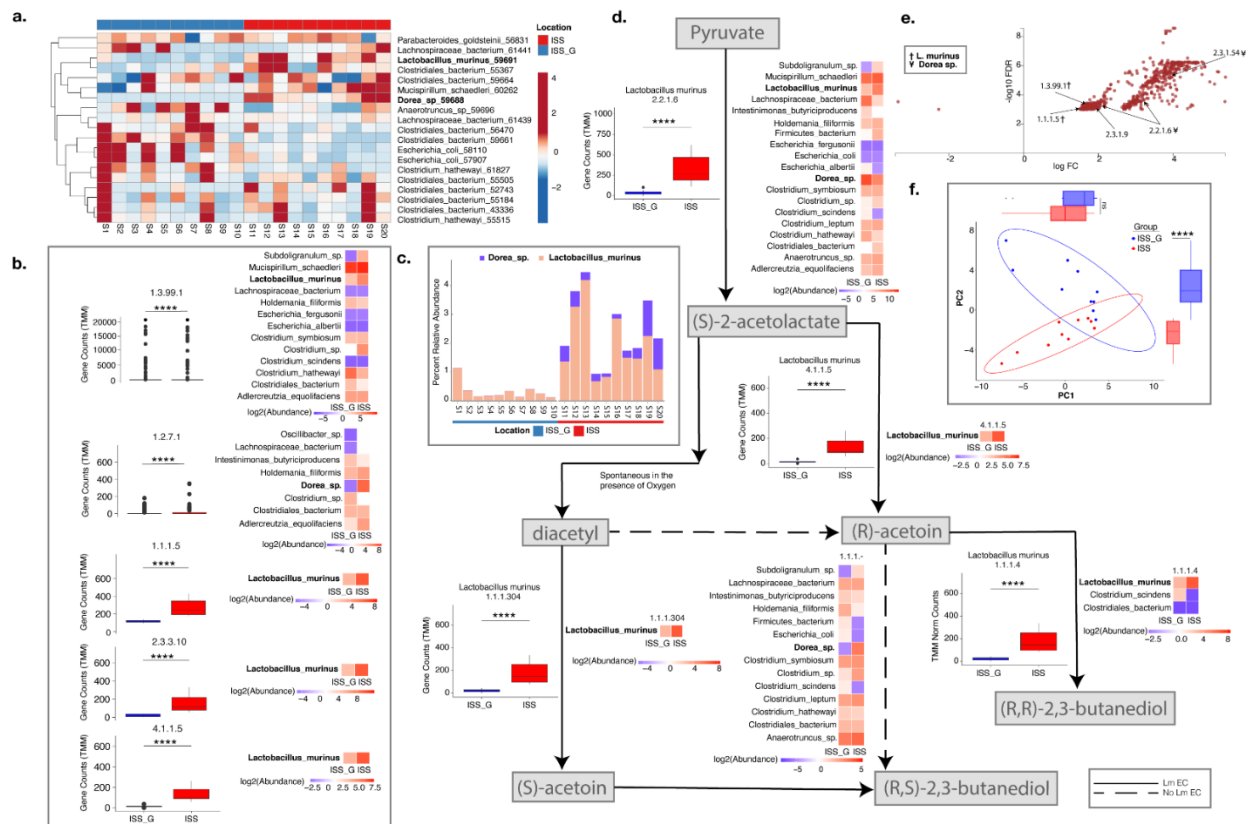
Fig. 4 | *Lactobacillus murinus and Dorea sp.* contribute differentially abundant genes encoding butanoate metabolic enzymes between ISS and ISS_G rodent as well as provides unique function within the community. Whole genome shotgun (WGS) sequencing was performed on a subset of ISS and ISS_G rodent fecal samples (N=20; 10 replicates for ISS and ISS_G respectively; 70,665,556 Average Reads/Sample, See Methods). Taxonomic assignment and gene characterization were performed using the Metagenomic Intra-Species Diversity Analysis System (MIDAS) (database v.1.2, Species Coverage Cutoff 0.01, Merge Sample Depth Cutoff 1.0, See Methods). **a.** Species diversity was filtered using mean relative abundance of Species Clustered Pangenomes assigned by MIDAS (≥95% ANI) between ISS and ISS_G rodent (cutoff min relative abundance ≥ 0.0001 and in 20% of the total samples). The top 19 differentially abundant Species clusters are highlighted as a heatmap showing Log Fold Change of relative

species abundance by sample and clustered by group (Clustvis, row z-score, See Methods). **b.** Significant differentially abundant genes with Enzyme Commission numbers (EC's) associated with Butanoate metabolism (BM; KO00650) identified by MIDAS were then further analyzed using RNAseq2G (Differential cutoff 10.0, Normalized by TMM, See methods). A total of 32 EC's hit BM KO00650; however, only 5 EC's were found to be significantly different between ISS and ISS_G rodent. Boxplots show differences in TMM normalized counts between ISS and ISS_G rodent (Wilcoxon Test, adjusted by FDR; See methods). Heatmaps show Log2 transformed TMM normalized counts between ISS and ISS_G rodent for BM associated EC's by taxonomy (See methods). EC 1.1.1.5, 2.3.3.10, and 4.1.1.5 associated with BM were only present in samples containing *Lactobacillus murinus* (*Lm*). **c.** Relative abundance of Lactobacillus murinus and Dorea sp. between ISS_G and ISS rodent. Barplot shows the relative percent of Lm and Dorea sp. in each sample clustered by the ISS_G and ISS group location. **d.** Synthesis of 2,3-butanediol is driven by the prevalence of *Lm* in ISS rodent compared to those in ISS_G. Pathway products are shown in grey boxes, starting from Pyruvate and ending with either para (R,R) or meso (R,S,)-2,3-butanediol. Solid line shows the specific conversion from Pyruvate to both para and meso 2,3-butanediol by *Lm*; whereas, dashed lines are indicative of other BM enzymes present within the community. Boxplots show differences in TMM normalized counts between ISS and ISS_G by EC (Wilcoxon Test, adjusted by FDR; See Methods). EC 1.1.1.5 is now known to have dual function as EC 1.1.1.4 and 1.1.1.304 (See Methods). Heatmaps show Log2 transformed TMM normalized counts between ISS and ISS_G rodent for BM associated EC's by taxonomy (See methods). **e.** Differential gene abundance was analyzed using Degust (Voom/Limma, Min Gene Read Count 1.0, Min Gen CPM 1.0, See Methods). Volcano plot shows significant differentially abundant genes (red dots) by Log Fold Change vs the inverse Log of the FDR adjusted P-value. Of the 396,080 total genes identified by MIDAS, 64,574 genes were determined to be differentially abundant (Voom/Limma, See Methods). Genes associated with BM were identified as one of the

125

most significantly differentially abundant orthologous gene groups (KO00650) between ISS and ISS_G rodent with a total of 604 of the 1,983 total gene hits associated with BM being differentially abundant. Using a stringent cutoff, 6 of the 651 top differentially abundant genes are associated with BM and identified differentially abundant species between ISS and ISS_G rodent (FDR adjusted p value < 0.001, abs Log Fold Change = 3 (> 8X Coverage)). **f.** Principle component analysis (PCA) was determined using Midas species TMM normalized counts by group, ISS_G and ISS. Marginal boxplots show the differences in PC distances for PC1 and PC2 by group (Wilcoxon Test, adjusted by FDR, See Methods). All boxplots show median and lower/upper quartiles; whiskers show inner fences (see Methods). All heatmaps show individual scales by EC or taxonomy. Stars show false discovery rate (FDR) corrected statistical significance (FDR: *P ≤ 0.05, **P ≤ 0.01, ***P ≤ 0.001, ****P ≤ 0.0001).
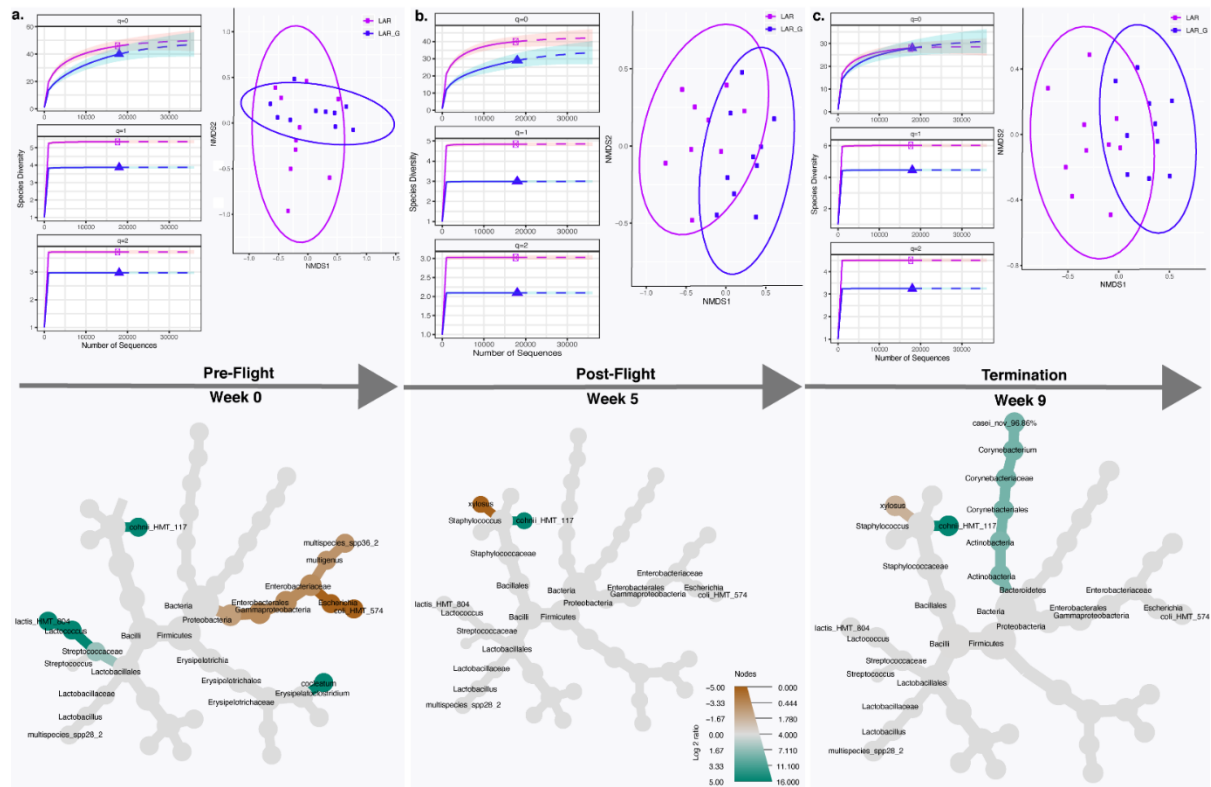
Supplementary Fig. 1 | Longitudinal Analysis of the Oral Microbiome in the LAR Flight Group versus LAR_G Ground Control. a, represents the sequence sample based upon sample size rarefaction and extrapolation for timepoints Pre-Flight, Post-Flight Return, and the Termination of the study. **a**, **b**, and **c**, represents differences found in bacterial richness (q=0), Shannon (q=1), and Simpson (q=2) diversity orders based upon sample-based rarefaction as described(Hsieh et al. 2016). The Wilcoxon Rank-Sum statistical test was employed to compare LAR vs LAR_G groups for alpha diversity analysis and statistical significance is designated with p value. **d**, represents Beta diversity analysis between LAR and LAR_G groups showing a non-statistically significant difference between the LAR and LAR_G groups represents analysis of species enriched or lost in the LAR compared with LAR_G control group. Taxa enriched or lost in the LAR group at a threshold of p<0.05 compared to taxa present in the LAR_G group are represented in the *metacoder* heat tree by a color intensity Log_2 median ratio scale.
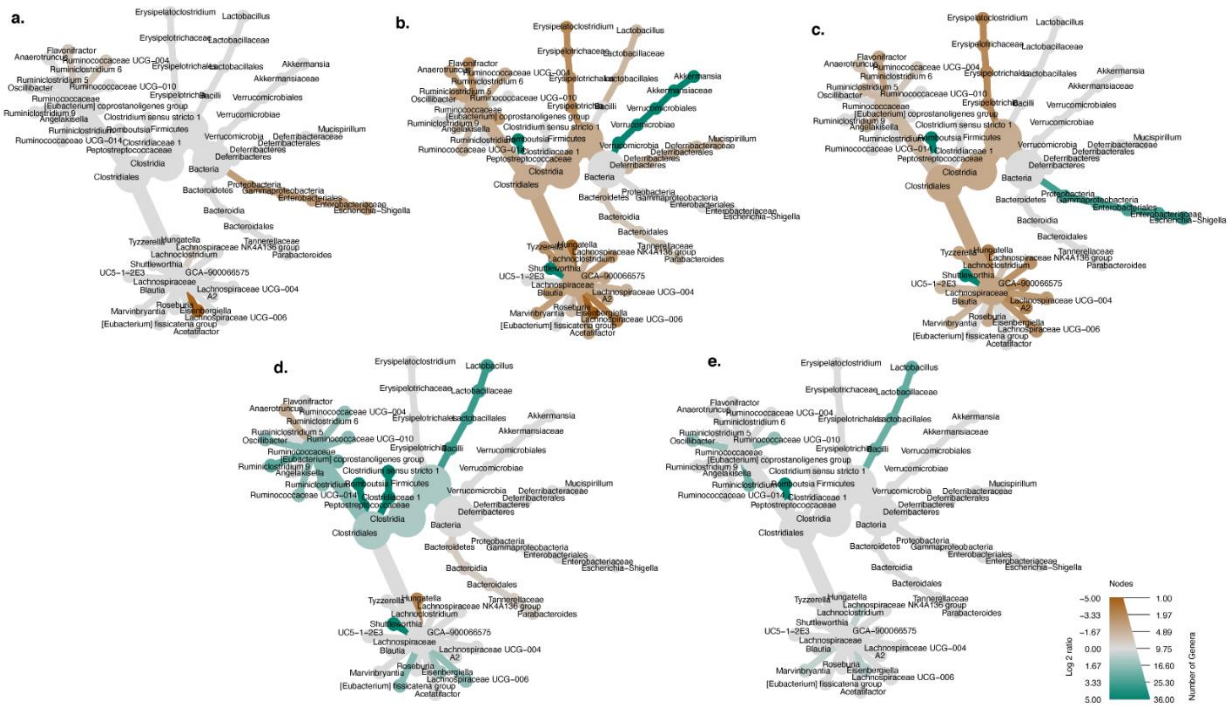
127

Supplementary Fig. 2 | Termination Analysis of Enriched or Lost Genera Evaluating Caging Effects. a. Analysis of genera enriched or lost in the LAR vs compared with LAR_G group. **b.** Analysis of genera enriched or lost in the LAR vs compared with baseline group. **c.** Analysis of genera enriched or lost in the LAR_G vs compared with baseline group. **d.** Analysis of genera enriched or lost in the ISS vs compared with baseline group. **e.** Analysis of genera enriched or lost in the ISS_G vs compared with baseline group. Taxa enriched or lost in the LAR group at a threshold of p<0.05 compared to taxa present in the LAR_G group are represented in the *metacoder* heat tree by a color intensity Log$_2$ median ratio scale.

Supplementary Data Table 1. MetacodeR_diff_table_Pre-Flight_LAR vs. Pre-Flight_LAR_G_Genus

Supplementary Data Table 1 is attached as an excel file (.xslx)

Supplementary Data Table 2. MetacodeR_diff_table_Post-Flight_LAR vs. Post-Flight_LAR_G_Genus

Supplementary Data Table 2 is attached as an excel file (.xslx)

Supplementary Data Table 3. MetacodeR_diff_table_Termination_LAR vs. Termination_LAR_G_Genus

Supplementary Data Table 3 is attached as an excel file (.xslx)

Supplementary Data Table 4. MetacodeR_diff_table_Termination ISS vs. Termination_LAR_Genus

Supplementary Data Table 4 is attached as an excel file (.xslx)

Supplementary Data Table 5. MetacodeR_diff_table_oral_Pre-Flight LAR vs. Pre-Flight LAR_G_species

Supplementary Data Table 5 is attached as an excel file (.xslx)

Supplementary Data Table 6. MetacodeR_diff_table_oral_Post-Flight_ LAR_vs Post-Flight_ LAR_G_species

Supplementary Data Table 6 is attached as an excel file (.xslx)

Supplementary Data Table 7. MetacodeR_diff_table_Termination_oral_

LAR_vs_Termination_LAR_G_species

Supplementary Data Table 7 is attached as an excel file (.xslx)

Supplementary Data Table 8. MetacodeR_diff_table_Termination_ISS vs. Termination_ISS_G_Genus

Supplementary Data Table 8 is attached as an excel file (.xslx)

Supplementary Data Table 9. MetacodeR_diff_table_Termination_LAR vs. Termination_LAR_G_Genus

Supplementary Data Table 9 is attached as an excel file (.xslx)

Supplementary Data Table 10. NASA RR5 Food Bar

Supplementary Data Table 10 is attached as an PDF file (.PDF)

Supplementary Data Table 11. meta_table_fecal

Supplementary Data Table 11 is attached as an text file (.txt)

Supplementary Data Table 12. otu_table_fecal

Supplementary Data Table 12 is attached as an text file (.txt)

Supplementary Data Table 13. tax_table_fecal

Supplementary Data Table 13 is attached as an text file (.txt)

Supplementary Data Table 14. meta_table_oral

Supplementary Data Table 14 is attached as an text file (.txt)

Supplementary Data Table 15. otu_table_oral

Supplementary Data Table 15 is attached as an text file (.txt)

Supplementary Data Table 16. tax_table_oral

Supplementary Data Table 16 is attached as an text file (.txt)

CONCLUSION

The co-cultivation of TM7x and XH001 presented a rare opportunity to enhance the current knowledge set regarding symbiotic and parasitic bacterial-bacterial interactions, but also illuminated poorly understood biological understanding of the new bacterial lineage, the Candidate Phyla Radiation, which comprises more than 25% of all bacterial diversity (Brown et al. 2015, Hug et al. 2016). Early transcriptomic profiling (RNA-seq) of TM7x-associated XH001 compared to XH001 alone revealed robust increases in expression of the AI-2 receptor ortholog encoding gene, *lsrB*, which was subsequently inactivated and demonstrated to be critical, along with *luxS*, in biofilm formation in the presence of TM7x (Bedree et al. 2018). Therefore, these data warranted more advanced genetic systems to tease out downstream effectors prompting the creation of a highly saturated Tn-seq library. This approach elucidated the conditionally essential genes in XH001 and the fitness of specific genes involved in sugar transport and biosynthetic genes likely involved in TM7x symbioses and/or parasitism as previously suggested (He et al. 2015, McLean et al. 2020).

Finally, exploration past the Van Allen Radiation belt intersects with augmenting durations of travel and demands upon the human body. The complex commensal microbial ecosystem intrinsically implicated in health and disease homeostasis, to inform safety health measure protocols to successfully navigate imminent deep-space travel, requires further understanding. Rodent Research 1 and human astronaut studies demonstrated increases in biodiversity of gut microbiome associated with microgravity exposure (Garrett-Bakelman et al. 2019, Jiang et al. 2019, Voorhies et al. 2019). This work recapitulates the previously observed increase in alpha and beta diversity of gut microbiome and furthermore, captures the effects on the first live animal return (LAR) rodent study in the US/NASA history to date. Gut microbial diversity reduction was correlated between the LAR and the flight group, ISS, which received double the microgravity exposure relative to LAR group and the previous RR1 study, upon return to earth as observed in human studies (Garrett-Bakelman et al. 2019, Voorhies et al. 2019). Furthermore, the LAR

maintained persistent community structure alterations longitudinally post-earth return, but stabilized relative to its terrestrial control, LAR_G. Lastly, *Lactobacillus murinus* was enriched in the ISS terminal cohort compared to the terrestrial control, ISS_G and bacterial-encoded short chain fatty acid production pathways involved in host bone homeostasis were enriched and functionally assigned to *L. murinus*. These data encourage higher resolution analyses of microgravity exposure via genomic, transcriptomic, and metabolomic studies aimed to elucidate the benefits and consequences of these microbial compositional shifts upon safely returning to earth, traversing past the Van Allen radiation belt, and beyond.

In conclusion, this work successfully sought to characterize a unique epibiotic parasitic relationship between XH001 and TM7x, a recent and the first uncultivatable CPR organism. Through powerful genetic screens to systematic single deletions, great insight was achieved into how TM7x associates with its host and potential impact on the oral microbiome. Finally, the fourth chapter enabled a broad scope view of microbial dynamics within the rodent microbiome on a macroscale relative to the microscope of bacterial-bacterial interactions.

References

Aas, J. A., B. J. Paster, L. N. Stokes, I. Olsen and F. E. Dewhirst (2005). "Defining the normal bacterial flora of the oral cavity." Journal of clinical microbiology **43**(11): 5721-5732.

Abrams, M., D. E. Barton, E. Vandaei, D. Romero, A. Caldwell and C. C. Ouverney (2012). "Genomic characteristics of an environmental microbial community harboring a novel human uncultivated TM7 bacterium associated with oral diseases." Open Access Scientific Reports **1**(5): 276.

Abusleme, L., A. K. Dupuy, N. Dutzan, N. Silva, J. A. Burleson, L. D. Strausbaugh, J. Gamonal and P. I. Diaz (2013). "The subgingival microbiome in health and periodontitis and its relationship with community biomass and inflammation." ISME J **7**(5): 1016-1025.

Agarwal, V., A. Kuchipudi, M. Fulde, K. Riesbeck, S. Bergmann and A. M. Blom (2013). "Streptococcus pneumoniae endopeptidase O (PepO) is a multifunctional plasminogen-and fibronectin-binding protein, facilitating evasion of innate immunity and invasion of host cells." Journal of Biological Chemistry **288**(10): 6849-6863.

Ahmed, N. A., F. C. Petersen and A. A. Scheie (2009). "AI-2/LuxS is involved in increased biofilm formation by Streptococcus intermedius in the presence of antibiotics." Antimicrobial agents and chemotherapy **53**(10): 4258-4263.

Akerley, B. J., E. J. Rubin, V. L. Novick, K. Amaya, N. Judson and J. J. Mekalanos (2002). "A genome-scale analysis for identification of genes required for growth or survival of Haemophilus influenzae." Proceedings of the National Academy of Sciences **99**(2): 966-971.

Al-Hebshi, N. N., A. T. Nasher, A. M. Idris and T. Chen (2015). "Robust species taxonomy assignment algorithm for 16S rRNA NGS reads: application to oral carcinoma samples." Journal of oral microbiology **7**(1): 28934.

Albertsen, M., P. Hugenholtz, A. Skarshewski, K. L. Nielsen, G. W. Tyson and P. H. Nielsen (2013). "Genome sequences of rare, uncultured bacteria obtained by differential coverage binning of multiple metagenomes." Nat Biotechnol **31**(6): 533-538.

Ali, T., D. Lam, M. S. Bronze and M. B. Humphrey (2009). "Osteoporosis in inflammatory bowel disease." The American journal of medicine **122**(7): 599-604.

Allen, H. K., D. O. Bayles, T. Looft, J. Trachsel, B. E. Bass, D. P. Alt, S. M. D. Bearson, T. Nicholson and T. A. Casey (2016). "Pipeline for amplifying and analyzing amplicons of the V1–V3 region of the 16S rRNA gene." BMC research notes **9**(1): 380.

Angiuoli, S. V., M. Matalka, A. Gussman, K. Galens, M. Vangala, D. R. Riley, C. Arze, J. R. White, O. White and W. F. Fricke (2011). "CloVR: a virtual machine for automated and portable sequence analysis from the desktop using cloud computing." BMC bioinformatics **12**(1): 356.

Arkin, A. P., R. W. Cottingham, C. S. Henry, N. L. Harris, R. L. Stevens, S. Maslov, P. Dehal, D. Ware, F. Perez, S. Canon, M. W. Sneddon, M. L. Henderson, W. J. Riehl, D. Murphy-Olson, S. Y. Chan, R. T. Kamimura, S. Kumari, M. M. Drake, T. S. Brettin, E. M. Glass, D. Chivian, D. Gunter, D. J. Weston, B. H. Allen, J. Baumohl, A. A. Best, B. Bowen, S. E. Brenner, C. C. Bun, J. M. Chandonia, J. M. Chia, R. Colasanti, N. Conrad, J. J. Davis, B. H. Davison, M. DeJongh, S. Devoid, E. Dietrich, I. Dubchak, J. N. Edirisinghe, G. Fang, J. P. Faria, P. M. Frybarger, W. Gerlach, M. Gerstein, A. Greiner, J. Gurtowski, H. L. Haun, F. He, R. Jain, M. P. Joachimiak, K. P. Keegan, S. Kondo, V. Kumar, M. L. Land, F. Meyer, M. Mills, P. S. Novichkov, T. Oh, G. J. Olsen, R. Olson, B. Parrello, S. Pasternak, E. Pearson, S. S. Poon, G. A. Price, S. Ramakrishnan, P. Ranjan, P. C. Ronald, M. C. Schatz, S. M. D. Seaver, M. Shukla, R. A. Sutormin, M. H. Syed, J. Thomason, N. L. Tintle, D. Wang, F. Xia, H. Yoo, S. Yoo and D. Yu (2018). "KBase: The United States Department of Energy Systems Biology Knowledgebase." Nat Biotechnol **36**(7): 566-569.

Attar, N. (2016). "Bacterial evolution: CPR breathes new air into the tree of life." Nat Rev Microbiol **14**(6): 332-333.

Baker, B. J., G. W. Tyson, R. I. Webb, J. Flanagan, P. Hugenholtz, E. E. Allen and J. F. Banfield (2006). "Lineages of acidophilic archaea revealed by community genomic analysis." Science **314**(5807): 1933-1935.

Baker, J. L., B. Bor, M. Agnello, W. Shi and X. He (2017). "Ecology of the Oral Microbiome: Beyond Bacteria." Trends Microbiol **25**(5): 362-374.

Baker, J. L., E. L. Lindsay, R. C. Faustoferri, T. T. To, E. L. Hendrickson, X. He, W. Shi, J. S. McLean and R. G. Quivey, Jr. (2018). "Characterization of the Trehalose Utilization Operon in Streptococcus mutans Reveals that the TreR Transcriptional Regulator Is Involved in Stress Response Pathways and Toxin Production." J Bacteriol **200**(12).

Bassler, B. L., E. P. Greenberg and A. M. Stevens (1997). "Cross-species induction of luminescence in the quorum-sensing bacterium Vibrio harveyi." Journal of bacteriology **179**(12): 4043-4045.

Bassler, B. L., M. Wright and M. R. Silverman (1994). "Multiple signalling systems controlling expression of luminescence in Vibrio harveyi: sequence and function of genes encoding a second sensory pathway." Molecular microbiology **13**(2): 273-286.

Becker, M. R., B. J. Paster, E. J. Leys, M. L. Moeschberger, S. G. Kenyon, J. L. Galvin, S. K. Boches, F. E. Dewhirst and A. L. Griffen (2002). "Molecular analysis of bacterial species associated with childhood caries." Journal of clinical microbiology **40**(3): 1001-1009.

Bedree, J. K., B. Bor, L. Cen, A. Edlund, R. Lux, J. S. McLean, W. Shi and X. He (2018). "Quorum Sensing Modulates the Epibiotic-Parasitic Relationship Between Actinomyces odontolyticus and Its Saccharibacteria epibiont, a Nanosynbacter lyticus Strain, TM7x." Front Microbiol **9**: 2049.

Bidartondo, M. I., D. Redecker, I. Hijri, A. Wiemken, T. D. Bruns, L. Dominguez, A. Sersic, J. R. Leake and D. J. Read (2002). "Epiparasitic plants specialized on arbuscular mycorrhizal fungi." Nature **419**(6905): 389-392.

Bidot, W. A., A. C. Ericsson and C. L. Franklin (2018). "Effects of water decontamination methods and bedding material on the gut microbiota." PloS one **13**(10).

Bor, B., J. K. Bedree, W. Shi, J. S. McLean and X. He (2019). "Saccharibacteria (TM7) in the Human Oral Microbiome." Journal of dental research **98**(5): 500-509.

Bor, B., A. J. Collins, P. P. Murugkar, S. Balasubramanian, T. T. To, E. L. Hendrickson, J. K. Bedree, F. B. Bidlack, C. D. Johnston and W. Shi (2020). "Insights Obtained by Culturing Saccharibacteria With Their Bacterial Hosts." Journal of dental research: 0022034520905792.

Bor, B., J. S. McLean, K. R. Foster, L. Cen, T. T. To, A. Serrato-Guillen, F. E. Dewhirst, W. Shi and X. He (2018). "Rapid evolution of decreased host susceptibility drives a stable relationship between ultrasmall parasite TM7x and its bacterial host." Proc Natl Acad Sci U S A.

Bor, B., J. S. McLean, K. R. Foster, L. Cen, T. T. To, A. Serrato-Guillen, F. E. Dewhirst, W. Shi and X. He (2018). "Rapid evolution of decreased host susceptibility drives a stable relationship between ultrasmall parasite TM7x and its bacterial host." Proceedings of the National Academy of Sciences **115**(48): 12277-12282.

Bor, B., N. Poweleit, J. S. Bois, L. Cen, J. K. Bedree, Z. H. Zhou, R. P. Gunsalus, R. Lux, J. S. McLean and X. He (2016). "Phenotypic and physiological characterization of the epibiotic interaction between TM7x and its basibiont Actinomyces." Microbial ecology **71**(1): 243-255.

Bor, B., N. Poweleit, J. S. Bois, L. Cen, J. K. Bedree, Z. H. Zhou, R. P. Gunsalus, R. Lux, J. S. McLean, X. He and W. Shi (2016). "Phenotypic and Physiological Characterization of the Epibiotic Interaction Between TM7x and Its Basibiont Actinomyces." Microb Ecol **71**(1): 243-255.

Bowen, W. H., R. A. Burne, H. Wu and H. Koo (2018). "Oral Biofilms: Pathogens, Matrix, and Polymicrobial Interactions in Microenvironments." Trends Microbiol **26**(3): 229-242.

Brinig, M. M., P. W. Lepp, C. C. Ouverney, G. C. Armitage and D. A. Relman (2003). "Prevalence of bacteria of division TM7 in human subgingival plaque and their association with disease." Applied and environmental microbiology **69**(3): 1687-1694.

Brinig, M. M., P. W. Lepp, C. C. Ouverney, G. C. Armitage and D. A. Relman (2003). "Prevalence of bacteria of division TM7 in human subgingival plaque and their association with disease." Appl Environ Microbiol **69**(3): 1687-1694.

Brown, C. T., L. A. Hug, B. C. Thomas, I. Sharon, C. J. Castelle, A. Singh, M. J. Wilkins, K. C. Wrighton, K. H. Williams and J. F. Banfield (2015). "Unusual biology across a group comprising more than 15% of domain Bacteria." Nature **523**(7559): 208.

Brown, C. T., L. A. Hug, B. C. Thomas, I. Sharon, C. J. Castelle, A. Singh, M. J. Wilkins, K. C. Wrighton, K. H. Williams and J. F. Banfield (2015). "Unusual biology across a group comprising more than 15% of domain Bacteria." Nature **523**(7559): 208-211.

Burgess, N. A., D. F. Kirke, P. Williams, K. Winzer, K. R. Hardie, N. L. Meyers, J. Aduse-Opoku, M. A. Curtis and M. Cámara (2002). "LuxS-dependent quorum sensing in Porphyromonas gingivalis modulates protease and haemagglutinin activities but is not essential for virulence." Microbiology **148**(3): 763-772.

Burstein, D., C. L. Sun, C. T. Brown, I. Sharon, K. Anantharaman, A. J. Probst, B. C. Thomas and J. F. Banfield (2016). "Major bacterial lineages are essentially devoid of CRISPR-Cas viral defence systems." Nat Commun **7**: 10613.

Callahan, B. J., P. J. McMurdie, M. J. Rosen, A. W. Han, A. J. A. Johnson and S. P. Holmes (2016). "DADA2: high-resolution sample inference from Illumina amplicon data." Nature methods **13**(7): 581.

Camanocha, A. and F. E. Dewhirst (2014). "Host-associated bacterial taxa from Chlorobi, Chloroflexi, GN02, Synergistetes, SR1, TM7, and WPS-2 Phyla/candidate divisions." J Oral Microbiol **6**.

Camelo-Castillo, A. J., A. Mira, A. Pico, L. Nibali, B. Henderson, N. Donos and I. Tomas (2015). "Subgingival microbiota in health compared to periodontitis and the influence of smoking." Front Microbiol **6**: 119.

Canali, C., E. Spillum, M. Valvik, N. Agersnap and T. Olesen (2018). Real-Time Digital Bright Field Technology for Rapid Antibiotic Susceptibility Testing. Antibiotic Resistance Protocols, Springer**:** 75-84.

Caporaso, J. G., C. L. Lauber, W. A. Walters, D. Berg-Lyons, J. Huntley, N. Fierer, S. M. Owens, J. Betley, L. Fraser and M. Bauer (2012). "Ultra-high-throughput microbial community analysis on the Illumina HiSeq and MiSeq platforms." The ISME journal **6**(8): 1621-1624.

Caspi, R., R. Billington, L. Ferrer, H. Foerster, C. A. Fulcher, I. M. Keseler, A. Kothari, M. Krummenacker, M. Latendresse, L. A. Mueller, Q. Ong, S. Paley, P. Subhraveti, D. S. Weaver

and P. D. Karp (2016). "The MetaCyc database of metabolic pathways and enzymes and the BioCyc collection of pathway/genome databases." Nucleic Acids Res **44**(D1): D471-480.

Castelle, C. J. and J. F. Banfield (2018). "Major new microbial groups expand diversity and alter our understanding of the tree of life." Cell **172**(6): 1181-1197.

Castelle, C. J., C. T. Brown, B. C. Thomas, K. H. Williams and J. F. Banfield (2017). "Unusual respiratory capacity and nitrogen metabolism in a Parcubacterium (OD1) of the Candidate Phyla Radiation." Sci Rep **7**: 40101.

Chao, A., C.-H. Chiu and L. Jost (2010). "Phylogenetic diversity measures based on Hill numbers." Philosophical Transactions of the Royal Society B: Biological Sciences **365**(1558): 3599-3609.

Chao, A., N. J. Gotelli, T. C. Hsieh, E. L. Sander, K. H. Ma, R. K. Colwell and A. M. Ellison (2014). "Rarefaction and extrapolation with Hill numbers: a framework for sampling and estimation in species diversity studies." Ecological monographs **84**(1): 45-67.

Chaudhuri, R. R., A. G. Allen, P. J. Owen, G. Shalom, K. Stone, M. Harrison, T. A. Burgis, M. Lockyer, J. Garcia-Lara and S. J. Foster (2009). "Comprehensive identification of essential Staphylococcus aureus genes using Transposon-Mediated Differential Hybridisation (TMDH)." BMC genomics **10**(1): 291.

Chen, T., W. H. Yu, J. Izard, O. V. Baranova, A. Lakshmanan and F. E. Dewhirst (2010). "The Human Oral Microbiome Database: a web accessible resource for investigating oral microbe taxonomic and genomic information." Database (Oxford) **2010**: baq013.

Chen, X., S. Schauder, N. Potier, A. Van Dorsselaer, I. Pelczer, B. L. Bassler and F. M. Hughson (2002). "Structural identification of a bacterial quorum-sensing signal containing boron." Nature **415**(6871): 545.

Choi, S. Y., A. Saravia-Butler, Y. Shirazi-Fard, D. Leveson-Gower, L. S. Stodieck, S. M. Cadena, J. Beegle, S. Solis, A. Ronca and R. K. Globus (2020). "Validation of a new Rodent experimental System to investigate consequences of Long Duration Space Habitation." Scientific reports **10**(1): 1-17.

Chung, W. O., Y. Park, R. J. Lamont, R. McNab, B. Barbieri and D. R. Demuth (2001). "Signaling system in Porphyromonas gingivalis based on a LuxS protein." Journal of bacteriology **183**(13): 3903-3909.

Colombo, A. V., C. M. Silva, A. Haffajee and A. P. V. Colombo (2006). "Identification of oral bacteria associated with crevicular epithelial cells from chronic periodontitis lesions." Journal of medical microbiology **55**(5): 609-615.

Costalonga, M. and M. C. Herzberg (2014). "The oral microbiome and the immunobiology of periodontal disease and caries." Immunol Lett **162**(2 Pt A): 22-38.

Cuadra-Saenz, G., D. L. Rao, A. J. Underwood, S. A. Belapure, S. R. Campagna, Z. Sun, S. Tammariello and A. H. Rickard (2012). "Autoinducer-2 influences interactions amongst pioneer colonizing streptococci in oral biofilms." Microbiology **158**(7): 1783-1795.

Danczak, R. E., M. D. Johnston, C. Kenah, M. Slattery, K. C. Wrighton and M. J. Wilkins (2017). "Members of the Candidate Phyla Radiation are functionally differentiated by carbon- and nitrogen-cycling capabilities." Microbiome **5**(1): 112.

Davison, J., M. Heusterspreute, N. Chevalier, V. Ha-Thi and F. Brunei (1987). "Vectors with restriction site banks V. pJRD215, a wide-host-range cosmid vector with multiple cloning sites." Gene **51**(2): 275-280.

De Berardinis, V., D. Vallenet, V. Castelli, M. Besnard, A. Pinet, C. Cruaud, S. Samair, C. Lechaplais, G. Gyapay and C. Richez (2008). "A complete collection of single-gene deletion mutants of Acinetobacter baylyi ADP1." Molecular systems biology **4**(1): 174.

de Bruyn, M., J. Sabino, D. Vandeputte, S. Vermeire, J. Raes and G. Opdenakker (2018). "Comparisons of gut microbiota profiles in wild-type and gelatinase B/matrix metalloproteinase-9-deficient mice in acute DSS-induced colitis." npj Biofilms and Microbiomes **4**(1): 18.

Denning, T. L., B. A. Norris, O. Medina-Contreras, S. Manicassamy, D. Geem, R. Madan, C. L. Karp and B. Pulendran (2011). "Functional specializations of intestinal dendritic cell and macrophage subsets that control Th17 and regulatory T cell responses are dependent on the T cell/APC ratio, source of mouse strain, and regional localization." The Journal of Immunology **187**(2): 733-747.

Dewhirst, F. E., T. Chen, J. Izard, B. J. Paster, A. C. Tanner, W. H. Yu, A. Lakshmanan and W. G. Wade (2010). "The human oral microbiome." J Bacteriol **192**(19): 5002-5017.

Dewhirst, F. E., E. A. Klein, E. C. Thompson, J. M. Blanton, T. Chen, L. Milella, C. M. Buckley, I. J. Davis, M. L. Bennett and Z. V. Marshall-Jones (2012). "The canine oral microbiome." PLoS One **7**(4): e36067.

Diaz, P. I., N. I. Chalmers, A. H. Rickard, C. Kong, C. L. Milburn, R. J. Palmer and P. E. Kolenbrander (2006). "Molecular characterization of subject-specific oral microflora during initial colonization of enamel." Applied and environmental microbiology **72**(4): 2837-2848.

Dige, I., H. Nilsson, M. Kilian and B. Nyvad (2007). "In situ identification of streptococci and other bacteria in initial dental biofilm by confocal laser scanning microscopy and fluorescence in situ hybridization." European journal of oral sciences **115**(6): 459-467.

Dige, I., J. R. Nyengaard, M. Kilian and B. Nyvad (2009). "Application of stereological principles for quantification of bacteria in intact dental biofilms." Molecular oral microbiology **24**(1): 69-75.

Dige, I., M. K. Raarup, J. R. Nyengaard, M. Kilian and B. Nyvad (2009). "Actinomyces naeslundii in initial dental biofilm formation." Microbiology **155**(7): 2116-2126.

Ding, A. M., R. J. Palmer, J. O. Cisar and P. E. Kolenbrander (2010). "Shear-enhanced oral microbial adhesion." Applied and environmental microbiology **76**(4): 1294-1297.

Dinis, J. M., D. E. Barton, J. Ghadiri, D. Surendar, K. Reddy, F. Velasquez, C. L. Chaffee, M. C. Lee, H. Gavrilova, H. Ozuna, S. A. Smits and C. C. Ouverney (2011). "In search of an uncultured human-associated TM7 bacterium in the environment." PLoS One **6**(6): e21280.

Domenech, M., E. García and M. Moscoso (2012). "Biofilm formation in Streptococcus pneumoniae." Microbial biotechnology **5**(4): 455-465.

Domenech, M., E. Ramos-Sevillano, E. Garcia, M. Moscoso and J. Yuste (2013). "Biofilm formation avoids complement immunity and phagocytosis of Streptococcus pneumoniae." Infect Immun **81**(7): 2606-2615.

Domenech, M., E. Ramos-Sevillano, E. García, M. Moscoso and J. Yuste (2013). "Biofilm formation avoids complement immunity and phagocytosis of Streptococcus pneumoniae." Infection and immunity **81**(7): 2606-2615.

Donlan, R. M. and J. W. Costerton (2002). "Biofilms: survival mechanisms of clinically relevant microorganisms." Clinical microbiology reviews **15**(2): 167-193.

Donlan, R. M. and J. W. Costerton (2002). "Biofilms: survival mechanisms of clinically relevant microorganisms." Clin Microbiol Rev **15**(2): 167-193.

Dudek, N. K., C. L. Sun, D. Burstein, R. S. Kantor, D. S. Aliaga Goltsman, E. M. Bik, B. C. Thomas, J. F. Banfield and D. A. Relman (2017). "Novel Microbial Diversity and Functional Potential in the Marine Mammal Oral Microbiome." Curr Biol **27**(24): 3752-3762 e3756.

Duerkop, B. A., C. V. Clements, D. Rollins, J. L. Rodrigues and L. V. Hooper (2012). "A composite bacteriophage alters colonization by an intestinal commensal bacterium." Proc Natl Acad Sci U S A **109**(43): 17621-17626.

Duncan, M. C., J. C. Forbes, Y. Nguyen, L. M. Shull, R. K. Gillette, D. W. Lazinski, A. Ali, R. M. Q. Shanks, D. E. Kadouri and A. Camilli (2018). "Vibrio cholerae motility exerts drag force to impede attack by the bacterial predator Bdellovibrio bacteriovorus." Nature communications **9**(1): 1-9.

Dunn, D. W., S. T. Segar, J. Ridley, R. Chan, R. H. Crozier, D. W. Yu and J. M. Cook (2008). "A role for parasites in stabilising the fig-pollinator mutualism." PLoS Biol **6**(3): e59.

Eckburg, P. B., E. M. Bik, C. N. Bernstein, E. Purdom, L. Dethlefsen, M. Sargent, S. R. Gill, K. E. Nelson and D. A. Relman (2005). "Diversity of the human intestinal microbial flora." Science **308**(5728): 1635-1638.

Edlund, A., Y. Yang, A. P. Hall, L. Guo, R. Lux, X. He, K. E. Nelson, K. H. Nealson, S. Yooseph, W. Shi and J. S. McLean (2013). "An in vitro biofilm model system maintaining a highly reproducible species and metabolic diversity approaching that of the human oral microbiome." Microbiome **1**(1): 25.

Edlund, A., Y. Yang, S. Yooseph, A. P. Hall, D. D. Nguyen, P. C. Dorrestein, K. E. Nelson, X. He, R. Lux, W. Shi and J. S. McLean (2015). "Meta-omics uncover temporal regulation of pathways across oral microbiome genera during in vitro sugar metabolism." ISME J **9**(12): 2605-2619.

Eren, A. M., G. G. Borisy, S. M. Huse and J. L. Mark Welch (2014). "Oligotyping analysis of the human oral microbiome." Proc Natl Acad Sci U S A **111**(28): E2875-2884.

Ericsson, A. C., J. W. Davis, W. Spollen, N. Bivens, S. Givan, C. E. Hagan, M. McIntosh and C. L. Franklin (2015). "Effects of vendor and genetic background on the composition of the fecal microbiota of inbred mice." PloS one **10**(2).

Ericsson, A. C., J. Gagliardi, D. Bouhan, W. G. Spollen, S. A. Givan and C. L. Franklin (2018). "The influence of caging, bedding, and diet on the composition of the microbiota in different regions of the mouse gut." Scientific reports **8**(1): 4065.

F. Escapa, I., Y. Huang, T. Chen, M. Lin, A. Kokaras, F. E. Dewhirst and K. P. Lemon (2020). "Construction of habitat-specific training sets to achieve species-level assignment in 16S rRNA gene datasets." Microbiome **8**: 1-16.

Ferrari, B. C., S. J. Binnerup and M. Gillings (2005). "Microcolony cultivation on a soil substrate membrane system selects for previously uncultured soil bacteria." Appl Environ Microbiol **71**(12): 8714-8720.

Fong, K. P., W. O. Chung, R. J. Lamont and D. R. Demuth (2001). "Intra-and interspecies regulation of gene expression by Actinobacillus actinomycetemcomitansLuxS." Infection and immunity **69**(12): 7625-7634.

Fong, K. P., L. Gao and D. R. Demuth (2003). "luxS and arcB control aerobic growth of Actinobacillus actinomycetemcomitans under iron limitation." Infection and immunity **71**(1): 298-308.

Foster, Z. S. L., T. J. Sharpton and N. J. Grünwald (2017). "Metacoder: An R package for visualization and manipulation of community taxonomic diversity data." PLoS computational biology **13**(2): e1005404.

Franklin, C. L. and A. C. Ericsson (2017). "Microbiota and reproducibility of rodent models." Lab animal **46**(4): 114.

Fredricks, D. N., T. L. Fiedler and J. M. Marrazzo (2005). "Molecular identification of bacteria associated with bacterial vaginosis." New England Journal of Medicine **353**(18): 1899-1911.

Fredricks, D. N., T. L. Fiedler and J. M. Marrazzo (2005). "Molecular identification of bacteria associated with bacterial vaginosis." N Engl J Med **353**(18): 1899-1911.

Freed, N. E., D. Bumann and O. K. Silander (2016). "Combining Shigella Tn-seq data with gold-standard E. coli gene deletion data suggests rare transitions between essential and non-essential gene functionality." BMC microbiology **16**(1): 203.

Frias, J., E. Olle and M. Alsina (2001). "Periodontal pathogens produce quorum sensing signal molecules." Infection and Immunity **69**(5): 3431-3434.

Gallagher, L. A., E. Ramage, M. A. Jacobs, R. Kaul, M. Brittnacher and C. Manoil (2007). "A comprehensive transposon mutant library of Francisella novicida, a bioweapon surrogate." Proceedings of the National Academy of Sciences **104**(3): 1009-1014.

Gao, L., T. Xu, G. Huang, S. Jiang, Y. Gu and F. Chen (2018). "Oral microbiomes: more and more importance in oral cavity and whole body." Protein & cell **9**(5): 488-500.

Gao, Z., C. H. Tseng, Z. Pei and M. J. Blaser (2007). "Molecular analysis of human forearm superficial skin bacterial biota." Proc Natl Acad Sci U S A **104**(8): 2927-2932.

Garrett-Bakelman, F. E., M. Darshi, S. J. Green, R. C. Gur, L. Lin, B. R. Macias, M. J. McKenna, C. Meydan, T. Mishra and J. Nasrini (2019). "The NASA Twins Study: A multidimensional analysis of a year-long human spaceflight." Science **364**(6436): eaau8650.

Ghafoor, A., I. D. Hay and B. H. A. Rehm (2011). "The role of exopolysaccharides in Pseudomonas aeruginosa biofilm formation and architecture." Applied and environmental microbiology: AEM-00637.

Gibson, D. G., G. A. Benders, C. Andrews-Pfannkoch, E. A. Denisova, H. Baden-Tillson, J. Zaveri, T. B. Stockwell, A. Brownley, D. W. Thomas and M. A. Algire (2008). "Complete chemical synthesis, assembly, and cloning of a Mycoplasma genitalium genome." Science **319**(5867): 1215-1220.

Giongo, A., K. A. Gano, D. B. Crabb, N. Mukherjee, L. L. Novelo, G. Casella, J. C. Drew, J. Ilonen, M. Knip and H. Hyöty (2011). "Toward defining the autoimmune microbiome for type 1 diabetes." The ISME journal **5**(1): 82.

Goodman, A. L., N. P. McNulty, Y. Zhao, D. Leip, R. D. Mitra, C. A. Lozupone, R. Knight and J. I. Gordon (2009). "Identifying genetic determinants needed to establish a human gut symbiont in its habitat." Cell host & microbe **6**(3): 279-289.

Goryshin, I. Y., J. Jendrisak, L. M. Hoffman, R. Meis and W. S. Reznikoff (2000). "Insertional transposon mutagenesis by electroporation of released Tn5 transposition complexes." Nature biotechnology **18**(1): 97-100.

Goryshin, I. Y. and W. S. Reznikoff (1998). "Tn5 in vitro transposition." Journal of Biological Chemistry **273**(13): 7367-7374.

Greenberg, E. P., J. W. Hastings and S. Ulitzur (1979). "Induction of luciferase synthesis in Beneckea harveyi by other marine bacteria." Archives of Microbiology **120**(2): 87-91.

Hart, M. L., A. C. Ericsson, K. C. K. Lloyd, K. N. Grimsrud, A. R. Rogala, V. L. Godfrey, J. N. Nielsen and C. L. Franklin (2018). "Development of outbred CD1 mouse colonies with distinct standardized gut microbiota profiles for use in complex microbiota targeted studies." Scientific reports **8**(1): 1-11.

Hart, M. L., A. Meyer, P. J. Johnson and A. C. Ericsson (2015). "Comparative evaluation of DNA extraction methods from feces of multiple host species for downstream next-generation sequencing." PloS one **10**(11).

He, X., J. S. McLean, A. Edlund, S. Yooseph, A. P. Hall, S.-Y. Liu, P. C. Dorrestein, E. Esquenazi, R. C. Hunter and G. Cheng (2015). "Cultivation of a human-associated TM7 phylotype reveals a reduced genome and epibiotic parasitic lifestyle." Proceedings of the National Academy of Sciences **112**(1): 244-249.

He, X., J. S. McLean, A. Edlund, S. Yooseph, A. P. Hall, S. Y. Liu, P. C. Dorrestein, E. Esquenazi, R. C. Hunter, G. Cheng, K. E. Nelson, R. Lux and W. Shi (2015). "Cultivation of a human-associated TM7 phylotype reveals a reduced genome and epibiotic parasitic lifestyle." Proc Natl Acad Sci U S A **112**(1): 244-249.

Henry, C. S., H. C. Bernstein, P. Weisenhorn, R. C. Taylor, J. Y. Lee, J. Zucker and H. S. Song (2016). "Microbial Community Metabolic Modeling: A Community Data-Driven Network Reconstruction." J Cell Physiol **231**(11): 2339-2345.

Henry, C. S., M. DeJongh, A. A. Best, P. M. Frybarger, B. Linsay and R. L. Stevens (2010). "High-throughput generation, optimization and analysis of genome-scale metabolic models." Nat Biotechnol **28**(9): 977-982.

Hernandez, C. J., J. D. Guss, M. Luna and S. R. Goldring (2016). "Links between the microbiome and bone." Journal of bone and mineral research **31**(9): 1638-1646.

Hilgers, M. T. and M. L. Ludwig (2001). "Crystal structure of the quorum-sensing protein LuxS reveals a catalytic metal site." Proceedings of the National Academy of Sciences **98**(20): 11169-11174.

Hill, M. O. (1973). "Diversity and evenness: a unifying notation and its consequences." Ecology **54**(2): 427-432.

Hoffman, L. M. and J. J. Jendrisak (2002). Transposomes: a system for identifying genes involved in bacterial pathogenesis. Methods in enzymology, Elsevier. **358:** 128-140.

Hsieh, T. C., K. H. Ma and A. Chao (2016). "iNEXT: an R package for rarefaction and extrapolation of species diversity (H ill numbers)." Methods in Ecology and Evolution **7**(12): 1451-1456.

Huang, S., Z. Li, T. He, C. Bo, J. Chang, L. Li, Y. He, J. Liu, D. Charbonneau, R. Li and J. Xu (2016). "Microbiota-based Signature of Gingivitis Treatments: A Randomized Study." Sci Rep **6**: 24705.

Huber, H., M. J. Hohn, R. Rachel, T. Fuchs, V. C. Wimmer and K. O. Stetter (2002). "A new phylum of Archaea represented by a nanosized hyperthermophilic symbiont." Nature **417**(6884): 63-67.

Hufeldt, M. R., D. S. Nielsen, F. K. Vogensen, T. Midtvedt and A. K. Hansen (2010). "Variation in the gut microbiota of laboratory mice is related to both genetic and environmental factors." Comparative medicine **60**(5): 336-347.

Hug, L. A., B. J. Baker, K. Anantharaman, C. T. Brown, A. J. Probst, C. J. Castelle, C. N. Butterfield, A. W. Hernsdorf, Y. Amano and K. Ise (2016). "A new view of the tree of life." Nature microbiology **1**: 16048.

Hug, L. A., B. J. Baker, K. Anantharaman, C. T. Brown, A. J. Probst, C. J. Castelle, C. N. Butterfield, A. W. Hernsdorf, Y. Amano, K. Ise, Y. Suzuki, N. Dudek, D. A. Relman, K. M. Finstad, R. Amundson, B. C. Thomas and J. F. Banfield (2016). "A new view of the tree of life." Nat Microbiol **1**: 16048.

Hugenholtz, P., B. M. Goebel and N. R. Pace (1998). "Impact of culture-independent studies on the emerging phylogenetic view of bacterial diversity." J Bacteriol **180**(18): 4765-4774.

Hugenholtz, P., G. W. Tyson, R. I. Webb, A. M. Wagner and L. L. Blackall (2001). "Investigation of candidate division TM7, a recently recognized major lineage of the domain Bacteria with no known pure-culture representatives." Appl Environ Microbiol **67**(1): 411-419.

Ibberson, C. B., A. Stacy, D. Fleming, J. L. Dees, K. Rumbaugh, M. S. Gilmore and M. Whiteley (2017). "Co-infecting microorganisms dramatically alter pathogen gene essentiality during polymicrobial infection." Nature microbiology **2**(8): 17079.

Ivanov, I. I., R. de Llanos Frutos, N. Manel, K. Yoshinaga, D. B. Rifkin, R. B. Sartor, B. B. Finlay and D. R. Littman (2008). "Specific microbiota direct the differentiation of IL-17-producing T-helper cells in the mucosa of the small intestine." Cell host & microbe **4**(4): 337-349.

Jahn, U., M. Gallenberger, W. Paper, B. Junglas, W. Eisenreich, K. O. Stetter, R. Rachel and H. Huber (2008). "Nanoarchaeum equitans and Ignicoccus hospitalis: new insights into a unique, intimate association of two archaea." J Bacteriol **190**(5): 1743-1750.

James, D., H. Shao, R. J. Lamont and D. R. Demuth (2006). "The Actinobacillus actinomycetemcomitans ribose binding protein RbsB interacts with cognate and heterologous autoinducer 2 signals." Infection and immunity **74**(7): 4021-4029.

Jiang, P., S. J. Green, G. E. Chlipala, F. W. Turek and M. H. Vitaterna (2019). "Reproducible changes in the gut microbiome suggest a shift in microbial and host metabolism during spaceflight." Microbiome **7**(1): 1-18.

Jones, D. T., W. R. Taylor and J. M. Thornton (1992). "The rapid generation of mutation data matrices from protein sequences." Bioinformatics **8**(3): 275-282.

Jost, L. (2007). "Partitioning diversity into independent alpha and beta components." Ecology **88**(10): 2427-2439.

Kanasi, E., F. E. Dewhirst, N. I. Chalmers, R. Kent Jr, A. Moore, C. V. Hughes, N. Pradhan, C. Y. Loo and A. C. R. Tanner (2010). "Clonal analysis of the microbiota of severe early childhood caries." Caries research **44**(5): 485-497.

Kantor, R. S., K. C. Wrighton, K. M. Handley, I. Sharon, L. A. Hug, C. J. Castelle, B. C. Thomas and J. F. Banfield (2013). "Small genomes and sparse metabolisms of sediment-associated bacteria from four candidate phyla." MBio **4**(5): e00708-00713.

Karp, P. D., M. Latendresse, S. M. Paley, M. Krummenacker, Q. D. Ong, R. Billington, A. Kothari, D. Weaver, T. Lee, P. Subhraveti, A. Spaulding, C. Fulcher, I. M. Keseler and R. Caspi

(2016). "Pathway Tools version 19.0 update: software for pathway/genome informatics and systems biology." Brief Bioinform **17**(5): 877-890.

Kelley, L. A. and M. J. E. Sternberg (2009). "Protein structure prediction on the Web: a case study using the Phyre server." Nature protocols **4**(3): 363.

Khatiwara, A., T. Jiang, S.-S. Sung, T. Dawoud, J. N. Kim, D. Bhattacharya, H.-B. Kim, S. C. Ricke and Y. M. Kwon (2012). "Genome scanning for conditionally essential genes in Salmonella enterica serotype Typhimurium." Applied and environmental microbiology **78**(9): 3098-3107.

Kianoush, N., C. J. Adler, K.-A. T. Nguyen, G. V. Browne, M. Simonian and N. Hunter (2014). "Bacterial profile of dentine caries and the impact of pH on bacterial population diversity." PloS one **9**(3): e92940.

Kindaichi, T., S. Yamaoka, R. Uehara, N. Ozaki, A. Ohashi, M. Albertsen, P. H. Nielsen and J. L. Nielsen (2016). "Phylogenetic diversity and ecophysiology of Candidate phylum Saccharibacteria in activated sludge." FEMS Microbiol Ecol **92**(6): fiw078.

Kistler, J. O., V. Booth, D. J. Bradshaw and W. G. Wade (2013). "Bacterial community development in experimental gingivitis." PLoS One **8**(8): e71227.

Klein, B. A., E. L. Tenorio, D. W. Lazinski, A. Camilli, M. J. Duncan and L. T. Hu (2012). "Identification of essential genes of the periodontal pathogen Porphyromonas gingivalis." BMC genomics **13**(1): 1-17.

Kolenbrander, P. E. (1997). "Oral microbiology and coaggregation." Bacteria as multicellular organisms: 245-269.

Kolenbrander, P. E. (2000). "Oral microbial communities: biofilms, interactions, and genetic systems 1." Annual Reviews in Microbiology **54**(1): 413-437.

Kolenbrander, P. E., R. J. Palmer, S. Periasamy and N. S. Jakubovics (2010). "Oral multispecies biofilm development and the key role of cell–cell distance." Nature Reviews Microbiology **8**(7): 471-480.

Koressaar, T. and M. Remm (2007). "Enhancements and modifications of primer design program Primer3." Bioinformatics **23**(10): 1289-1291.

Kuehbacher, T., A. Rehman, P. Lepage, S. Hellmig, U. R. Folsch, S. Schreiber and S. J. Ott (2008). "Intestinal TM7 bacterial phylogenies in active inflammatory bowel disease." J Med Microbiol **57**(Pt 12): 1569-1576.

Kuehbacher, T., A. Rehman, P. Lepage, S. Hellmig, U. R. Fölsch, S. Schreiber and S. J. Ott (2008). "Intestinal TM7 bacterial phylogenies in active inflammatory bowel disease." Journal of medical microbiology **57**(12): 1569-1576.

Kumar, P. S., A. L. Griffen, J. A. Barton, B. J. Paster, M. L. Moeschberger and E. J. Leys (2003). "New bacterial species associated with chronic periodontitis." Journal of dental research **82**(5): 338-344.

Kumar, P. S., A. L. Griffen, J. A. Barton, B. J. Paster, M. L. Moeschberger and E. J. Leys (2003). "New bacterial species associated with chronic periodontitis." J Dent Res **82**(5): 338-344.

Kumar, S., G. Stecher and K. Tamura (2016). "MEGA7: molecular evolutionary genetics analysis version 7.0 for bigger datasets." Molecular biology and evolution **33**(7): 1870-1874.

Kumar, S., S. Suman, A. J. Fornace and K. Datta (2018). "Space radiation triggers persistent stress response, increases senescent signaling, and decreases cell migration in mouse intestine." Proceedings of the National Academy of Sciences **115**(42): E9832-E9841.

Lazinski, D. W. and A. Camilli (2013). "Homopolymer tail-mediated ligation PCR: a streamlined and highly efficient method for DNA cloning and library construction." Biotechniques **54**(1): 25-34.

Lee, W.-H., H.-M. Chen, S.-F. Yang, C. Liang, C.-Y. Peng, F.-M. Lin, L.-L. Tsai, B.-C. Wu, C.-H. Hsin and C.-Y. Chuang (2017). "Bacterial alterations in salivary microbiota and their association in oral cancer." Scientific reports **7**(1): 1-11.

Lewin, G. R., A. Stacy, K. L. Michie, R. J. Lamont and M. Whiteley (2019). "Large-scale identification of pathogen essential genes during coinfection with sympatric and allopatric microbes." Proceedings of the National Academy of Sciences **116**(39): 19685-19694.

Ley, R. E., D. A. Peterson and J. I. Gordon (2006). "Ecological and evolutionary forces shaping microbial diversity in the human intestine." Cell **124**(4): 837-848.

Ling, Z., J. Kong, P. Jia, C. Wei, Y. Wang, Z. Pan, W. Huang, L. Li, H. Chen and C. Xiang (2010). "Analysis of oral microbiota in children with dental caries by PCR-DGGE and barcoded pyrosequencing." Microbial ecology **60**(3): 677-690.

Liu, B., L. L. Faller, N. Klitgord, V. Mazumdar, M. Ghodsi, D. D. Sommer, T. R. Gibbons, T. J. Treangen, Y.-C. Chang and S. Li (2012). "Deep sequencing of the oral microbiome reveals signatures of periodontal disease." PloS one **7**(6): e37919.

Liu, B., L. L. Faller, N. Klitgord, V. Mazumdar, M. Ghodsi, D. D. Sommer, T. R. Gibbons, T. J. Treangen, Y. C. Chang, S. Li, O. C. Stine, H. Hasturk, S. Kasif, D. Segre, M. Pop and S. Amar (2012). "Deep sequencing of the oral microbiome reveals signatures of periodontal disease." PLoS One **7**(6): e37919.

Liu, L., R. Wu, J. Zhang, N. Shang and P. Li (2017). "D-Ribose Interferes with Quorum Sensing to Inhibit Biofilm Formation of Lactobacillus paraplantarum L-ZS9." Frontiers in microbiology **8**: 1860.

Lowe, B. A., T. L. Marsh, N. Isaacs-Cosgrove, R. N. Kirkwood, M. Kiupel and M. H. Mulks (2012). "Defining the "core microbiome" of the microbial communities in the tonsils of healthy pigs." BMC Microbiol **12**: 20.

Lucas, S., Y. Omata, J. Hofmann, M. Böttcher, A. Iljazovic, K. Sarter, O. Albrecht, O. Schulz, B. Krishnacoumar and G. Krönke (2018). "Short-chain fatty acids regulate systemic bone mass and protect from pathological bone loss." Nature communications **9**(1): 55.

Luef, B., K. R. Frischkorn, K. C. Wrighton, H.-Y. N. Holman, G. Birarda, B. C. Thomas, A. Singh, K. H. Williams, C. E. Siegerist and S. G. Tringe (2015). "Diverse uncultivated ultra-small bacterial cells in groundwater." Nature communications **6**: 6372.

Luef, B., K. R. Frischkorn, K. C. Wrighton, H. Y. Holman, G. Birarda, B. C. Thomas, A. Singh, K. H. Williams, C. E. Siegerist, S. G. Tringe, K. H. Downing, L. R. Comolli and J. F. Banfield (2015). "Diverse uncultivated ultra-small bacterial cells in groundwater." Nat Commun **6**: 6372.

Luna, R. A. and J. A. Foster (2015). "Gut brain axis: diet microbiota interactions and implications for modulation of anxiety and depression." Current opinion in biotechnology **32**: 35-41.

Luo, R., B. Mann, W. S. Lewis, A. Rowe, R. Heath, M. L. Stewart, A. E. Hamburger, S. Sivakolundu, E. R. Lacy and P. J. Bjorkman (2005). "Solution structure of choline binding protein A, the major adhesin of Streptococcus pneumoniae." The EMBO journal **24**(1): 34-43.

Lutz, R. and H. Bujard (1997). "Independent and tight regulation of transcriptional units in Escherichia coli via the LacR/O, the TetR/O and AraC/I1-I2 regulatory elements." Nucleic acids research **25**(6): 1203-1210.

Ma, B. W., N. A. Bokulich, P. A. Castillo, A. Kananurak, M. A. Underwood, D. A. Mills and C. L. Bevins (2012). "Routine habitat change: a source of unrecognized transient alteration of intestinal microbiota in laboratory mice." PloS one **7**(10).

Marchler-Bauer, A., Y. Bo, L. Han, J. He, C. J. Lanczycki, S. Lu, F. Chitsaz, M. K. Derbyshire, R. C. Geer and N. R. Gonzales (2016). "CDD/SPARCLE: functional classification of proteins via subfamily domain architectures." Nucleic acids research **45**(D1): D200-D203.

Marchler-Bauer, A., M. K. Derbyshire, N. R. Gonzales, S. Lu, F. Chitsaz, L. Y. Geer, R. C. Geer, J. He, M. Gwadz and D. I. Hurwitz (2014). "CDD: NCBI's conserved domain database." Nucleic acids research **43**(D1): D222-D226.

Marchler-Bauer, A., S. Lu, J. B. Anderson, F. Chitsaz, M. K. Derbyshire, C. DeWeese-Scott, J. H. Fong, L. Y. Geer, R. C. Geer and N. R. Gonzales (2010). "CDD: a Conserved Domain Database for the functional annotation of proteins." Nucleic acids research **39**(suppl_1): D225-D229.

Marcy, Y., C. Ouverney, E. M. Bik, T. Losekann, N. Ivanova, H. G. Martin, E. Szeto, D. Platt, P. Hugenholtz, D. A. Relman and S. R. Quake (2007). "Dissecting biological "dark matter" with single-cell genetic analysis of rare and uncultivated TM7 microbes from the human mouth." Proc Natl Acad Sci U S A **104**(29): 11889-11894.

Mariat, D., O. Firmesse, F. Levenez, V. D. Guimarães, H. Sokol, J. Doré, G. Corthier and J. P. Furet (2009). "The Firmicutes/Bacteroidetes ratio of the human microbiota changes with age." BMC microbiology **9**(1): 123.

Martin, M. (2011). "Cutadapt removes adapter sequences from high-throughput sequencing reads." EMBnet. journal **17**(1): 10-12.

McCutcheon, J. P. and N. A. Moran (2011). "Extreme genome reduction in symbiotic bacteria." Nat Rev Microbiol **10**(1): 13-26.

McIver, L. J., G. Abu-Ali, E. A. Franzosa, R. Schwager, X. C. Morgan, L. Waldron, N. Segata and C. Huttenhower (2018). "bioBakery: a meta'omic analysis environment." Bioinformatics **34**(7): 1235-1237.

McLean, J. S., B. Bor, K. A. Kerns, Q. Liu, T. T. To, L. Solden, E. L. Hendrickson, K. Wrighton, W. Shi and X. He (2020). "Acquisition and adaptation of ultra-small parasitic reduced genome bacteria to mammalian hosts." Cell reports **32**(3): 107939.

McLean, J. S., B. Bor, T. T. To, Q. Liu, K. A. Kearns, L. M. Solden, K. C. Wrighton, X. He and W. Shi (2018). "Evidence of independent acquisition and adaption of ultra-small bacteria to human hosts across the highly diverse yet reduced genomes of the phylum Saccharibacteria." bioRxiv: 258137.

McLean, J. S., B. Bor, T. T. To, Q. Liu, K. A. Kearns, L. M. Solden, K. C. Wrighton, X. He and W. Shi (2018). "Independent Acquisition and Adaptation of Ultra-Small Bacteria with Reduced Genomes from the Phylum Saccharibacteria to Human Hosts." CELL Sneak Peek Preprint Papers Under Review doi:10.2139/ssrn.3192029.

McLean, J. S., B. Bor, T. T. To, Q. Liu, K. A. Kearns, L. M. Solden, K. C. Wrighton, X. He and W. Shi (2018). "Independent Acquisition and Adaptation of Ultra-Small Bacteria with Reduced Genomes from the Phylum Saccharibacteria to Human Hosts. ." CELL Sneak Peek Preprint Papers Under Review.

McLean, J. S., Q. Liu, B. Bor, J. K. Bedree, L. Cen, M. Watling, T. T. To, R. E. Bumgarner, X. He and W. Shi (2016). "Draft Genome Sequence of Actinomyces odontolyticus subsp. actinosynbacter Strain XH001, the Basibiont of an Oral TM7 Epibiont." Genome Announc **4**(1).

McLean, J. S., Q. Liu, B. Bor, J. K. Bedree, L. Cen, M. Watling, T. T. To, R. E. Bumgarner, X. He and W. Shi (2016). "Draft genome sequence of Actinomyces odontolyticus subsp. actinosynbacter strain XH001, the basibiont of an oral TM7 epibiont." Genome announcements **4**(1): e01685-01615.

McLean, J. S., M. J. Lombardo, J. H. Badger, A. Edlund, M. Novotny, J. Yee-Greenbaum, N. Vyahhi, A. P. Hall, Y. Yang, C. L. Dupont, M. G. Ziegler, H. Chitsaz, A. E. Allen, S. Yooseph, G. Tesler, P. A. Pevzner, R. M. Friedman, K. H. Nealson, J. C. Venter and R. S. Lasken (2013). "Candidate phylum TM6 genome recovered from a hospital sink biofilm provides genomic insights into this uncultivated phylum." Proc Natl Acad Sci U S A **110**(26): E2390-2399.

McMurdie, P. J. and S. Holmes (2013). "phyloseq: an R package for reproducible interactive analysis and graphics of microbiome census data." PloS one **8**(4): e61217.

McNab, R., S. K. Ford, A. El-Sabaeny, B. Barbieri, G. S. Cook and R. J. Lamont (2003). "LuxS-based signaling in Streptococcus gordonii: autoinducer 2 controls carbohydrate metabolism and biofilm formation with Porphyromonas gingivalis." Journal of bacteriology **185**(1): 274-284.

Merritt, J., J. Kreth, W. Shi and F. Qi (2005). "LuxS controls bacteriocin production in Streptococcus mutans through a novel regulatory component." Molecular microbiology **57**(4): 960-969.

Merritt, J., F. Qi, S. D. Goodman, M. H. Anderson and W. Shi (2003). "Mutation of luxS affects biofilm formation in Streptococcus mutans." Infection and Immunity **71**(4): 1972-1979.

Metsalu, T. and J. Vilo (2015). "ClustVis: a web tool for visualizing clustering of multivariate data using Principal Component Analysis and heatmap." Nucleic acids research **43**(W1): W566-W570.

Miller, S. T., K. B. Xavier, S. R. Campagna, M. E. Taga, M. F. Semmelhack, B. L. Bassler and F. M. Hughson (2004). "Salmonella typhimurium recognizes a chemically distinct form of the bacterial quorum-sensing signal AI-2." Molecular cell **15**(5): 677-687.

Mishra, A., A. Das, J. O. Cisar and H. Ton-That (2007). "Sortase-catalyzed assembly of distinct heteromeric fimbriae in Actinomyces naeslundii." Journal of bacteriology **189**(8): 3156-3165.

Mishra, A., C. Wu, J. Yang, J. O. Cisar, A. Das and H. Ton-That (2010). "The Actinomyces oris type 2 fimbrial shaft FimA mediates co-aggregation with oral streptococci, adherence to red blood cells and biofilm development." Molecular microbiology **77**(4): 841-854.

Molina-Quiroz, R. C., D. W. Lazinski, A. Camilli and S. B. Levy (2016). "Transposon-sequencing analysis unveils novel genes involved in the generation of persister cells in uropathogenic Escherichia coli." Antimicrobial agents and chemotherapy **60**(11): 6907-6910.

Montonye, D. R., A. C. Ericsson, S. B. Busi, C. Lutz, K. Wardwell and C. L. Franklin (2018). "Acclimation and institutionalization of the mouse microbiota following transportation." Frontiers in microbiology **9**: 1085.

Mosca, A., M. Leclerc and J. P. Hugot (2016). "Gut microbiota diversity and human diseases: should we reintroduce key predators in our ecosystem?" Frontiers in microbiology **7**: 455.

Moscoso, M., E. García and R. López (2006). "Biofilm formation by Streptococcus pneumoniae: role of choline, extracellular DNA, and capsular polysaccharide in microbial accretion." Journal of bacteriology **188**(22): 7785-7795.

Moyer, E. L., P. M. Dumars, G.-S. Sun, K. J. Martin, D. G. Heathcote, R. D. Boyle and M. G. Skidmore (2016). "Evaluation of rodent spaceflight in the NASA animal enclosure module for an extended operational period (up to 35 days)." NPJ microgravity **2**: 16002.

Murugkar, P. P., A. J. Collins, T. Chen and F. E. Dewhirst (2020). "Isolation and cultivation of candidate phyla radiation Saccharibacteria (TM7) bacteria in coculture with bacterial hosts." Journal of oral microbiology **12**(1): 1814666.

Nagy, K. N., I. Sonkodi, I. Szöke, E. Nagy and H. N. Newman (1998). "The microflora associated with human oral carcinomas." Oral oncology **34**(4): 304-308.

Nakajima, H., Y. Hongoh, R. Usami, T. Kudo and M. Ohkuma (2005). "Spatial distribution of bacterial phylotypes in the gut of the termite Reticulitermes speratus and the bacterial community colonizing the gut epithelium." FEMS Microbiol Ecol **54**(2): 247-255.

Nishihara, T. and T. Koseki (2004). "Microbial etiology of periodontitis." Periodontol 2000 **36**: 14-26.

Nouioui, I., L. Carro, M. García-López, J. P. Meier-Kolthoff, T. Woyke, N. C. Kyrpides, R. Pukall, H.-P. Klenk, M. Goodfellow and M. Göker (2018). "Genome-based taxonomic classification of the phylum Actinobacteria." Frontiers in microbiology **9**: 2007.

Nowicki, E. M., R. Shroff, J. A. Singleton, D. E. Renaud, D. Wallace, J. Drury, J. Zirnheld, B. Colleti, A. D. Ellington, R. J. Lamont, D. A. Scott and M. Whiteley (2018). "Microbiota and Metatranscriptome Changes Accompanying the Onset of Gingivitis." MBio **9**(2).

Nyvad, B. and M. Kilian (1987). "Microbiology of the early colonization of human enamel and root surfaces in vivo." European journal of oral sciences **95**(5): 369-380.

Nyvad, B. and M. Kilian (1990). "Comparison of the initial streptococcal microflora on dental enamel in caries-active and in caries-inactive individuals." Caries research **24**(4): 267-272.

Orth, J. D., I. Thiele and B. O. Palsson (2010). "What is flux balance analysis?" Nat Biotechnol **28**(3): 245-248.

Palmer Jr, R. J., S. M. Gordon, J. O. Cisar and P. E. Kolenbrander (2003). "Coaggregation-mediated interactions of streptococci and actinomyces detected in initial human dental plaque." Journal of bacteriology **185**(11): 3400-3409.

Paster, B. J., S. K. Boches, J. L. Galvin, R. E. Ericson, C. N. Lau, V. A. Levanos, A. Sahasrabudhe and F. E. Dewhirst (2001). "Bacterial diversity in human subgingival plaque." Journal of bacteriology **183**(12): 3770-3783.

Paster, B. J., M. K. Russell, T. Alpagot, A. M. Lee, S. K. Boches, J. L. Galvin and F. E. Dewhirst (2002). "Bacterial diversity in necrotizing ulcerative periodontitis in HIV-positive subjects." Annals of periodontology **7**(1): 8-16.

Paster, B. J., M. K. Russell, T. Alpagot, A. M. Lee, S. K. Boches, J. L. Galvin and F. E. Dewhirst (2002). "Bacterial diversity in necrotizing ulcerative periodontitis in HIV-positive subjects." Ann Periodontol **7**(1): 8-16.

Pecharki, D., F. C. Petersen and A. A. Scheie (2008). "LuxS and expression of virulence factors in Streptococcus intermedius." Molecular oral microbiology **23**(1): 79-83.

Pereira, C. S., A. K. de Regt, P. H. Brito, S. T. Miller and K. B. Xavier (2009). "Identification of functional LsrB-like autoinducer-2 receptors." Journal of bacteriology **191**(22): 6975-6987.

Pereira, C. S., J. R. McAuley, M. E. Taga, K. B. Xavier and S. T. Miller (2008). "Sinorhizobium meliloti, a bacterium lacking the autoinducer-2 (AI-2) synthase, responds to AI-2 supplied by other bacteria." Molecular microbiology **70**(5): 1223-1235.

Periasamy, S. and P. E. Kolenbrander (2009). "Aggregatibacter actinomycetemcomitans builds mutualistic biofilm communities with Fusobacterium nucleatum and Veillonella species in saliva." Infection and immunity **77**(9): 3542-3551.

Peterson, J., S. Garges, M. Giovanni, P. McInnes, L. Wang, J. A. Schloss, V. Bonazzi, J. E. McEwen, K. A. Wetterstrand, C. Deal, C. C. Baker, V. Di Francesco, T. K. Howcroft, R. W. Karp, R. D. Lunsford, C. R. Wellington, T. Belachew, M. Wright, C. Giblin, H. David, M. Mills, R. Salomon, C. Mullins, B. Akolkar, L. Begg, C. Davis, L. Grandison, M. Humble, J. Khalsa, A. R. Little, H. Peavy, C. Pontzer, M. Portnoy, M. H. Sayre, P. Starke-Reed, S. Zakhari, J. Read, B. Watson and M. Guyer (2009). "The NIH Human Microbiome Project." Genome Res **19**(12): 2317-2323.

Pham, V. H. and J. Kim (2012). "Cultivation of unculturable soil bacteria." Trends Biotechnol **30**(9): 475-484.

Picardeau, M. (2010). "Transposition of fly mariner elements into bacteria as a genetic tool for mutagenesis." Genetica **138**(5): 551-558.

Podar, M., C. B. Abulencia, M. Walcher, D. Hutchison, K. Zengler, J. A. Garcia, T. Holland, D. Cotton, L. Hauser and M. Keller (2007). "Targeted access to the genomes of low-abundance organisms in complex microbial communities." Appl Environ Microbiol **73**(10): 3205-3214.

Powell, D. (2015). Degust: interactive RNA-seq analysis.

Quast, C., E. Pruesse, P. Yilmaz, J. Gerken, T. Schweer, P. Yarza, J. Peplies and F. O. Glöckner (2012). "The SILVA ribosomal RNA gene database project: improved data processing and web-based tools." Nucleic acids research **41**(D1): D590-D596.

Rabot, S., O. Szylit, L. Nugon-Baudon, J.-C. Meslin, P. Vaissade, F. Popot and M. Viso (2000). "Variations in digestive physiology of rats after short duration flights aboard the US space shuttle." Digestive diseases and sciences **45**(9): 1687-1695.

Rappé, M. S. and S. J. Giovannoni (2003). "The uncultured microbial majority." Annual Reviews in Microbiology **57**(1): 369-394.

Rheims, H., F. A. Rainey and E. Stackebrandt (1996). "A molecular approach to search for diverstiy among bacteria in the environment." J Ind Microbiol **17**: 159-169.

Rheims, H., C. Sproer, F. A. Rainey and E. Stackebrandt (1996). "Molecular biological evidence for the occurrence of uncultured members of the actinomycete line of descent in different environments and geographical locations." Microbiology **142 (Pt 10)**: 2863-2870.

Rickard, A. H., R. J. Palmer, D. S. Blehert, S. R. Campagna, M. F. Semmelhack, P. G. Egland, B. L. Bassler and P. E. Kolenbrander (2006). "Autoinducer 2: a concentration-dependent signal for mutualistic bacterial biofilm growth." Molecular microbiology **60**(6): 1446-1456.

Ritchie, L. E., S. S. Taddeo, B. R. Weeks, F. Lima, S. A. Bloomfield, M. A. Azcarate-Peril, S. R. Zwart, S. M. Smith and N. D. Turner (2015). "Space environmental factor impacts upon murine colon microbiota and mucosal homeostasis." PloS one **10**(6).

Ronca, A. E., E. L. Moyer, Y. Talyansky, M. Lowe, S. Padmanabhan, S. Choi, C. Gong, S. M. Cadena, L. Stodieck and R. K. Globus (2019). "Behavior of mice aboard the International Space Station." Scientific reports **9**(1): 1-14.

Rosenow, C., P. Ryan, J. N. Weiser, S. Johnson, P. Fontan, A. Ortqvist and H. R. Masure (1997). "Contribution of novel choline-binding proteins to adherence, colonization and immunogenicity of Streptococcus pneumoniae." Molecular microbiology **25**(5): 819-829.

Rueden, C. T., J. Schindelin, M. C. Hiner, B. E. DeZonia, A. E. Walter, E. T. Arena and K. W. Eliceiri (2017). "ImageJ2: ImageJ for the next generation of scientific image data." BMC bioinformatics **18**(1): 529.

Rylev, M., M. Bek-Thomsen, J. Reinholdt, O. K. Ennibi and M. Kilian (2011). "Microbiological and immunological characteristics of young Moroccan patients with aggressive periodontitis with and without detectable Aggregatibacter actinomycetemcomitans JP2 infection." Mol Oral Microbiol **26**(1): 35-51.

Rylev, M., M. Bek-Thomsen, J. Reinholdt, O. K. Ennibi and M. Kilian (2011). "Microbiological and immunological characteristics of young Moroccan patients with aggressive periodontitis with and without detectable Aggregatibacter actinomycetemcomitans JP2 infection." Molecular oral microbiology **26**(1): 35-51.

Sanz, M., D. Beighton, M. A. Curtis, J. A. Cury, I. Dige, H. Dommisch, R. Ellwood, R. A. Giacaman, D. Herrera, M. C. Herzberg, E. Kononen, P. D. Marsh, J. Meyle, A. Mira, A. Molina, A. Mombelli, M. Quirynen, E. C. Reynolds, L. Shapira and E. Zaura (2017). "Role of microbial biofilms in the maintenance of oral health and in the development of dental caries and periodontal diseases. Consensus report of group 1 of the Joint EFP/ORCA workshop on the boundaries between caries and periodontal disease." J Clin Periodontol **44 Suppl 18**: S5-S11.

Sanz, Y. and A. Moya-Pérez (2014). Microbiota, inflammation and obesity. Microbial endocrinology: The microbiota-gut-brain axis in health and disease, Springer**:** 291-317.

Sassetti, C. M., D. H. Boyd and E. J. Rubin (2003). "Genes required for mycobacterial growth defined by high density mutagenesis." Molecular microbiology **48**(1): 77-84.

Sato, T., K. Watanabe, H. Kumada, T. Toyama, N. Tani-Ishii and N. Hamada (2012). "Peptidoglycan of Actinomyces naeslundii induces inflammatory cytokine production and stimulates osteoclastogenesis in alveolar bone resorption." Archives of oral biology **57**(11): 1522-1528.

Saulnier, D. M., K. Riehle, T. A. Mistretta, M. A. Diaz, D. Mandal, S. Raza, E. M. Weidler, X. Qin, C. Coarfa and A. Milosavljevic (2011). "Gastrointestinal microbiome signatures of pediatric patients with irritable bowel syndrome." Gastroenterology **141**(5): 1782-1791.

Schindelin, J., I. Arganda-Carreras, E. Frise, V. Kaynig, M. Longair, T. Pietzsch, S. Preibisch, C. Rueden, S. Saalfeld and B. Schmid (2012). "Fiji: an open-source platform for biological-image analysis." Nature methods **9**(7): 676-682.

Schommer, N. N., M. Christner, M. Hentschke, K. Ruckdeschel, M. Aepfelbacher and H. Rohde (2011). "Staphylococcus epidermidis uses distinct mechanisms of biofilm formation to interfere with phagocytosis and activation of mouse macrophage-like cells 774A. 1." Infection and immunity **79**(6): 2267-2276.

Schwabe, R. F. and C. Jobin (2013). "The microbiome and cancer." Nature Reviews Cancer **13**(11): 800.

Segata, N., S. K. Haake, P. Mannon, K. P. Lemon, L. Waldron, D. Gevers, C. Huttenhower and J. Izard (2012). "Composition of the adult digestive tract bacterial microbiome based on seven mouth surfaces, tonsils, throat and stool samples." Genome Biol **13**(6): R42.

Shao, H., D. James, R. J. Lamont and D. R. Demuth (2007). "Differential interaction of Aggregatibacter (Actinobacillus) actinomycetemcomitans LsrB and RbsB proteins with autoinducer 2." Journal of bacteriology **189**(15): 5559-5565.

Shao, H., R. J. Lamont and D. R. Demuth (2007). "Autoinducer 2 is required for biofilm growth of Aggregatibacter (Actinobacillus) actinomycetemcomitans." Infection and Immunity **75**(9): 4211-4218.

Shevchuk, N. A., A. V. Bryksin, Y. A. Nusinovich, F. C. Cabello, M. Sutherland and S. Ladisch (2004). "Construction of long DNA molecules using long PCR-based fusion of several fragments simultaneously." Nucleic acids research **32**(2): e19-e19.

Shi, J. (2019). "Systemic Therapy of Inactivated-Bisphosphonate-Conjugated PEGylated NELL-1 (BP-NELL-PEG) for Spaceflight-Induced Osteoporosis."

Shields, R. C., A. R. Walker, N. Maricic, B. Chakraborty, S. A. M. Underhill and R. A. Burne (2020). "Repurposing the Streptococcus mutans CRISPR-Cas9 System to Understand Essential Gene Function." PLoS pathogens **16**(3): e1008344.

Shields, R. C., L. Zeng, D. J. Culp and R. A. Burne (2018). "Genomewide identification of essential genes and fitness determinants of Streptococcus mutans UA159." MSphere **3**(1).

Sievers, F., A. Wilm, D. Dineen, T. J. Gibson, K. Karplus, W. Li, R. Lopez, H. McWilliam, M. Remmert and J. Söding (2011). "Fast, scalable generation of high-quality protein multiple sequence alignments using Clustal Omega." Molecular systems biology **7**(1): 539.

Sjögren, K., C. Engdahl, P. Henning, U. H. Lerner, V. Tremaroli, M. K. Lagerquist, F. Bäckhed and C. Ohlsson (2012). "The gut microbiota regulates bone mass in mice." Journal of bone and mineral research **27**(6): 1357-1367.

Smego Jr, R. A. and G. Foglia (1998). "Actinomycosis." Clinical infectious diseases: 1255-1261.

Soro, V., L. C. Dutton, S. V. Sprague, A. H. Nobbs, A. J. Ireland, J. R. Sandy, M. A. Jepson, M. Micaroni, P. R. Splatt and D. Dymock (2014). "Axenic culture of a candidate division TM7 bacterium from the human oral cavity and biofilm interactions with other oral bacteria." Applied and environmental microbiology **80**(20): 6480-6489.

Sousa, V., L. Nibali, D. Spratt, J. Dopico, N. Mardas, A. Petrie and N. Donos (2017). "Peri-implant and periodontal microbiome diversity in aggressive periodontitis patients: a pilot study." Clin Oral Implants Res **28**(5): 558-570.

Sperandio, V., J. L. Mellies, W. Nguyen, S. Shin and J. B. Kaper (1999). "Quorum sensing controls expression of the type III secretion gene transcription and protein secretion in enterohemorrhagic and enteropathogenic Escherichia coli." Proceedings of the National Academy of Sciences **96**(26): 15196-15201.

Staley, J. T. and A. Konopka (1985). "Measurement of in situ activities of nonphotosynthetic microorganisms in aquatic and terrestrial habitats." Annual Reviews in Microbiology **39**(1): 321-346.

Starr, E. P., S. Shi, S. J. Blazewicz, A. J. Probst, D. J. Herman, M. K. Firestone and J. F. Banfield (2018). "Stable isotope informed genome-resolved metagenomics reveals that Saccharibacteria utilize microbially-processed plant-derived carbon." Microbiome **6**(1): 122.

Strati, F., D. Cavalieri, D. Albanese, C. De Felice, C. Donati, J. Hayek, O. Jousson, S. Leoncini, D. Renzi and A. Calabrò (2017). "New evidences on the altered gut microbiota in autism spectrum disorders." Microbiome **5**(1): 24.

Taga, M. E., S. T. Miller and B. L. Bassler (2003). "Lsr-mediated transport and processing of AI-2 in Salmonella typhimurium." Molecular microbiology **50**(4): 1411-1427.

Taga, M. E., J. L. Semmelhack and B. L. Bassler (2001). "The LuxS-dependent autoinducer AI-2 controls the expression of an ABC transporter that functions in AI-2 uptake in Salmonella typhimurium." Molecular microbiology **42**(3): 777-793.

Taga, M. E. and K. B. Xavier (2005). "Methods for Analysis of Bacterial Autoinducer-2 Production." Current protocols in microbiology: 1C-1.

Team, R. C. (2013). "R: A language and environment for statistical computing."

Thiel, V., R. Vilchez, H. Sztajer, I. Wagner-Döbler and S. Schulz (2009). "Identification, Quantification, and Determination of the Absolute Configuration of the Bacterial Quorum-Sensing Signal Autoinducer-2 by Gas Chromatography–Mass Spectrometry." ChemBioChem **10**(3): 479-485.

Thurlow, L. R., M. L. Hanke, T. Fritz, A. Angle, A. Aldrich, S. H. Williams, I. L. Engebretsen, K. W. Bayles, A. R. Horswill and T. Kielian (2011). "Staphylococcus aureus biofilms prevent macrophage phagocytosis and attenuate inflammation in vivo." J Immunol **186**(11): 6585-6596.

Thurlow, L. R., M. L. Hanke, T. Fritz, A. Angle, A. Aldrich, S. H. Williams, I. L. Engebretsen, K. W. Bayles, A. R. Horswill and T. Kielian (2011). "Staphylococcus aureus biofilms prevent macrophage phagocytosis and attenuate inflammation in vivo." The Journal of Immunology **186**(11): 6585-6596.

Tian, Y., X. He, M. Torralba, S. Yooseph, K. E. Nelson, R. Lux, J. S. McLean, G. Yu and W. Shi (2010). "Using DGGE profiling to develop a novel culture medium suitable for oral microbial communities." Mol Oral Microbiol **25**(5): 357-367.

Tong, M., J. P. Jacobs, I. H. McHardy and J. Braun (2014). "Sampling of intestinal microbiota and targeted amplification of bacterial 16S rRNA genes for microbial ecologic analysis." Current protocols in immunology **107**(1): 7-41.

Tsai, C.-Y., C. Y. Tang, T.-S. Tan, K.-H. Chen, K.-H. Liao and M.-L. Liou (2018). "Subgingival microbiota in individuals with severe chronic periodontitis." Journal of microbiology, immunology and infection **51**(2): 226-234.

Untergasser, A., I. Cutcutache, T. Koressaar, J. Ye, B. C. Faircloth, M. Remm and S. G. Rozen (2012). "Primer3—new capabilities and interfaces." Nucleic acids research **40**(15): e115-e115.

Utter, D. R., X. He, C. M. Cavanaugh, J. S. McLean and B. Bor (2020). "The saccharibacterium TM7x elicits differential responses across its host range." The ISME journal: 1-14.

Van Opijnen, T., K. L. Bodi and A. Camilli (2009). "Tn-seq: high-throughput parallel sequencing for fitness and genetic interaction studies in microorganisms." Nature methods **6**(10): 767-772.

Vartoukian, S. R., R. M. Palmer and W. G. Wade (2010). "Strategies for culture of 'unculturable' bacteria." FEMS Microbiol Lett **309**(1): 1-7.

Vidal, J. E., J. Chen, J. Li and B. A. McClane (2009). "Use of an EZ-Tn 5-based random mutagenesis system to identify a novel toxin regulatory locus in Clostridium perfringens strain 13." PloS one **4**(7): e6232.

Voorhies, A. A. and H. A. Lorenzi (2016). "The challenge of maintaining a healthy microbiome during long-duration space missions." Frontiers in Astronomy and Space Sciences **3**: 23.

Voorhies, A. A., C. M. Ott, S. Mehta, D. L. Pierson, B. E. Crucian, A. Feiveson, C. M. Oubre, M. Torralba, K. Moncera and Y. Zhang (2019). "Study of the impact of long-duration space missions at the International Space Station on the astronaut microbiome." Scientific reports **9**.

Wang, L., J. Li, J. C. March, J. J. Valdes and W. E. Bentley (2005). "luxS-dependent gene regulation in Escherichia coli K-12 revealed by genomic expression profiling." Journal of bacteriology **187**(24): 8350-8360.

Weyrich, L. S., S. Duchene, J. Soubrier, L. Arriola, B. Llamas, J. Breen, A. G. Morris, K. W. Alt, D. Caramelli, V. Dresely, M. Farrell, A. G. Farrer, M. Francken, N. Gully, W. Haak, K. Hardy, K. Harvati, P. Held, E. C. Holmes, J. Kaidonis, C. Lalueza-Fox, M. de la Rasilla, A. Rosas, P. Semal, A. Soltysiak, G. Townsend, D. Usai, J. Wahl, D. H. Huson, K. Dobney and A. Cooper (2017). "Neanderthal behaviour, diet, and disease inferred from ancient DNA in dental calculus." Nature **544**(7650): 357-361.

Winsley, T. J., I. Snape, J. McKinlay, J. Stark, J. M. van Dorst, M. Ji, B. C. Ferrari and S. D. Siciliano (2014). "The ecological controls on the prevalence of candidate division TM7 in polar regions." Front Microbiol **5**: 345.

Wu, C., I. H. Huang, C. Chang, M. E. Reardon-Robinson, A. Das and H. Ton-That (2014). "Lethality of sortase depletion in A ctinomyces oris caused by excessive membrane accumulation of a surface glycoprotein." Molecular microbiology **94**(6): 1227-1241.

Wu, C., M. E. Reardon-Robinson and H. Ton-That (2016). Genetics and cell morphology analyses of the Actinomyces oris srtA mutant. Bacterial Cell Wall Homeostasis, Springer**:** 109-122.

Wu, C. and H. Ton-That (2010). "Allelic exchange in Actinomyces oris with mCherry fluorescence counterselection." Appl. Environ. Microbiol. **76**(17): 5987-5989.

Wurch, L., R. J. Giannone, B. S. Belisle, C. Swift, S. Utturkar, R. L. Hettich, A. L. Reysenbach and M. Podar (2016). "Genomics-informed isolation and characterization of a symbiotic Nanoarchaeota system from a terrestrial geothermal environment." Nat Commun **7**: 12115.

Xavier, K. B. and B. L. Bassler (2005). "Regulation of uptake and processing of the quorum-sensing autoinducer AI-2 in Escherichia coli." Journal of bacteriology **187**(1): 238-248.

Xavier, K. B., S. T. Miller, W. Lu, J. H. Kim, J. Rabinowitz, I. Pelczer, M. F. Semmelhack and B. L. Bassler (2007). "Phosphorylation and processing of the quorum-sensing molecule autoinducer-2 in enteric bacteria." ACS chemical biology **2**(2): 128-136.

Yan, J., J. W. Herzog, K. Tsang, C. A. Brennan, M. A. Bower, W. S. Garrett, B. R. Sartor, A. O. Aliprantis and J. F. Charles (2016). "Gut microbiota induce IGF-1 and promote bone formation and growth." Proceedings of the National Academy of Sciences **113**(47): E7554-E7563.

Yeung, M. K. (1995). "Construction and use of integration plasmids to generate site-specific mutations in the Actinomyces viscosus T14V chromosome." Infection and Immunity **63**(8): 2924-2930.

Yeung, M. K. (1999). "Molecular and genetic analyses of Actinomyces spp." Critical Reviews in Oral Biology & Medicine **10**(2): 120-138.

Yeung, M. K., J. A. Donkersloot, J. O. Cisar and P. A. Ragsdale (1998). "Identification of a Gene Involved in Assembly ofActinomyces naeslundii T14V Type 2 Fimbriae." Infection and immunity **66**(4): 1482-1491.

Yeung, M. K. and C. S. Kozelsky (1994). "Transformation of Actinomyces spp. by a gram-negative broad-host-range plasmid." Journal of bacteriology **176**(13): 4173-4176.

Yeung, M. K. and C. S. Kozelsky (1997). "Transfection ofActinomycesspp. by Genomic DNA of Bacteriophages from Human Dental Plaque." Plasmid **37**(2): 141-153.

Zengler, K., G. Toledo, M. Rappe, J. Elkins, E. J. Mathur, J. M. Short and M. Keller (2002). "Cultivating the uncultured." Proc Natl Acad Sci U S A **99**(24): 15681-15686.

Zhang, R. and Y. Lin (2009). "DEG 5.0, a database of essential genes in both prokaryotes and eukaryotes." Nucleic acids research **37**(suppl_1): D455-D458.

Zhang, R., H. Y. Ou and C. T. Zhang (2004). "DEG: a database of essential genes." Nucleic acids research **32**(suppl_1): D271-D272.

Zhang, S. L., L. Bai, N. Goel, A. Bailey, C. J. Jang, F. D. Bushman, P. Meerlo, D. F. Dinges and A. Sehgal (2017). "Human and rat gut microbiome composition is maintained following sleep restriction." Proc Natl Acad Sci U S A **114**(8): E1564-E1571.

Zhang, Z., Y. Zhang, P. Evans, A. Chinwalla and D. Taylor (2017). "RNA-seq 2G: online analysis of differential gene expression with comprehesive options of statistical methods." bioRxiv: 122747.

Zheng, H., L. Xu, Z. Wang, L. Li, J. Zhang, Q. Zhang, T. Chen, J. Lin and F. Chen (2015). "Subgingival microbiome in patients with healthy and ailing dental implants." <u>Scientific reports</u> **5**: 10948.

Zhou, M., A. Bhasin and W. S. Reznikoff (1998). "Molecular genetic analysis of transposase-end DNA sequence recognition: cooperativity of three adjacent base-pairs in specific interaction with a mutant Tn5 transposase." <u>Journal of molecular biology</u> **276**(5): 913-925.